Computer-Aided Design Software for the Undamped Two-Dimensional Static and Dynamic Analysis of Beams and Rotors

Anaita R. Dolasa

Thesis submitted to the Faculty of the
Virginia Polytechnic Institute and State University
in partial fulfillment of the requirements for the degree of

Master of Science
In
Mechanical Engineering

Larry D. Mitchell, Chairman
Reginald G. Mitchiner
Robert L. West, Jr.

May 3, 1998
Blacksburg, Virginia

Keywords: Beam, Rotor, Transfer Matrix, Vibration, Eigenvalues, Forced Response, Frequency Response

Computer–Aided Design Software for the Undamped Two-Dimensional Static and Dynamic Analysis of Beams and Rotors

by

Anaita Dolasa

Dr. Larry D. Mitchell, Chairman

Department of Mechanical Engineering

Abstract

The objective of this research work was to develop a design tool to analyze and design undamped beam and rotor systems in two dimensions. Systems modeled in two dimensions, such as beams with different moments of inertia, could produce varying responses in the each direction of motion. A coupling between the vertical and horizontal motions also exists in rotor systems mounted of fluid film bearings. The computer program called 2DBEAM has been developed to model and provide analyses of such systems in two dimensions.

The tool has been based on an existing design package, BEAM9, which in its present state provides the response of beams and rotors in one plane of motion. The 2DBEAM program has the capability of performing the static response, free vibration, forced dynamic response, and frequency response analyses of a system.

The Transfer Matrix Method has been used in the development of the software and an explanation of the method is included in this thesis. Mathematical problems and solutions encountered while developing 2DBEAM are also documented in this study. The code has been tested against analytical and published solutions for the types of analysis mentioned above and on coupled and uncoupled system models.

Acknowledgements

My sincerest gratitude is extended to my advisor, Dr. Larry D. Mitchell, for his guidance, advice, and support, throughout the course of my graduate years at Virginia Tech. His immeasurable patience and support has made this work possible. I would like to thank Dr. Reginald G. Mitchiner and Dr. Robert L. West for serving on my committee and reviewing this work.

I would also like to thank my colleagues Tim Poppe and Tim Griffin for their help and support particularly with the software development. I sincerely appreciate Pavan Thallapragada's willingness to help me at all times especially while I was away from Blacksburg.

I am greatly appreciative of my parents for their unconditional love and support. The close relationship I share with them and my sisters, Navaz, Shehrnaz, and Ayesha, has brought confidence and reassurance to my life.

To my friend Piyush without whom life would not be as colorful. Last but not least, to Dutch, my furry companion, who always reminds me about the simple joys in life.

Table of Contents

List of Figures

List of Tables

Chapter 1
Introduction

Beams and rotors are important structural and mechanical elements in engineering. Beams are commonly found in the deck of a bridge, the boom of a crane, wing of an aircraft, and axles of vehicles, while rotor systems are found in industrial machines such as steam and gas turbines, turbogenerators, and internal combustion engines.

As beam elements and rotor systems are widely used in industry it is important to ensure that their design is reliable and safe. Preliminary analyses of the systems also help to optimize the design and avoid future investments on repairs. It is, therefore, essential for design engineers to evaluate the static and dynamic characteristics of the systems. The intention of this study is to develop a software tool to be used by design engineers to perform these evaluations with ease and efficiency.

1.1 Research Overview

The concentration of this research effort is to produce a computer-aided design package that performs the two-dimensional static and dynamic analyses of beams and rotor systems. The term two-dimensional is used to describe the planes of motion of the system in the directions of the two principal axes of the cross section of the structure. For the remainder of the thesis these two planes are referred to as the horizontal and vertical planes or directions of motion.

The tool, called 2DBEAM, expands the capability of an existing design package, BEAM9. BEAM9 in its present state provides the response of beams and rotors in one plane of motion.

The extended 2DBEAM program broadens the solution to beam and rotor vibration problems to include systems in which a coupling exists between the vertical and horizontal directions of motion. An example of such a system is a rotor system supported on fluid-film bearings. The response of a system with uncoupled motions is also available and is a time saver as obtaining the computations of the two directions of motion can be carried out with a single run of the program. Such systems include the support of floors of buildings or the straight beams in a frame. The cross section of these members could have different moments of inertia in the two principal axes or be acted upon by loads perpendicular to but at angles about the axis of the members, both of which would produce varying responses in the two directions.

1.2 Research Approach

The transfer matrix method described in Pestel and Leckie [1] has been used to develop the code for the 2DBEAM program. The basic concept of the method is that a system can be broken up into smaller, simpler elements that can be expressed as matrices comprised of elastic and dynamic properties. These element matrices or *transfer matrices* relate the *state vector* (a column vector composed of displacements and internal forces) on the left side of an element to the *state vector* located on the right side of an element by a simple matrix multiplication. That is, output state on the right equals the element *transfer matrix* times the input state on the left of the element. The *state vectors* and *transfer matrices* link adjacent sections of the structure to one another.

The *transfer matrix* that describes an element of finite length is known as the *field transfer matrix*. A point element, namely one with zero length, is referred to as a *point transfer matrix*. These *transfer matrices* when combined through successive matrix multiplication produce the *global transfer matrix* that relates the left end of the entire system to the right end of the system.

1.3 Goals of the Research

The objective of this research work is to develop 2DBEAM, a design tool to aid engineers in their task of analyzing and designing beam and rotor systems in two dimensions. The software tool has been developed using Visual Basic® 4.0, a product of the Microsoft Corporation, which is an interactive Windows® programming language.

The analyses of undamped beams and rotors included in 2DBEAM are:

1. the static and stress analysis whose results are the deflection, slope, moment, and shear values in the horizontal and vertical planes of motions along with the shear and tensile stresses,
2. the free vibration analysis to obtain the undamped natural frequencies and corresponding mode shapes using a visual method of determining the natural frequency or an automatic Muller Method [2] of determining the roots,
3. the forced dynamic response to a specified harmonic excitation, and
4. the frequency response at a point along the structure for a given frequency range.

Note that the beam model can take into account the effects of shear deformation and rotary inertia.

Disclaimer:

An important warning about 2DBEAM (which is also seen while using the program) is the following limitation in the code. The program can handle axisymmetric sections of a structure whose principal axes coincide with one another. However, sections that have different orientations of the principal axes can not be assembled correctly by this version of the code and should be avoided when using 2DBEAM.

The usage of the tool by industrial and academic users is made easier due to a user-friendly interface. The output from 2DBEAM can be viewed graphically or obtained in

the form of tables. Both the graphical plots and tables can be generated as printouts or saved into files for future work. Appendix B provides an overview of screen displays seen while using 2DBEAM. Shown are the various input screens to enter the model's information, the different types of analysis that can be performed on a system, and the resulting output screen shots in graphical and tabular formats. The appendix has been provided as a preview of all available screens that users will encounter as they step through the software package.

Chapter 2
Transfer Matrix Method

This chapter outlines the basic concept of the transfer matrix method. Pestel and Leckie [3] provide an excellent reference for a detailed explanation and application of the method.

The first three sections of this chapter define terminology and terms as used by the transfer matrix method. Section 2.4 and 2.5 deal with the method's procedure to perform free and forced vibrations analyses of systems.

2.1 State Vector

In the transfer matrix method the term *state vector* denoted as $\{z\}_i$ is used to describe a column vector of displacements and internal forces at point *i* located along the length of the structure.

In a spring-mass system the *state vector* at the point *i* on the spring is comprised of the displacement x_i and spring internal force N_i. This would symbolically be written as

$$\{z\}_i = \begin{Bmatrix} x \\ N \end{Bmatrix}_i \tag{2.1}$$

For a torsional system made up of disks attached along the length of a shaft, the *state vector's* displacement component is the angle of twist of the shaft, ϕ, while the internal force is the torque, *T*. At a given point *i* this would be

$$\{z\}_i = \begin{Bmatrix} \phi \\ T \end{Bmatrix}_i \tag{2.2}$$

This notation can also be extended to describe a straight beam structure. The flexural vibration of a beam in three-dimensional space can be resolved into two mutually perpendicular planes of motion. The *state vector* at a point contains the deflection, the slope, the internal moment, and the internal shear. For the vertical direction of motion the deflection, slope, moment, and shear is denoted by w, ψ, M_y, and V_z and for the horizontal direction is v, ϑ, M_z, and V_y respectively. The notation will be made more apparent in Section 2.2. For now, the *state vector* at a point i is expressed as

$$\{z\}_i = \begin{Bmatrix} w \\ v \\ \hline M_y \\ V_z \\ \hline v \\ \vartheta \\ \hline M_z \\ V_y \end{Bmatrix}_i \tag{2.3}$$

Note that in the above *state vector* the displacement terms are above the force terms for a given direction of motion. The displacements are defined as complements of the forces. That is, deflection w is the complement of shear V_z and ψ is the complement of M_y. Complements are those state variables that directly interact with one another. For example, if one constrains the deflection w to zero this must be done by applying the complement V_z shear to hold the structure in place. Consider Equation (2.3)'s vertical states. These are the states above the solid horizontal line in the column vector. Now the complements of the vertical states are mirror imaged across the dashed divide line. That is, w is the complement of V_z and ψ is the complement of M_y. The components of the vertical direction are lumped together above those of the horizontal direction.

2.2 Coordinate System and Sign Convention

The right-handed cartesian coordinate system is employed for the transfer matrix method (Figure 2.1). The *x*-axis runs along the central axis of the structure while the *y* and *z* axes coincide with the principal axes of inertia of the cross-sectional area.

As this matrix method deals with displacements and internal forces within the structure it is important to establish the sign convention for the positive and negative values of these components. If a constant cross-sectioned element is cut, two cross-section surfaces are exposed (Figure 2.1). The positive face is the cross-section surface on which the outward normal is directed in the positive *x*-direction. The negative face is the one whose outward normal points in the negative *x*-direction. The displacements are considered positive when they occur in the coordinate's positive direction. A force is one of a positive force pair when it is positively directed in the coordinate system while acting upon a positive face. In other words, the force pair sign is the face sign times the force vector sign.

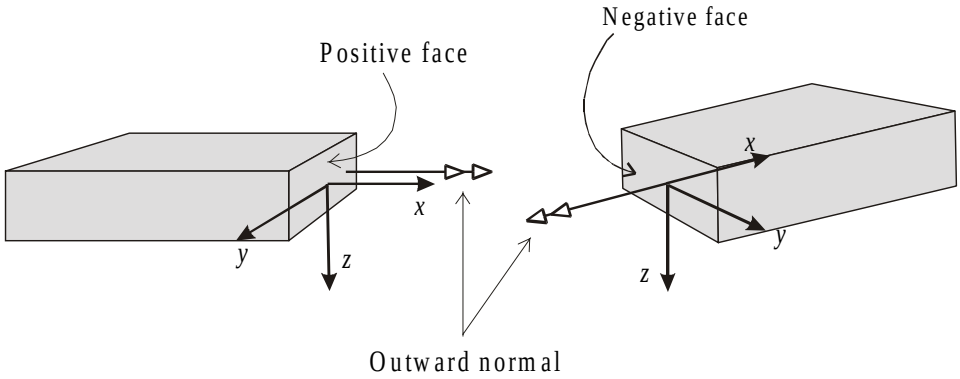

Figure 2.1: Coordinate system, adapted from Pestel and Leckie [4].

As mentioned in the previous section the terms in the *state vector* of a beam structure is comprised of deflection, slope, moment, and shear in two directions. Figure 2.2 below helps in the understanding of the notation of components for the structure's vibration in the two separate planes. The symbols will be used for the remainder of this and the following chapters.

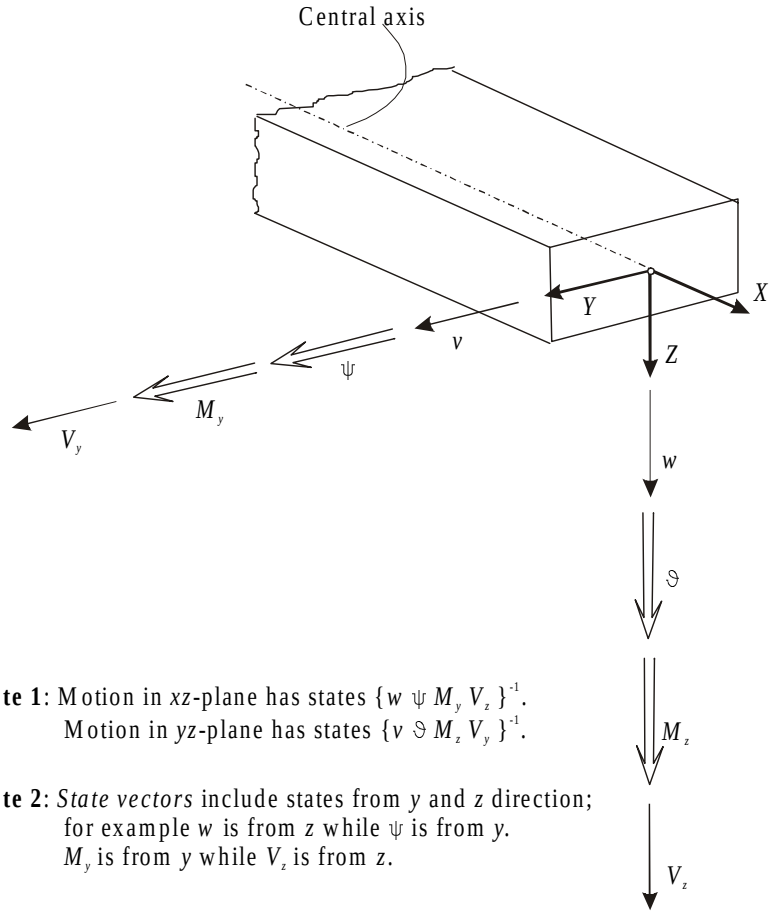

Figure 2.2: Displacements and forces of a straight beam in the two perpendicular directions, after Pestel and Leckie [5].

Symbols used in Figure 2.2:

v, *w*	Displacements in the *y* and *z* direction, respectively
ψ, ϑ	Rotations around the *y* and *z* axes, respectively
M_y, M_z	Bending moment about *y* and *z* axes, respectively

V_y, V_z Shear in y and z direction, respectively

2.3 Field, Point, and Global Transfer Matrix

Having established the sign convention that will be used, we return to the explanation of the method and define several new terms.

A complicated elastic structure containing various mechanical elements can be broken down into smaller easier to manage components. These smaller components fall into two categories: elements with a finite length and those with no length or at a point. To evaluate the effect of the elements, equations of equilibrium and strength of materials are utilized to form relations from one end or side of an element to another. In the transfer matrix method these equations are then written into a matrix form relating the *state vector* of one point on the system to the *state vector* of an adjacent point.

Field Transfer Matrix. Consider an element of non-zero length such as the massless elastic shaft of length l_i. Illustrated in Figures 2.3(a) and 2.3(b) are the free-body diagrams, from two different views, of the shaft isolated into a section between points i-1 and i.

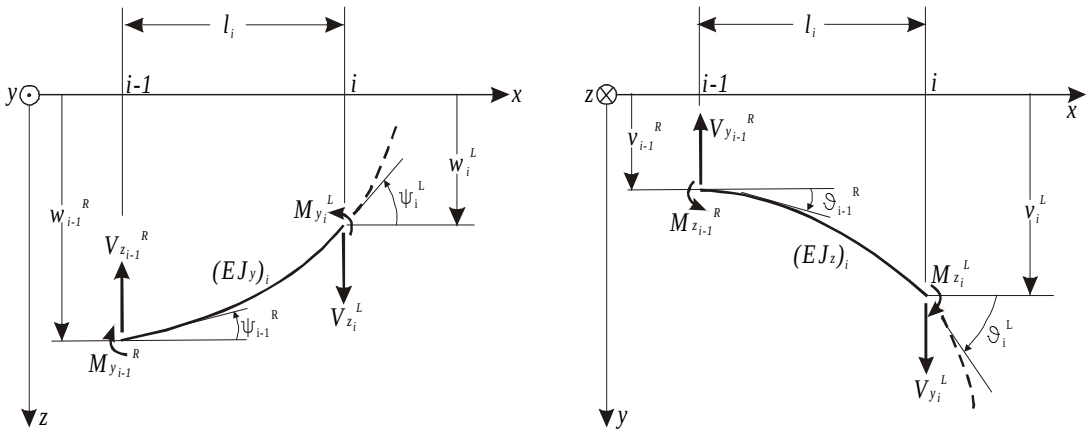

(a) (b)

Figure 2.3: (a) Free-body diagram of shaft in *xz*-plane; (b) free-body diagram of shaft in *xy*-plane, after Pestel and Leckie [6].

The displacements and internal forces at both ends of the beam allow *state vectors* to be formulated. To maintain the section in equilibrium the sum of vertical and horizontal forces and the sum of moments about a point must be zero. Using these principles the following four equations arise.

In the *xz*-plane:

$$V_{z_i}^{\ L} - V_{z_{i-1}}^{\ R} = 0 \tag{2.4}$$

$$M_{y_i}^{\ L} - M_{y_{i-1}}^{\ R} + V_{z_i}^{\ L} l_i = 0 \tag{2.5}$$

In the *xy*-plane:

`

$$V_{y_i}^{\ L} - V_{y_{i-1}}^{\ R} = 0 \tag{2.6}$$

$$M_{z_i}^{\ L} - M_{z_{i-1}}^{\ R} + V_{y_i}^{\ L} l_i = 0 \tag{2.7}$$

To obtain the deflection and slope equations for this beam section we consider the deflection and slope equations obtained from a cantilever beam subjected to an end load of shear and moment. Assuming the beam has a constant cross-section and the flexural stiffness affecting motion in the *xz*-plane is $(EJ_y)_i$ and motion in the *xy*-plane is $(EJ_z)_i$, the equations are:

$$w_i^L = -\frac{M_{y_i}^{\ L} l_i^2}{2(EJ_y)_i^L} + \frac{V_{z_i}^{\ L} l_i^3}{3(EJ_y)_i^L} \tag{2.8}$$

$$\psi_i^L = \frac{M_{y_i}^{\ L} l_i}{(EJ_y)_i^L} - \frac{V_{z_i}^{\ L} l_i^2}{2(EJ_y)_i^L} \tag{2.9}$$

$$v_i^L = \frac{M_{z_i}^{\ L} l_i^2}{2(EJ_z)_i^L} + \frac{V_{y_i}^{\ L} l_i^3}{3(EJ_z)_i^L} \tag{2.10}$$

$$\vartheta_i^L = \frac{M_{z_i}^{\ L} l_i}{(EJ_z)_i^L} + \frac{V_{y_i}^{\ L} l_i^2}{2(EJ_z)_i^L} \tag{2.11}$$

Using the method of superposition the above equations can be combined with the displacement terms at point *i*-1 to obtain,

$$w_i^L = w_{i-1}^R - \psi_{i-1}^R l_i - \frac{M_{y_i}^L l_i^2}{2(EJ_y)_i^L} + \frac{V_{z_i}^L l_i^3}{3(EJ_y)_i^L} \tag{2.12}$$

$$\psi_i^L = \psi_{i-1}^R + \frac{M_{y_i}^L l_i}{(EJ_y)_i^L} - \frac{V_{z_i}^L l_i^2}{2(EJ_y)_i^L} \tag{2.13}$$

$$v_i^L = v_{i-1}^R + \vartheta_{i-1}^R l_i + \frac{M_{z_i}^L l_i^2}{2(EJ_z)_i^L} + \frac{V_{y_i}^L l_i^3}{3(EJ_z)_i^L} \tag{2.14}$$

$$\vartheta_i^L = \vartheta_{i-1}^R + \frac{M_{z_i}^L l_i}{(EJ_z)_i^L} + \frac{V_{y_i}^L l_i^2}{2(EJ_z)_i^L} \tag{2.15}$$

Notice that Equations (2.12) to (2.15) are not in the form *ouput = f(input)*. Both the output and inputs are included on the right-hand side of the equation. So rearranging Equations (2.4), (2.5), (2.6), and (2.7) and substituting them into Equations (2.12), (2.13), (2.14), and (2.15) gives the following four equations that express displacement components of point *i*-1 as a function of point *i*:

(in the xz-plane)

$$w_i^L = w_{i-1}^R - \psi_{i-1}^R l_i - \frac{M_{y_{i-1}}^R l_i^2}{2(EJ_y)_i^L} - \frac{V_{z_{i-1}}^R l_i^3}{6(EJ_y)_i^L} \tag{2.16}$$

$$\psi_i^L = \psi_{i-1}^R + \frac{M_{y_{i-1}}^R l_i}{(EJ_y)_i^L} + \frac{V_{z_{i-1}}^R l_i^2}{2(EJ_y)_i^L} \tag{2.17}$$

(in the yz-plane)

$$v_i^L = v_{i-1}^R + \vartheta_{i-1}^R l_i + \frac{M_{z_{i-1}}^R l_i^2}{2(EJ_z)_i^L} - \frac{V_{y_{i-1}}^R l_i^3}{6(EJ_z)_i^L} \tag{2.18}$$

$$\vartheta_i^L = \vartheta_{i-1}^R + \frac{M_{z_{i-1}}^R l_i}{(EJ_z)_i^L} - \frac{V_{y_{i-1}}^R l_i^2}{2(EJ_z)_i^L} \tag{2.19}$$

After rearranging the shear and moment Equations (2.4), (2.5), (2.6), and (2.7), they can be assembled with the Equations (2.16), (2.17), (2.18), and (2.19) and written as the matrix equation as

$$\begin{Bmatrix} w \\ \psi \\ M_y \\ V_z \\ \hdashline v \\ \vartheta \\ M_z \\ V_y \end{Bmatrix}_i^L = \left[\begin{array}{cccc:cccc} 1 & -l & -\frac{l^2}{2EJ_y} & -\frac{l^3}{6EJ_y} & 0 & 0 & 0 & 0 \\ 0 & 1 & \frac{l}{EJ_y} & \frac{l^2}{2EJ_y} & 0 & 0 & 0 & 0 \\ 0 & 0 & 1 & l & 0 & 0 & 0 & 0 \\ 0 & 0 & 0 & 1 & 0 & 0 & 0 & 0 \\ \hdashline 0 & 0 & 0 & 0 & 1 & l & \frac{l^2}{2EJ_z} & -\frac{l^3}{6EJ_z} \\ 0 & 0 & 0 & 0 & 0 & 1 & \frac{l}{EJ_z} & -\frac{l^2}{2EJ_z} \\ 0 & 0 & 0 & 0 & 0 & 0 & 1 & -l \\ 0 & 0 & 0 & 0 & 0 & 0 & 0 & 1 \end{array}\right]_i \cdot \begin{Bmatrix} w \\ \psi \\ M_y \\ V_z \\ \hdashline v \\ \vartheta \\ M_z \\ V_y \end{Bmatrix}_{i-1}^R \tag{2.20}$$

or symbolically as:

$$\{z\}_i^L = [F]_i \{z\}_{i-1}^R \tag{2.21}$$

where $[F]_i$ is referred to as the i^{th} *field transfer matrix*, or in short *field matrix*, that aids in describing the *state vector* at point *i* in terms of the *state vector* at point *i*-1.

Point Transfer Matrix. The other category of elements is those with zero length or of point length. A concentrated mass is an example of such an element and is considered below.

Figures 2.4(a) and 2.4(b) show the free-body diagrams of the concentrated mass as observed from the two different directions.

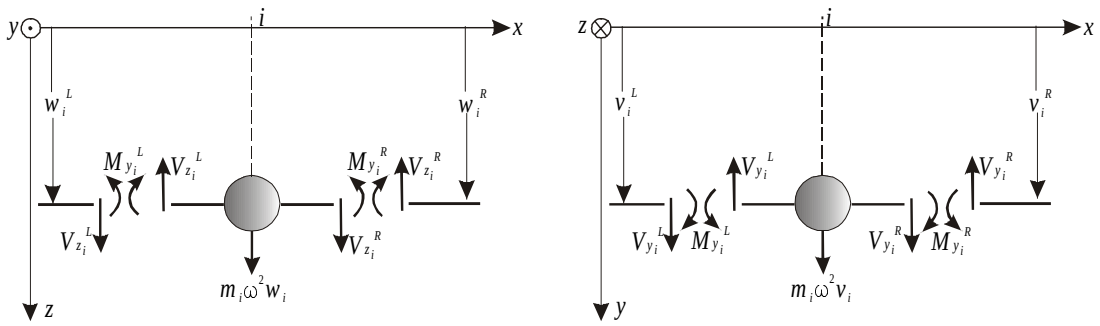

Figure 2.4: (a) Free-body diagram of a concentrated mass in *xz*-plane; (b) free-body diagram of a concentrated mass in *xy*-plane, adapted from Pestel and Leckie [7].

The point mass is considered to be the point i and is denoted as m_i. From the free-body diagrams of Figure 2.4(a) and 2.4(b) we see that the deflection, slope, and moment terms are equal on either side of the mass. This leads to,

$$\begin{aligned} w_i^R &= w_i^L \\ \varphi_i^R &= \varphi_i^L \\ M_{y_i}^R &= M_{y_i}^L \end{aligned} \tag{2.22}$$

and

$$\begin{aligned} v_i^R &= v_i^L \\ \vartheta_i^R &= \vartheta_i^L \\ M_{z_i}^R &= M_{z_i}^L \end{aligned} \tag{2.23}$$

To maintain the element in equilibrium the sum of forces in the vertical direction, that is the *xz*-plane, give

$$V_{z_i}^R = V_{z_i}^L - m_i \omega^2 w_i \tag{2.24}$$

while the sum of forces in the horizontal direction, the *xy*-plane, lead to

$$V_{y_i}^R = V_{y_i}^L - m_i \omega^2 v_i \tag{2.25}$$

Once again to formulate a matrix that relates the *state vector* on the left side of the mass, to the right side, namely $\{z\}_i^L$ to $\{z\}_i^R$, the Equations (2.22), (2.23), (2.24), and (2.25) are brought together in the matrix form as

$$\begin{Bmatrix} w \\ \psi \\ M_y \\ V_z \\ \hdashline v \\ \vartheta \\ M_z \\ V_y \end{Bmatrix}_i^R = \left[\begin{array}{cccc:cccc} 1 & 0 & 0 & 0 & 0 & 0 & 0 & 0 \\ 0 & 1 & 0 & 0 & 0 & 0 & 0 & 0 \\ 0 & 0 & 1 & 0 & 0 & 0 & 0 & 0 \\ -m\omega^2 & 0 & 0 & 1 & 0 & 0 & 0 & 0 \\ \hdashline 0 & 0 & 0 & 0 & 1 & 0 & 0 & 0 \\ 0 & 0 & 0 & 0 & 0 & 1 & 0 & 0 \\ 0 & 0 & 0 & 0 & 0 & 0 & 1 & 0 \\ 0 & 0 & 0 & 0 & -m\omega^2 & 0 & 0 & 1 \end{array}\right]_i \begin{Bmatrix} w \\ \psi \\ M_y \\ V_z \\ \hdashline v \\ \vartheta \\ M_z \\ V_y \end{Bmatrix}_i^L \tag{2.26}$$

This can be written as:

$$\{z\}_i^R = [P]_i \{z\}_i^L \tag{2.27}$$

where $[P]_i$ is known as the i^{th} *point transfer matrix*, or in short *point matrix*.

Global Transfer Matrix. With the smaller sections of a structure defined as either a *field* or a *point matrix* we now approach the handling of a more complex system. Figure 2.5 is an example of a part of a structure that has concentrated masses along the length of its massless shaft. The numbering convention shown in the diagram helps in the construction of the *global transfer matrix*. They are used in the numbering of *state vectors* and *field* and *point matrices*.

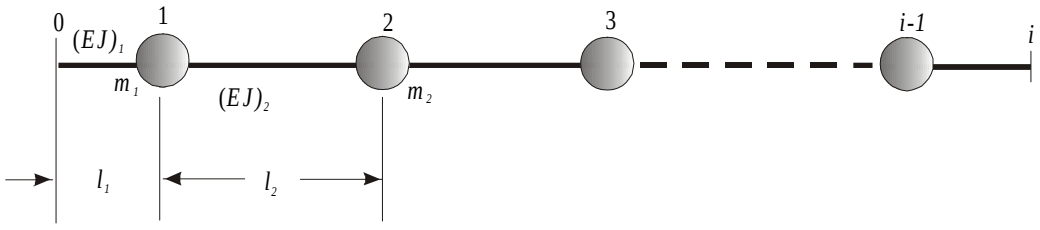

Figure 2.5: Beam with discrete masses, after Pestel and Leckie [8].

As a stepwise progress is made along the beam from left to right an element represented by either a *field*, $[F]$, or a *point matrix*, $[P]$, is encountered. The series of beam segments and lumped masses of Figure 2.5 are depicted in terms of *field* and *point matrices* in the figure shown below.

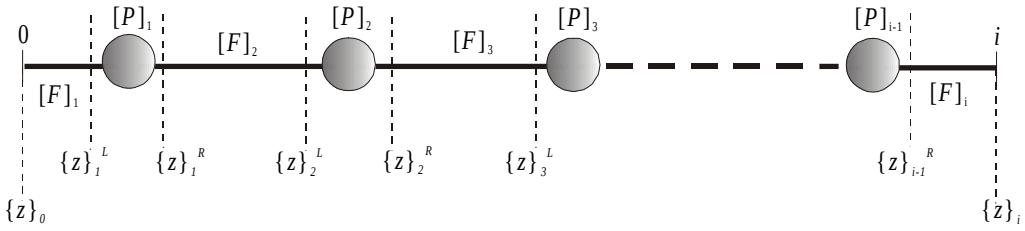

Figure 2.6: Beam with discrete masses, adapted from Pestel and Leckie [9].

Figure 2.6 helps to formulate the following relations between adjacent *state vectors*:

$$\begin{aligned}
\{z\}_1^L &= [F]_1\{z\}_0 \\
\{z\}_1^R &= [P]_1\{z\}_1^L \\
\{z\}_2^L &= [F]_2\{z\}_1^R \ \ldots \\
&\ldots \\
\ldots \{z\}_{i-1}^L &= [F]_{i-2}\{z\}_{i-2}^R \\
\{z\}_{i-1}^R &= [P]_{i-1}\{z\}_{i-1}^L \\
\{z\}_i &= [F]_i\{z\}_{i-1}^R
\end{aligned} \tag{2.28}$$

Substituting the first equation in the set above into the second, followed by the second into the third, and so on results in

$$\{z\}_i = [F]_i[P]_{i-1}[F]_{i-1}\ldots[P]_2[F]_2[P]_1[F]_1\{z\}_0 \tag{2.29}$$

Thus, the intermediate *state vectors* have been eliminated. Following the systematic multiplication of a *field* or *point matrix*, the *global transfer matrix*, written as $[U]$, is obtained,

$$\{z\}_i = [U]\{z\}_0 \tag{2.30}$$

The *global transfer matrix* contains a series of equations that relate the left end of the system to the right.

The following sections explain how to perform the free and forced vibration analyses of a system.

2.4 Free Vibration Analysis (Eigenvalue – Eigenvector Analysis)

Performing the free vibration analysis involves obtaining the system's natural frequencies (eigenvalue) and corresponding mode shapes (eigenvector). To illustrate the method of obtaining this information the system in Figure 2.5 is used. The algebraic matrix multiplication of *field* and *point matrices* was carried out to obtain the *global transfer matrix* $[U]$ of the model. Rewriting Equation (2.30) in terms of matrix elements u_{ij},

$$\begin{Bmatrix} w \\ \psi \\ M_y \\ V_z \\ \hdashline v \\ \vartheta \\ M_z \\ V_y \end{Bmatrix}_i = \left[\begin{array}{cccc:cccc} u_{11} & u_{12} & u_{13} & u_{14} & u_{15} & u_{16} & u_{17} & u_{18} \\ u_{21} & u_{22} & u_{23} & u_{24} & u_{25} & u_{26} & u_{27} & u_{28} \\ u_{31} & u_{32} & u_{33} & u_{34} & u_{35} & u_{36} & u_{37} & u_{38} \\ u_{41} & u_{42} & u_{43} & u_{44} & u_{45} & u_{46} & u_{47} & u_{48} \\ \hdashline u_{51} & u_{52} & u_{53} & u_{54} & u_{55} & u_{56} & u_{57} & u_{58} \\ u_{61} & u_{62} & u_{63} & u_{64} & u_{65} & u_{66} & u_{67} & u_{68} \\ u_{71} & u_{72} & u_{73} & u_{74} & u_{75} & u_{76} & u_{77} & u_{78} \\ u_{81} & u_{82} & u_{83} & u_{84} & u_{85} & u_{86} & u_{87} & u_{88} \end{array}\right]_i \begin{Bmatrix} w \\ \psi \\ M_y \\ V_z \\ \hdashline v \\ \vartheta \\ M_z \\ V_y \end{Bmatrix}_0 \tag{2.31}$$

In the equation above the coefficients u_{11} to u_{88} are known functions of the natural frequency ω_n. Note that some of the elements u_{ij} may be equal to zero.

Expanding the matrix Equation (2.31) gives

$$w_i = u_{11}w_0 + u_{12}\psi_0 + u_{13}M_{y_0} + u_{14}V_{z_0} + u_{15}v_0 + u_{16}\vartheta_0 + u_{17}M_{z_0} + u_{18}V_{y_0} \quad (2.32a)$$

$$\psi_i = u_{21}w_0 + u_{22}\psi_0 + u_{23}M_{y_0} + u_{24}V_{z_0} + u_{25}v_0 + u_{26}\vartheta_0 + u_{27}M_{z_0} + u_{28}V_{y_0} \quad (2.32b)$$

$$M_{y_i} = u_{31}w_0 + u_{32}\psi_0 + u_{33}M_{y_0} + u_{34}V_{z_0} + u_{35}v_0 + u_{36}\vartheta_0 + u_{37}M_{z_0} + u_{38}V_{y_0} \quad (2.32c)$$

$$V_{z_i} = u_{41}w_0 + u_{42}\psi_0 + u_{43}M_{y_0} + u_{44}V_{z_0} + u_{45}v_0 + u_{46}\vartheta_0 + u_{47}M_{z_0} + u_{48}V_{y_0} \quad (2.32d)$$

$$v_i = u_{51}w_0 + u_{52}\psi_0 + u_{53}M_{y_0} + u_{54}V_{z_0} + u_{55}v_0 + u_{56}\vartheta_0 + u_{57}M_{z_0} + u_{58}V_{y_0} \quad (2.32e)$$

$$\vartheta_i = u_{61}w_0 + u_{62}\psi_0 + u_{63}M_{y_0} + u_{64}V_{z_0} + u_{65}v_0 + u_{66}\vartheta_0 + u_{67}M_{z_0} + u_{68}V_{y_0} \quad (2.32f)$$

$$M_{z_i} = u_{71}w_0 + u_{72}\psi_0 + u_{73}M_{y_0} + u_{74}V_{z_0} + u_{75}v_0 + u_{76}\vartheta_0 + u_{77}M_{z_0} + u_{78}V_{y_0} \quad (2.32g)$$

$$V_{y_i} = u_{81}w_0 + u_{82}\psi_0 + u_{83}M_{y_0} + u_{84}V_{z_0} + u_{85}v_0 + u_{86}\vartheta_0 + u_{87}M_{z_0} + u_{88}V_{y_0} \quad (2.32h)$$

The systems boundary conditions are now applied. Below are some of the basic cases of boundary conditions and how they affect the parameters of the *state vector*.

Table 2.1: Beam Boundary conditions

Pinned	Fixed	Free	Guided
$w = 0$	$w = 0$	$M_y = 0$	$\psi = 0$
$v = 0$	$v = 0$	$M_z = 0$	$\vartheta = 0$
$M_y = 0$	$\psi = 0$	$V_z = 0$	$V_z = 0$
$M_z = 0$	$\vartheta = 0$	$V_y = 0$	$V_y = 0$

If the shaft of Figure 2.5 was simply supported at both ends, the boundary condition values at the right end of the system are,

$$w_i = 0 \qquad M_{y_i} = 0$$
$$v_i = 0 \qquad M_{z_i} = 0$$

and for the left end are,

$$w_0 = 0 \qquad M_{y_0} = 0$$
$$v_0 = 0 \qquad M_{z_0} = 0.$$

Substituting these boundary conditions into Equations (2.32a), (2.32c), (2.32e), and (2.32g) give,

$$0 = u_{12}\psi_0 + u_{14}V_{z_0} + u_{16}\vartheta_0 + u_{18}V_{y_0}$$
$$0 = u_{32}\psi_0 + u_{34}V_{z_0} + u_{36}\vartheta_0 + u_{38}V_{y_0}$$
$$0 = u_{52}\psi_0 + u_{54}V_{z_0} + u_{56}\vartheta_0 + u_{58}V_{y_0}$$
$$0 = u_{72}\psi_0 + u_{74}V_{z_0} + u_{76}\vartheta_0 + u_{78}V_{y_0}$$

For the non-trivial solution the determinant of the coefficient of these equations must be zero [10], that is

$$\begin{vmatrix} u_{12} & u_{14} & u_{16} & u_{18} \\ u_{32} & u_{34} & u_{36} & u_{38} \\ u_{52} & u_{54} & u_{56} & u_{58} \\ u_{72} & u_{74} & u_{76} & u_{78} \end{vmatrix} = 0 \tag{2.33}$$

The determinant is referred to as the *characteristic determinant* as it gives the characteristic equation which when solved for its zeroes gives the natural frequencies, ω_{n_i}, of the system. Discussion on how to obtain the corresponding mode shape of the natural frequencies has been deferred until Chapter 3. This is because certain mathematical issues concerning the computation of the mode shapes have risen.

2.5 Forced Vibration Analysis

From the theory of vibrations a system subjected to the steady-state condition of a harmonic excitation will cause the system to vibrate in its steady-state [11]. If the forcing term has a circular frequency of Ω the linear system will vibrate with the same circular frequency. This enables the transfer matrix method to be extended to solve the steady-state forced vibration case where the forcing term has a circular frequency of Ω and the static case where the circular frequency Ω is equal to zero.

To account for the forcing term, the *field or point matrix* equation is expanded to include the identity 1≡1 row so that an additional column can be had. The forcing term is inserted into the additional column that results in the partitioned *field* or *point matrix*.

The *state vector,* $\{z\}_i$, with the additional row is referred to as the *extended state vector*. The newly partitioned *field* and *point matrices* are known as the *extended field* and *point matrices*. These terms and the analysis procedure are more clearly illustrated in the example that follows.

A simple cantilever beam is subjected to a concentrated force, *P*, acting at an angle, θ, measured counterclockwise from the positive *y*-axis (Figure 2.6).

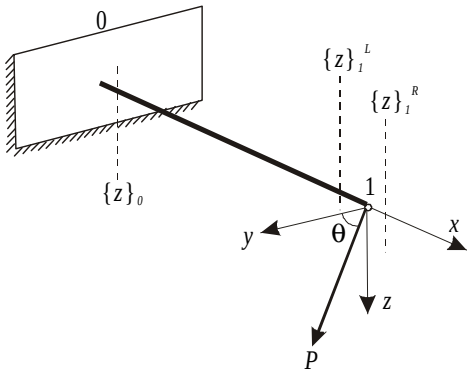

Figure 2.6: Cantilever subjected to a force P at an angle θ

To begin with the force is resolved into two perpendicular components, namely into its y (P_y) and z-direction (P_z) components where,

$$P_y = P\cos\theta \tag{2.34}$$

and

$$P_z = P\sin\theta. \tag{2.35}$$

As seen in Figure 2.7, the free body diagram of the force acting at point 1, in both the xz and xy-plane, helps to determine the equations for the matrix equation.

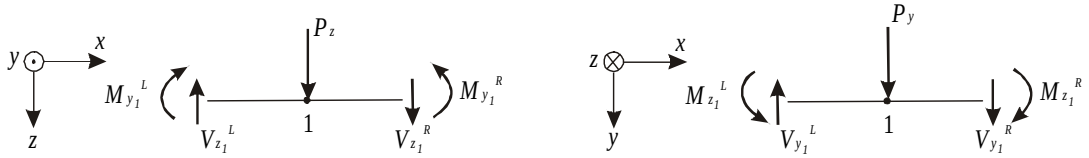

Figure 2.7: (a) External force at point 1 in xz-plane; (b) External force acting at point 1 in xy-plane, adapted from Beam V Documentation [12].

The displacements and moments remain unchanged but a discontinuity in the shear force due the external force gives rise to:

$$V_{z_1}^R = V_{z_1}^L - P_z \tag{2.36}$$

in the xz-plane and

$$V_{y_1}^R = V_{y_1}^L - P_y \tag{2.37}$$

in the *xy*-plane.

Compiling the equations into the matrix form leads to the partitioned *extended point matrix* resembling

$$\begin{Bmatrix} w \\ \psi \\ M_y \\ V_z \\ \hdashline v \\ \vartheta \\ M_z \\ V_y \\ \hdashline 1 \end{Bmatrix}_1^R = \left[\begin{array}{cccc:cccc:c} 1 & 0 & 0 & 0 & 0 & 0 & 0 & 0 & 0 \\ 0 & 1 & 0 & 0 & 0 & 0 & 0 & 0 & 0 \\ 0 & 0 & 1 & 0 & 0 & 0 & 0 & 0 & 0 \\ 0 & 0 & 0 & 1 & 0 & 0 & 0 & 0 & -P_z \\ \hdashline 0 & 0 & 0 & 0 & 1 & 0 & 0 & 0 & 0 \\ 0 & 0 & 0 & 0 & 0 & 1 & 0 & 0 & 0 \\ 0 & 0 & 0 & 0 & 0 & 0 & 1 & 0 & 0 \\ 0 & 0 & 0 & 0 & 0 & 0 & 0 & 1 & -P_y \\ \hdashline 0 & 0 & 0 & 0 & 0 & 0 & 0 & 0 & 1 \end{array}\right]_1 . \begin{Bmatrix} w \\ \psi \\ M_y \\ V_z \\ \hdashline v \\ \vartheta \\ M_z \\ V_y \\ \hdashline 1 \end{Bmatrix}_1^L \tag{2.38}$$

To solve the system of Figure 2.6, the method of obtaining the *global transfer matrix* explained in Section 2.3 is utilized. Starting from the left end and working toward the right, the massless shaft is the first element to be encountered. This is expressed as an *extended field matrix* and in symbolic form is,

$$\{z\}_1^L = [F_{Shaft}]_1 \{z\}_0 \tag{2.39}$$

At point 1 the concentrated force is encountered and the *extended point matrix* equation relating the *state vectors* on either sides is

$$\{z\}_1^R = [P_{Force}]_1 \{z\}_1^L \tag{2.40}$$

Combining the equations above, the *state vector* left of the massless shaft is related to the *state vector* on the right side of the applied force by

$$\{z\}_1^R = [P_{Force}]_1 [F_{Shaft}]_1 \{z\}_0 \tag{2.41}$$

and in terms of the system's properties looks like

$$\begin{Bmatrix} w \\ \psi \\ M_y \\ V_z \\ \hdashline v \\ \vartheta \\ M_z \\ V_y \\ \hdashline 1 \end{Bmatrix}_1^R = \left[\begin{array}{cccc:cccc:c} 1 & 0 & 0 & 0 & 0 & 0 & 0 & 0 & 0 \\ 0 & 1 & 0 & 0 & 0 & 0 & 0 & 0 & 0 \\ 0 & 0 & 1 & 0 & 0 & 0 & 0 & 0 & 0 \\ 0 & 0 & 0 & 1 & 0 & 0 & 0 & 0 & -P_z \\ \hdashline 0 & 0 & 0 & 0 & 1 & 0 & 0 & 0 & 0 \\ 0 & 0 & 0 & 0 & 0 & 1 & 0 & 0 & 0 \\ 0 & 0 & 0 & 0 & 0 & 0 & 1 & 0 & 0 \\ 0 & 0 & 0 & 0 & 0 & 0 & 0 & 1 & -P_y \\ \hdashline 0 & 0 & 0 & 0 & 0 & 0 & 0 & 0 & 1 \end{array}\right]_1 \left[\begin{array}{cccc:cccc:c} 1 & -l & -\frac{l^2}{2EI_y} & -\frac{l^3}{6EI_y} & 0 & 0 & 0 & 0 & 0 \\ 0 & 1 & \frac{l}{EI_y} & \frac{l^2}{2EI_y} & 0 & 0 & 0 & 0 & 0 \\ 0 & 0 & 1 & l & 0 & 0 & 0 & 0 & 0 \\ 0 & 0 & 0 & 1 & 0 & 0 & 0 & 0 & 0 \\ \hdashline 0 & 0 & 0 & 0 & 1 & l & \frac{l^2}{2EI_z} & \frac{l^3}{6EI_z} & 0 \\ 0 & 0 & 0 & 0 & 0 & 1 & \frac{l}{EI_z} & -\frac{l^2}{2EI_z} & 0 \\ 0 & 0 & 0 & 0 & 0 & 0 & 1 & -l & 0 \\ 0 & 0 & 0 & 0 & 0 & 0 & 0 & 1 & 0 \\ \hdashline 0 & 0 & 0 & 0 & 0 & 0 & 0 & 0 & 1 \end{array}\right]_1 \cdot \begin{Bmatrix} w \\ \psi \\ M_y \\ V_z \\ \hdashline v \\ \vartheta \\ M_z \\ V_y \\ \hdashline 1 \end{Bmatrix}_0 \quad (2.42)$$

After performing the matrix multiplication the equation simplifies to

$$\begin{Bmatrix} w \\ \psi \\ M_y \\ V_z \\ \hdashline v \\ \vartheta \\ M_z \\ V_y \\ \hdashline 1 \end{Bmatrix}_1^R = \left[\begin{array}{cccc:cccc:c} 1 & -l & -\frac{l^2}{2EI_y} & -\frac{l^3}{6EI_y} & 0 & 0 & 0 & 0 & 0 \\ 0 & 1 & \frac{l}{EI_y} & \frac{l^2}{2EI_y} & 0 & 0 & 0 & 0 & 0 \\ 0 & 0 & 1 & l & 0 & 0 & 0 & 0 & 0 \\ 0 & 0 & 0 & 1 & 0 & 0 & 0 & 0 & -P_z \\ \hdashline 0 & 0 & 0 & 0 & 1 & l & \frac{l^2}{2EI_z} & \frac{l^3}{6EI_z} & 0 \\ 0 & 0 & 0 & 0 & 0 & 1 & \frac{l}{EI_z} & -\frac{l^2}{2EI_z} & 0 \\ 0 & 0 & 0 & 0 & 0 & 0 & 1 & -l & 0 \\ 0 & 0 & 0 & 0 & 0 & 0 & 0 & 1 & -P_y \\ \hdashline 0 & 0 & 0 & 0 & 0 & 0 & 0 & 0 & 1 \end{array}\right]_1 \cdot \begin{Bmatrix} w \\ \psi \\ M_y \\ V_z \\ \hdashline v \\ \vartheta \\ M_z \\ V_y \\ \hdashline 1 \end{Bmatrix}_0 \quad (2.43)$$

The left side boundary condition of the system is fixed and the right is free as shown in Figure 2.6. On making the boundary condition substitutions $w_0 = 0$, $\psi_0 = 0$, $v_0 = 0$, and

ϑ_0 =0 for the fixed end and $M_{y_1}^R = 0$, $M_{z_1}^R = 0$, $V_{z_1}^R = 0$, and $V_{y_1}^R = 0$ for the free end, the resulting equations are:

(in the *xy*-plane)

$$w_1^R = -\frac{M_{y_0} l^2}{2EI_y} - \frac{V_{z_0} l^3}{6EI_y} \tag{2.44a}$$

$$\psi_1^R = \frac{M_{y_0} l}{EI_y} + \frac{V_{z_0} l^2}{2EI_y} \tag{2.44b}$$

$$0 = M_{y_0} + V_{z_0} l \tag{2.44c}$$

$$0 = V_{z_0} - P_z \tag{2.44d}$$

and

(in the yz-plane)

$$v_1^R = \frac{M_{z_0} l^2}{2EI_z} + \frac{V_{y_0} l^3}{6EI_z} \tag{2.44e}$$

$$\vartheta_1^R = \frac{M_{z_0} l}{EI_z} - \frac{V_{y_0} l^2}{2EI_z} \tag{2.44f}$$

$$0 = M_{z_0} - V_{y_0} l \tag{2.44g}$$

$$0 = V_{y_0} - P_y \tag{2.44h}$$

From Equation (2.44c) we obtain V_{z_0} and using this in Equation (2.44d) we get the value for M_{y_0}.

$$V_{z_0} = P_z \tag{2.45a}$$

$$M_{y_0} = -P_z l \tag{2.45b}$$

Similarly Equation (2.44g) gives us V_{y_0} with which we obtain M_{z_0} from Equation (2.44h).

$$V_{y_0} = P_y \tag{2.45c}$$

$$M_{z_0} = P_y l \tag{2.45d}$$

The initial *state vector* located at the fixed end of the cantilever, as shown in Figure 2.6, will be:

$$\{z\}_0 = \begin{Bmatrix} 0 \\ 0 \\ -P_z l \\ P_z \\ \hdashline 0 \\ 0 \\ P_y l \\ P_y \\ \hdashline 1 \end{Bmatrix} \tag{2.46}$$

The Equation (2.46) along with increasing values for the length parameter, l, in Equation (2.43) can be used in obtaining the intermediate *state vector* parameters of deflection, slope, moment, and shear at points along the length of the structure.

Chapter 3

Mathematical Issues

In writing the program to analyze systems in two dimensions using the transfer matrix method some mathematical difficulties arose. The problems and solutions to overcome them are addressed in this chapter.

The manner in which the computer code handles system models input by users is by initially separating the input model into the two possible categories of systems namely a coupled or uncoupled system. Section 3.1 outlines the definition of the two systems and the effect each of them has on the type of matrices that arise when using the transfer matrix method. Section 3.3 and 3.4 address the mathematics of obtaining corresponding mode shapes of natural frequencies for the coupled and uncoupled system.

3.1 Coupled and Uncoupled Systems

Depending on the type of system that is being analyzed the *global transfer matrix* (Equation (2.31)) falls into two basic arrangements. It is necessary to differentiate between the two systems as each one leads to a unique element arrangement within the *global transfer matrix* that have to be dealt with differently. The two types of systems and their arrangements when assembled into a matrix are:

3.1.1 The Uncoupled System

The *global transfer matrix* of a system, Equation (2.31), is modified to resemble the spread of an uncoupled system:

$$\begin{Bmatrix} w \\ \psi \\ M_y \\ V_z \\ \hdashline v \\ \vartheta \\ M_z \\ V_y \end{Bmatrix}_i = \left[\begin{array}{cccc:cccc} u_{11} & u_{12} & u_{13} & u_{14} & 0 & 0 & 0 & 0 \\ u_{21} & u_{22} & u_{23} & u_{24} & 0 & 0 & 0 & 0 \\ u_{31} & u_{32} & u_{33} & u_{34} & 0 & 0 & 0 & 0 \\ u_{41} & u_{42} & u_{43} & u_{44} & 0 & 0 & 0 & 0 \\ \hdashline 0 & 0 & 0 & 0 & u_{55} & u_{56} & u_{57} & u_{58} \\ 0 & 0 & 0 & 0 & u_{65} & u_{66} & u_{67} & u_{68} \\ 0 & 0 & 0 & 0 & u_{75} & u_{76} & u_{77} & u_{78} \\ 0 & 0 & 0 & 0 & u_{85} & u_{86} & u_{87} & u_{88} \end{array}\right]_i \cdot \begin{Bmatrix} w \\ \psi \\ M_y \\ V_z \\ \hdashline v \\ \vartheta \\ M_z \\ V_y \end{Bmatrix}_0 \tag{3.1}$$

The system represented by this matrix equation can be resolved into two perpendicular directions of motions independent of each other. In other words, motion in the horizontal direction has no bearing or effect on the vertical direction and vice versa. This uncoupled *global transfer matrix* results in a *characteristic determinant* arrangement,

$$\begin{vmatrix} x & x & 0 & 0 \\ x & x & 0 & 0 \\ 0 & 0 & x & x \\ 0 & 0 & x & x \end{vmatrix} \tag{3.2}$$

3.1.2 The Coupled System

The *global transfer matrix* of a coupled system could have several different types of elemental spreads. It is necessary, however, that Equation (2.31) contain at least one non-
zero element in the upper right or lower left half.

Unlike the uncoupled system, the coupling represents a system in which the forces or displacements occurring in one direction affect the orthogonal direction motions and/or forces. The resultant *characteristic determinant* would also be coupled. Equation (3.3) shows the direct terms in bold face type and the cross-coupled terms in regular face type.

$$\begin{vmatrix} \mathbf{x} & \mathbf{x} & x & x \\ \mathbf{x} & \mathbf{x} & x & x \\ x & x & \mathbf{x} & \mathbf{x} \\ x & x & \mathbf{x} & \mathbf{x} \end{vmatrix} \tag{3.3}$$

3.2 Double Eigenvalue of an Uncoupled System

3.2.1 Plot of Determinant versus Frequency

In Section 2.4 of Chapter 2, the method of obtaining the natural frequencies, ωn_i, in the free vibration analysis of a system was discussed. To recap, it involves obtaining the *global transfer matrix* of the system, substituting the boundary conditions thereby reducing the matrix to a 4 by 4, and computing the determinant (Equation (2.26)) of the resulting matrix. The determinant results in the *characteristic equation*, containing ωn_i^2 to the n^{th} power, the roots of which are the natural frequencies of the system.

As complicated systems are encountered the *characteristic equation* becomes more complex containing the frequency variable, ωn_i^2, to a high degree. For instance, if Figure 2.5 was comprised of six discrete masses the resulting *characteristic equation* would be of the sixth degree in ωn_i^2. This would, indeed, make solving the equation tedious and difficult, if done by hand.

To combat this difficulty the following procedure was adopted from Pestel and Leckie [13] and implemented in the earlier version of this computer code (BEAM 9) to obtain the values for the natural frequencies. Increasing values of frequencies are substituted into the *characteristic equation* and the corresponding determinant values are obtained. The result is a plot of the determinant versus frequency and resembles,

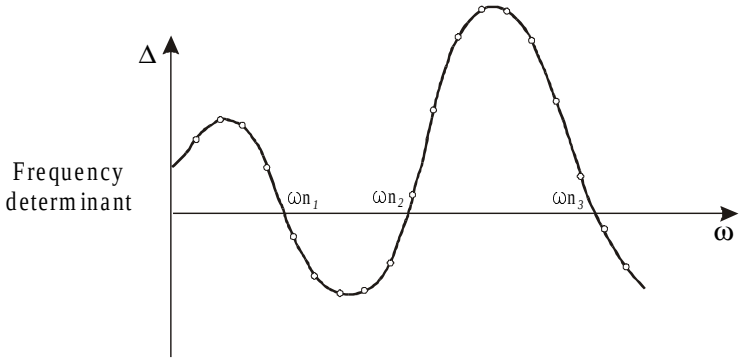

Figure 3.1: Plot of frequency determinant versus frequency, adapted from Pestel and Leckie [14].

The frequencies at which the determinant is zero, as indicated on the plot above, are the natural frequencies, ωn_i, of the system.

To visually determine an accurate root value from the determinant versus frequency plot, an upper and lower bound that encompasses the natural frequency is first obtained followed by using the false position method to find the root. The bounds around the natural frequency are obtained as a result of a change in sign that occurs as the determinant crosses the zero value.

3.2.2 Obtaining the uncoupled double eigenvalue

The visual method of obtaining the natural frequencies as described above runs into difficulties when faced with solving a particular instance of an uncoupled *characteristic determinant*.

The method can handle obtaining the natural frequencies of a system provided the natural frequency in the horizontal direction does not coincide with the vertical direction. When the natural frequency in each of the two perpendicular directions coincides, an uncoupled double eigenvalue problem is encountered. The *characteristic determinant* approaches zero but does not cross the zero determinant line on the plot. Not crossing

the zero determinant line causes a problem with the code since the bounds on the frequency range trapping the eigenvalue can not be obtained. The sign change of the determinant is used to establish this range. Since there is no sign change there is no range. A general plot for double eigenvalues at ωn_1 and ωn_2 as well as ωn_4 and ωn_5 would look like Figure 3.2.

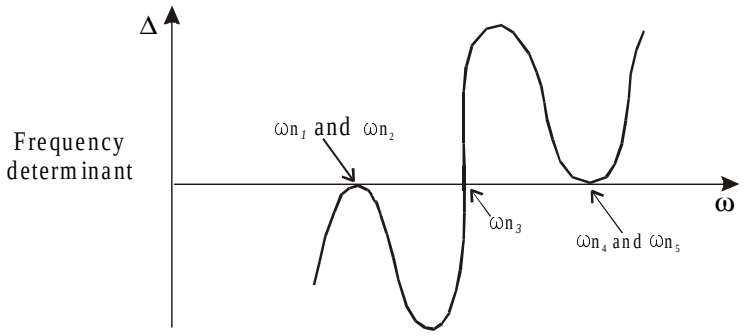

Figure 3.2: Plot of frequency determinant versus frequency.

Depending on whether the curve points are made up of positive or negative determinant values, the natural frequency is at the minimum or maximum point of the curve section that touches the zero determinant line.

To obtain the natural frequency values of the special uncoupled case the steps below have been implemented in the 2DBEAM code.

Step 1: Obtaining bounds around the double eigenvalue:

A variation in method exists in obtaining the bounds around a double eigenvalue depending on whether a curve lies on the positive side or on the negative side of the zero determinant line. The 2DBEAM code, therefore, maintains a variable to constantly note the sign of the curve's determinant co-ordinate.

The bounds of double eigenvalue occurring on the negative determinant side, as in the case of ωn_1 and ωn_2 in Figure 3.2, are obtained when the positive slope to the left of the eigenvalue changes to a negative slope without crossing the zero determinant mark. If

the curve crosses over the zero marker, as is the case for ωn_3 in Figure 3.2, thereby changing its determinant sign then the earlier described false position method is carried out to obtain an accurate eigenvalue.

When a double eigenvalue such as ωn_4 and ωn_5 in Figure 3.2 occurs, the curve section lies on the positive determinant side. The bounds are obtained when the negative slope changes to a positive slope while only touching the zero determinant line.

In this manner the code in 2DBEAM determines the left and right bracketing frequencies that surround a double eigenvalue.

Step 2: Obtaining the double eigenvalue:

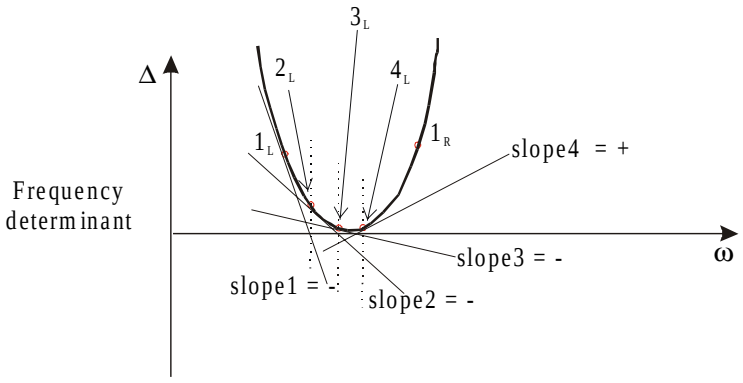

Figure 3.3: The modified false position method.

A modified false position method is used to decrease the interval between the initial bounding frequencies and locate a more accurate estimate of the double eigenvalue. Use Figure 3.3 in conjunction with the explanation of the method given below.

The two initial bounding frequencies from *Step 1* are 1_L on the left and 1_R on the right. The method begins by determining the slope of the left bracketing frequency point (1_L). The sign of this slope (slope1) is recorded. The next point on the curve to be evaluated is

2_L. The frequency of this value is the point where the slope1 line met the zero determinant line. The slope at 2_L is now determined and its sign recorded.
This process is repeated until a change in sign of the slope occurs, indicating that the double eigenvalue point on the curve section has been passed. The new left frequency bracket now becomes the last point (3_L) before the changing of the slope signs.

In the same manner, the double eigenvalue is converged on from the initial right bounding frequency (1_R). Again, when the slope of the curve changes sign, the last point before this occurrence is recorded. This is the new right frequency bracket.

A better estimate of the double eigenvalue is then evaluated by interpolating between the slope of the left and right closer frequency bounds. Since there is a sign change between the slopes of the bracketing frequencies, the frequency at which the curve's slope equals zero is calculated thereby obtaining a more accurate double eigenvalue.

3.3 Mode Shapes of Uncoupled Systems

Having obtained the natural frequencies of a system the corresponding mode shapes remain to be computed. In an uncoupled system when the *characteristic determinant* equals zero, the direction in which the natural frequency occurred needs to be determined in order to calculate the correct mode shape. The method used to determine the direction follows.

3.3.1 Computing Mode Shapes of Uncoupled Systems

Consider the uncoupled system of a massless beam of length *l* with a concentrated end mass, fixed at one end and free at the other (Figure 3.4).

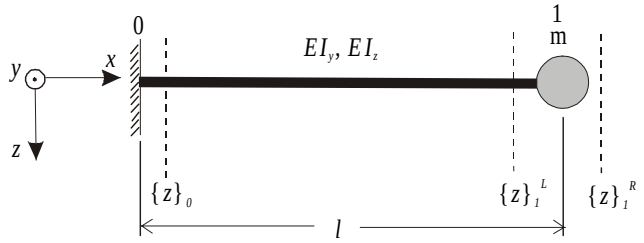

Figure 3.4: Cantilever with concentrated end mass, adapted from Pestel and Leckie [15].

It is assumed that the area moments of inertia of this beam about the *y* and *z*-axis are not equal and hence the flexural stiffness $EI_y \neq EI_z$. The uncoupled *global transfer matrix* is first built using the relation

$$\{z\}_1^R = [P_{Mass}]_1 [F_{Shaft}]_1 \{z\}_0^R \tag{3.4}$$

Equation (3.4) results in,

$$\begin{Bmatrix} w \\ \psi \\ M_y \\ V_z \\ \hdashline v \\ \vartheta \\ M_z \\ V_y \end{Bmatrix}_1^R = \left[\begin{array}{cccc:cccc} 1 & -l & -\frac{l^2}{2EI_y} & -\frac{l^3}{6EI_y} & 0 & 0 & 0 & 0 \\ 0 & 1 & \frac{l}{EI_y} & \frac{l^2}{2EI_y} & 0 & 0 & 0 & 0 \\ 0 & 0 & 1 & l & 0 & 0 & 0 & 0 \\ -m\omega^2 & m\omega^2 l & \frac{m\omega^2 l^2}{2EI_y} & \left(1+\frac{m\omega^2 l^3}{6EI_y}\right) & 0 & 0 & 0 & 0 \\ \hdashline 0 & 0 & 0 & 0 & 1 & l & \frac{l^2}{2EI_z} & -\frac{l^3}{6EI_z} \\ 0 & 0 & 0 & 0 & 0 & 1 & \frac{l}{EI_z} & -\frac{l^2}{2EI_z} \\ 0 & 0 & 0 & 0 & 0 & 0 & 1 & -l \\ 0 & 0 & 0 & 0 & -m\omega^2 & -m\omega^2 l & -\frac{m\omega^2 l^2}{2EI_z} & \left(1+\frac{m\omega^2 l^3}{6EI_z}\right) \end{array}\right] \begin{Bmatrix} w \\ \psi \\ M_y \\ V_z \\ \hdashline v \\ \vartheta \\ M_z \\ V_y \end{Bmatrix}_0^R \tag{3.5}$$

The boundary conditions for the left fixed end of system leads to

$$w_0 = 0 \qquad \psi_0 = 0$$
$$v_0 = 0 \qquad \vartheta_0 = 0 \tag{3.6}$$

and for the right free end gives

$$V_{z_1}^R = 0 \qquad M_{y_1}^R = 0$$
$$V_{y_1}^R = 0 \qquad M_{z_1}^R = 0\,. \tag{3.7}$$

On substituting the above boundary conditions into Equation (3.5),

$$\begin{Bmatrix} w \\ \psi \\ 0 \\ 0 \\ \cdots \\ v \\ \vartheta \\ 0 \\ 0 \end{Bmatrix}^R_1 = \left[\begin{array}{cc:cc} -\frac{l^2}{2EI_y} & -\frac{l^3}{6EI_y} & 0 & 0 \\ \frac{l}{EI_y} & \frac{l^2}{2EI_y} & 0 & 0 \\ 1 & l & 0 & 0 \\ \frac{m\omega^2 l^2}{2EI_y} & 1+\frac{m\omega^2 l^3}{6EI_y} & 0 & 0 \\ \hdashline 0 & 0 & \frac{l^2}{2EI_z} & -\frac{l^3}{6EI_z} \\ 0 & 0 & \frac{l}{EI_z} & -\frac{l^2}{2EI_z} \\ 0 & 0 & 1 & -l \\ 0 & 0 & -\frac{m\omega^2 l^2}{2EI_z} & 1+\frac{m\omega^2 l^3}{6EI_z} \end{array}\right] \cdot \begin{Bmatrix} M_y \\ V_z \\ \cdots \\ M_z \\ V_y \end{Bmatrix}^R_0 \tag{3.8}$$

Extracting the equations whose right boundary conditions are known yield,

$$0 = M_{y_0}^R + lV_{z_0}^R \tag{3.9a}$$

$$0 = \frac{m\omega^2 l^2}{2EI_y} M_{y_0}^R + \left(1+\frac{m\omega^2 l^3}{6EI_y}\right) V_{z_0}^R \tag{3.9b}$$

$$0 = M_{z_0}^R - lV_{y_0}^R \tag{3.10a}$$

$$0 = -\frac{m\omega^2 l^2}{2EI_z} M_{y_0}^R + \left(1 + \frac{m\omega^2 l^3}{6EI_z}\right) V_{z_0}^R \tag{3.10b}$$

Re-arranging Equation (3.9a) and Equation (3.10a),

$$V_{z_0}^R = -\left(\frac{1}{l}\right) M_{y_0}^R \tag{3.11}$$

$$V_{y_0}^R = \left(\frac{1}{l}\right) M_{z_0}^R \tag{3.12}$$

Rewriting the internal shear components in terms of M_{y_0} and M_{z_0}, still leaves the moment values unknown. As the mode shape is a scaled function the value of unity for the moments may be assumed temporarily. Substituting this unity value into Equations (3.11) and (3.12), and inserting the equations into the right-hand column vector of Equation (3.8) gives the result,

$$z_1^R = \left[\begin{array}{cc:cc} -\frac{l^2}{2EI_y} & -\frac{l^3}{6EI_y} & 0 & 0 \\ \frac{l}{EI_y} & \frac{l^2}{2EI_y} & 0 & 0 \\ 1 & l & 0 & 0 \\ \frac{m\omega^2 l^2}{2EI_y} & 1+\frac{m\omega^2 l^3}{6EI_y} & 0 & 0 \\ \hdashline 0 & 0 & \frac{l^2}{2EI_z} & -\frac{l^3}{6EI_z} \\ 0 & 0 & \frac{l}{EI_z} & -\frac{l^2}{2EI_z} \\ 0 & 0 & 1 & -l \\ 0 & 0 & -\frac{m\omega^2 l^2}{2EI_z} & 1+\frac{m\omega^2 l^3}{6EI_z} \end{array}\right] \cdot \left\{\begin{array}{c} 1 \\ -1/l \\ \hdashline 1 \\ 1/l \end{array}\right\}_0^R \tag{3.13}$$

This result is used to calculate the intermediate *state vectors* that are required to obtain the mode shape over the entire length of the structure.

3.3.2 Determining Directions of Mode Shapes

As mentioned in the opening paragraph of Section 3.3, the direction or directions in which the natural frequency has occurred needs to be determined in order to obtain the correct plane of the resulting mode shape. In other words, if the natural frequency occurred due to vibration in the vertical direction then the mode shape values or image must reflect the change of the structure in the vertical direction leaving the shape in the horizontal plane unchanged (zero).

To illustrate the procedure adopted to identify the correct direction of the natural frequency, the example system of Figure 3.4 is used. To simplify this illustration further, the following parameter values are assumed:

Length, $l = 1$
Modulus of Elasticity, $E = 1$
Mass, $m = 1$ (3.14)
Moment of Inertia about y-axis, $I_y = 2$
and Moment of Inertia about z-axis, $I_z = 3$.

As explained in Chapter 2, Section 2.4 (Free Vibration Analysis), the eigenvalues of the system cause the *characteristic determinant* to equate to zero. The uncoupled *characteristic determinant* in this case, obtained from Equations (3.9a), (3.9b), (3.10a), and (3.10b), is:

$$\begin{vmatrix} 1 & l & 0 & 0 \\ \dfrac{m\omega^2 l^2}{2EI_y} & 1+\dfrac{m\omega^2 l^3}{6EI_y} & 0 & 0 \\ 0 & 0 & 1 & -l \\ 0 & 0 & -\dfrac{m\omega^2 l^2}{2EI_z} & 1+\dfrac{m\omega^2 l^3}{6EI_z} \end{vmatrix} = 0 \qquad (3.15)$$

By hand we can calculate that the eigenvalue, $\omega_n = 3$, occurs causing the Equation (3.15) to equal zero. A closer inspection of Equation (3.15) helps us identify that this natural frequency occurred in the *xy*-plane (horizontal plane), in other words, the determinant in Equation (3.15) equaled zero as a result of the lower right quarter of the determinant becoming zero.

The code, however, is not able to discern that the determinant of the equations in the horizontal plane caused the *characteristic determinant* to become zero. The procedure it uses to obtain this information begins by the assumption that for all cases of an uncoupled system, a double eigenvalue has occurred. The appropriate numerical substitutions for Equation (3.13) are made followed by a matrix multiplication to obtain the right-end *state vector*, z_1^R.

$$z_1^R = \left[\begin{array}{cc:cc} -1/4 & -1/12 & 0 & 0 \\ 1/2 & 1/4 & 0 & 0 \\ 1 & 1 & 0 & 0 \\ 2\,1/4 & 1\,3/4 & 0 & 0 \\ \hdashline 0 & 0 & 1/6 & -1/18 \\ 0 & 0 & 1/3 & -1/6 \\ 0 & 0 & 1 & -1 \\ 0 & 0 & -1\,1/2 & 1\,1/2 \end{array}\right] \cdot \left\{\begin{array}{c} 1 \\ -1 \\ \hdashline 1 \\ 1 \end{array}\right\}_0^R$$

$$z_1^R = \left\{\begin{array}{c} w \\ \psi \\ M_y \\ V_z \\ \hdashline v \\ \vartheta \\ M_z \\ V_y \end{array}\right\}_1^R = \left\{\begin{array}{c} -1/6 \\ 1/4 \\ 0 \\ 1/2 \\ \hdashline 1/9 \\ 1/6 \\ 0 \\ 0 \end{array}\right\}_1^R \qquad (3.16)$$

From the *state vector* that results (Equation (3.16)), the code determines which of the right-end boundary conditions match those originally input by the user of the program (Equation (3.7)). From Equation (3.16) it is evident that the boundary conditions in the *xy*-plane, namely $M_{z_1}^R$ and $V_{y_1}^R$, are the ones that are satisfied.

Using this method, the computer code correctly identified that the eigenvalue occurred in the horizontal direction. It now returns to Equation (3.13) and sets the vertical plane components of initial *state vector*, z_0^R, to zero and allows the mode shape of the horizontal plane to be evaluated.

For cases where an uncoupled double eigenvalue results, the components of the initial *state vector* are not modified and the mode shapes for both the horizontal and vertical planes are determined.

3.4 Mode Shapes of Coupled Systems

A different mathematical approach is utilized to compute the mode shapes of coupled systems. This section outlines the procedure used to make this computation which has been implemented in the 2DBEAM program.

For a coupled system such as a simple rotor mounted on fluid film bearings, the cross-coupling coefficients arise due to the bearings having stiffness coefficients K_{ij}, where i represents the direction of force and j represents the direction of displacement [16]. These stiffnesses are in addition to direct stiffnesses of K_{ii} and K_{jj}. A more detailed look at this *point transfer matrix* can be found in Appendix A.

To tackle such coupled systems the following procedure has been adopted. With elements giving rise to cross coupling in the matrices, the *global transfer matrix* (Equation 2.31) that results will also be coupled. The boundary condition of the rotor

problem on both the left and right is free. Making these boundary equation substitutions in the *global transfer matrix* reduces the matrix to,

$$\begin{Bmatrix} w \\ \psi \\ 0 \\ 0 \\ \cdots \\ v \\ \vartheta \\ 0 \\ 0 \end{Bmatrix}_i^R = \left[\begin{array}{cc:cc} u_{13} & u_{14} & u_{17} & u_{18} \\ u_{23} & u_{24} & u_{27} & u_{28} \\ u_{33} & u_{34} & u_{37} & u_{38} \\ u_{43} & u_{44} & u_{47} & u_{48} \\ \hdashline u_{53} & u_{54} & u_{57} & u_{58} \\ u_{63} & u_{64} & u_{67} & u_{68} \\ u_{73} & u_{74} & u_{77} & u_{78} \\ u_{83} & u_{84} & u_{87} & u_{88} \end{array}\right]_i . \begin{Bmatrix} w \\ \psi \\ \cdots \\ v \\ \vartheta \end{Bmatrix}_0^L \tag{3.17}$$

where the elements $u_{17} - u_{47}$, $u_{18} - u_{48}$, $u_{53} - u_{83}$, and $u_{54} - u_{84}$ are the cross coupling coeffiecients.

As before, the equations whose right-boundary conditions are know are extracted to give the following four equations:

$$u_{33}w_0^L + u_{34}\psi_0^L + u_{37}v_0^L + u_{38}\vartheta_0^L = 0 \tag{3.18a}$$

$$u_{43}w_0^L + u_{44}\psi_0^L + u_{47}v_0^L + u_{48}\vartheta_0^L = 0 \tag{3.18b}$$

$$u_{73}w_0^L + u_{74}\psi_0^L + u_{77}v_0^L + u_{78}\vartheta_0^L = 0 \tag{3.18c}$$

$$u_{83}w_0^L + u_{84}\psi_0^L + u_{87}v_0^L + u_{88}\vartheta_0^L = 0 \tag{3.18d}$$

In computing the eigenvalues of the system, the coefficients of Equation (3.18a) to Equation (3.18d) form the *characteristic determinant*, which equals zero when an eigenvalue of the system is found. Mathematically, the determinant equaling zero means that at least one equation of the four is linearly dependent on one or more of the others [17].

To obtain the mode shape of this eigenvalue, we need to isolate the three linearly independent equations. The manner of determining the correct equations is to select any

three of the four equations and compute their determinant. This selecting process is repeated using three equations at a time until the calculated determinant *does not* equal zero. When this occurs the three linearly independent equations have been found.

The three linearly independent equations have four unknowns. As the mode shape is an arbitrarily scaled function, the value of unity may be assumed for one of the unknowns and using Cramer's rule [18] the unknowns can be solved to provide the values of the input *state vector* for the mode shape.

Chapter 4
Test Examples

In this chapter, the results obtained from the computer code of 2DBEAM are tested for accuracy.

4.1 Static Response

Three cases have been evaluated to verify the static response of 2DBEAM. The results from the program are compared to analytical solutions.

4.1.1 Uniformly Distributed Load at an Angle on a Massless Beam

The first example is a simply-supported stainless steel (18-8) beam subjected to uniformly distributed load (Q) acting at an angle θ_Q of 45^o measured counter-clockwise from the positive y-axis. The circular cross-section with a radius of 0.5m, gives equal area moment of inertias (I_y and I_z) about the y and z-axis. The quantity of these variables along with the length (l) of the beam and its modulus of elasticity (E) are depicted in Figure 4.1.

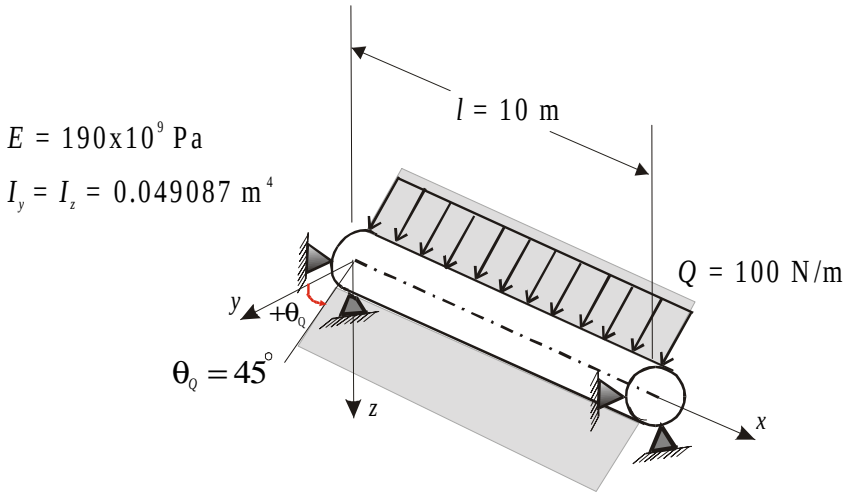

Figure 4.1: Simply supported beam with uniformly distributed load at angle θ_Q.

To verify the 2DBEAM output, the static response of the model in Figure 4.1 was calculated by hand. The distributed load was first resolved into its *y* and *z*-components. Following this the equations found in Shigley and Mitchell [19] were used to obtain the deflection, moment, and shear along the length of the beam. The signs of the equations were modified depending on the orientation of the axis and direction that was being evaluated. The equation used in the hand calculation of each *state vector* component is found directly below the table in which its result is compared to that from the 2DBEAM program. Note that in the equations, *x* represents the axial location from the left end of the beam.

As the calculated result is compared to the 2DBEAM output in Table 4.1 to Table 4.6, it can be seen that for an equivalent number of decimal places, the result is exact. The stress response is dealt with following Table 4.6.

Table 4.1: Analytical and 2DBEAM results of deflection in the *z*-direction.

Axial Location (m)	†Calculated *z* -Deflection (m)	2DBEAM *z* -Deflection (m)	Percent Difference
0.00E+00	0.000000E+00	0.000000E+00	0.00E+00
1.00E+00	3.098984E-07	3.098984E-07	0.00E+00
2.00E+00	5.863113E-07	5.863113E-07	0.00E+00
3.00E+00	8.027031E-07	8.027031E-07	0.00E+00
4.00E+00	9.401198E-07	9.401198E-07	0.00E+00
5.00E+00	9.871889E-07	9.871889E-07	0.00E+00
6.00E+00	9.401198E-07	9.401198E-07	0.00E+00
7.00E+00	8.027031E-07	8.027031E-07	0.00E+00
8.00E+00	5.863113E-07	5.863113E-07	0.00E+00
9.00E+00	3.098984E-07	3.098984E-07	0.00E+00
1.00E+01	0.000000E+00	-8.470329E-22	N/A

†Equation used in calculation: $w = -\frac{(Q\sin\theta)x}{24EI_y}(2lx^2 - x^3 - l^3)$

Table 4.2: Analytical and 2DBEAM results of deflection in the *y*-direction.

Axial Location (m)	††Calculated *y*- Deflection (m)	2DBEAM *y* -Deflection (m)	Percent Difference
0.00E+00	0.000000E+00	0.000000E+00	0.00E+00
1.00E+00	3.098984E-07	3.098984E-07	0.00E+00
2.00E+00	5.863113E-07	5.863113E-07	0.00E+00
3.00E+00	8.027031E-07	8.027031E-07	0.00E+00
4.00E+00	9.401198E-07	9.401198E-07	0.00E+00
5.00E+00	9.871889E-07	9.871889E-07	0.00E+00
6.00E+00	9.401198E-07	9.401198E-07	0.00E+00
7.00E+00	8.027031E-07	8.027031E-07	0.00E+00
8.00E+00	5.863113E-07	5.863113E-07	0.00E+00
9.00E+00	3.098984E-07	3.098984E-07	0.00E+00
1.00E+01	0.000000E+00	-4.235165E-22	N/A

††Equation used in calculation: $v = -\frac{(Q\cos\theta_Q)x}{24EI_z}(2lx^2 - x^3 - l^3)$

Table 4.3: Analytical and 2DBEAM results of moment in the *y*-direction.

Axial Location (m)	†Calculated *y* -Moment (N-m)	2DBEAM *y* -Moment (N-m)	Percent Difference
0.00E+00	0.000000E+00	0.000000E+00	0.00E+00
1.00E+00	3.181981E+02	3.181981E+02	0.00E+00
2.00E+00	5.656854E+02	5.656854E+02	0.00E+00
3.00E+00	7.424621E+02	7.424621E+02	0.00E+00
4.00E+00	8.485281E+02	8.485281E+02	0.00E+00
5.00E+00	8.838835E+02	8.838835E+02	0.00E+00
6.00E+00	8.485281E+02	8.485281E+02	0.00E+00
7.00E+00	7.424621E+02	7.424621E+02	0.00E+00
8.00E+00	5.656854E+02	5.656854E+02	0.00E+00
9.00E+00	3.181981E+02	3.181981E+02	0.00E+00
1.00E+01	0.000000E+00	4.547474E-13	N/A

†Equation used in calculation: $M_y = \frac{(Q\sin\theta_Q)x}{2}(l-x)$

Table 4.4: Analytical and 2DBEAM results of moment in the *z*-direction.

Axial Location (m)	††Calculated *z* -Moment (N-m)	2DBEAM *z* -Moment (N-m)	Percent Difference
0.00E+00	0.000000E+00	0.000000E+00	0.00E+00
1.00E+00	-3.181981E+02	-3.181981E+02	0.00E+00
2.00E+00	-5.656854E+02	-5.656854E+02	0.00E+00
3.00E+00	-7.424621E+02	-7.424621E+02	0.00E+00
4.00E+00	-8.485281E+02	-8.485281E+02	0.00E+00
5.00E+00	-8.838835E+02	-8.838835E+02	0.00E+00
6.00E+00	-8.485281E+02	-8.485281E+02	0.00E+00
7.00E+00	-7.424621E+02	-7.424621E+02	0.00E+00
8.00E+00	-5.656854E+02	-5.656854E+02	0.00E+00
9.00E+00	-3.181981E+02	-3.181981E+02	0.00E+00
1.00E+01	0.000000E+00	0.000000E+00	0.00E+00

††Equation used in calculation: $M_z = -\frac{(Q\cos\theta_Q)x}{2}(l-x)$

Table 4.5: Analytical and 2DBEAM results of shear in the *z*-direction.

Axial Location (m)	†Calculated *z* -Shear (N)	2DBEAM *z* -Shear (N)	Percent Difference
0.00E+00	3.535534E+02	3.535534E+02	0.00E+00
1.00E+00	2.828427E+02	2.828427E+02	0.00E+00
2.00E+00	2.121320E+02	2.121320E+02	0.00E+00
3.00E+00	1.414214E+02	1.414214E+02	0.00E+00
4.00E+00	7.071068E+01	7.071068E+01	0.00E+00
5.00E+00	0.000000E+00	5.684342E-14	0.00E+00
6.00E+00	-7.071068E+01	-7.071068E+01	0.00E+00
7.00E+00	-1.414214E+02	-1.414214E+02	0.00E+00
8.00E+00	-2.121320E+02	-2.121320E+02	0.00E+00
9.00E+00	-2.828427E+02	-2.828427E+02	0.00E+00
1.00E+01	-3.535534E+02	-3.535534E+02	0.00E+00

†Equation used in calculation: $V_z = \frac{(Q\sin\theta_Q)l}{2} - (Q\sin\theta_Q)x$

Table 4.6: Analytical and 2DBEAM results of shear in the *y*-direction.

Axial Location (m)	††Calculated *y* -Shear (N)	2DBEAM *y* -Shear (N)	Percent Difference
0.00E+00	3.535534E+02	3.535534E+02	0.00E+00
1.00E+00	2.828427E+02	2.828427E+02	0.00E+00
2.00E+00	2.121320E+02	2.121320E+02	0.00E+00
3.00E+00	1.414214E+02	1.414214E+02	0.00E+00
4.00E+00	7.071068E+01	7.071068E+01	0.00E+00
5.00E+00	0.000000E+00	0.000000E+00	0.00E+00
6.00E+00	-7.071068E+01	-7.071068E+01	0.00E+00
7.00E+00	-1.414214E+02	-1.414214E+02	0.00E+00
8.00E+00	-2.121320E+02	-2.121320E+02	0.00E+00
9.00E+00	-2.828427E+02	-2.828427E+02	0.00E+00
1.00E+01	-3.535534E+02	-3.535534E+02	0.00E+00

††Equation used in calculation: $V_y = \frac{(Q\cos\theta_Q)l}{2} - (Q\cos\theta_Q)x$

The 2DBEAM stress response of the model in Figure 4.1 was also verified by hand calculations. For the tensile stress, the equation for unsymmetrical bending found in Hibbeler [20] was used. The shear stress makes use of the basic shear stress formula also found in Hibbeler [21]. The vectorial resultant of the shear stress is then calculated from the *y* and *z* components. From Table 4.7 and 4.8, it is evident that the values match those from the program's output.

Table 4.7: Analytical and 2DBEAM results for maximum tensile stress.

Axial Location (m)	Calculated Max. Tensile Stress (MPa)	2DBEAM Max. Tensile Stress (MPa)	Percent Difference
0.00E+00	0.000000E+00	0.000000E+00	0.00E+00
1.00E+00	6.482277E-03	6.482277E-03	0.00E+00
2.00E+00	1.152405E-02	1.152405E-02	0.00E+00
3.00E+00	1.512531E-02	1.512531E-02	0.00E+00
4.00E+00	1.728607E-02	1.728607E-02	0.00E+00
5.00E+00	1.800633E-02	1.800633E-02	0.00E+00
6.00E+00	1.728607E-02	1.728607E-02	0.00E+00
7.00E+00	1.512531E-02	1.512531E-02	0.00E+00
8.00E+00	1.152405E-02	1.152405E-02	0.00E+00
9.00E+00	6.482277E-03	6.482277E-03	0.00E+00
1.00E+01	0.000000E+00	4.632018E-18	N/A

Table 4.8: Analytical and 2DBEAM results for maximum shear stress.

Axial Location (m)	Calculated Max. Shear Stress (MPa)	2DBEAM Max. Shear Stress (MPa)	Percent Difference
0.00E+00	8.488264E-04	8.488264E-04	0.00E+00
1.00E+00	6.790611E-04	6.790611E-04	0.00E+00
2.00E+00	5.092958E-04	5.092958E-04	0.00E+00
3.00E+00	3.395305E-04	3.395305E-04	0.00E+00
4.00E+00	1.697653E-04	1.697653E-04	0.00E+00
5.00E+00	0.000000E+00	9.650039E-20	N/A
6.00E+00	1.697653E-04	1.697653E-04	0.00E+00
7.00E+00	3.395305E-04	3.395305E-04	0.00E+00
8.00E+00	5.092958E-04	5.092958E-04	0.00E+00
9.00E+00	6.790611E-04	6.790611E-04	0.00E+00
1.00E+01	8.488264E-04	8.488264E-04	0.00E+00

4.1.2 Concentrated Force and Moment at Different Angles on a Massless Beam

The case in Figure 4.2 involves an aluminum cantilever beam with an external force (*P*) and moment (*M*) acting at its free end. The force acts at an angle θ_P of 225° and the moment at an angle θ_M of 45°, both measured counter-clockwise from the positive *y*-axis. Here the cross-section is a solid rectangle with a height of 10in and width of 5in. The cross-section leads to dissimilar area moment of inertias about the *y* and *z*-axis.

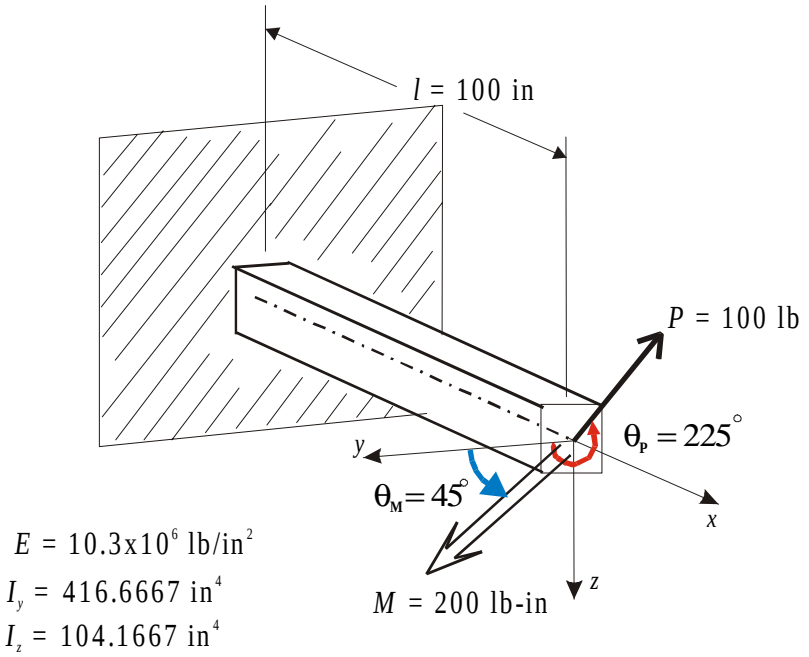

Figure 4.2: Cantilever acted upon by external force (*P*) and moment (*M*)

To compare with the output obtained from 2DBEAM, the static response of Figure 4.2 was calculated using equations from Shigley and Mitchell. As the model contains two loading vectors, the response of the force load is superpositioned on the moment load. The signs of the equations were modified where necessary.

The results from 2DBEAM are again seen to match those computed analytically.

Table 4.9: Analytical and 2DBEAM results of deflection in the *z*-direction.

Axial Location (in)	†Calculated *z* -Deflection (in)	2DBEAM *z* -Deflection (in)	Percent Difference
0.00E+00	0.000000E+00	0.000000E+00	0.00E+00
1.00E+01	-8.128295E-05	-8.128295E-05	0.00E+00
2.00E+01	-3.141476E-04	-3.141476E-04	0.00E+00
3.00E+01	-6.821178E-04	-6.821178E-04	0.00E+00
4.00E+01	-1.168717E-03	-1.168717E-03	0.00E+00
5.00E+01	-1.757469E-03	-1.757469E-03	0.00E+00
6.00E+01	-2.431898E-03	-2.431898E-03	0.00E+00
7.00E+01	-3.175527E-03	-3.175527E-03	0.00E+00
8.00E+01	-3.971881E-03	-3.971881E-03	0.00E+00
9.00E+01	-4.804482E-03	-4.804482E-03	0.00E+00
1.00E+02	-5.656854E-03	-5.656854E-03	0.00E+00

†Equation used in calculation: $w = -\frac{(P\sin\theta_P)x^2}{6EI_y}(x-3l) - \frac{(M\cos\theta_M)x^2}{2EI_y}$

Table 4.10: Analytical and 2DBEAM results of deflection in the *y*-direction.

Axial Location (in)	††Calculated *y*- Deflection (in)	2DBEAM *y* -Deflection (in)	Percent Difference
0.00E+00	0.000000E+00	0.000000E+00	0.00E+00
1.00E+01	-3.119508E-04	-3.119508E-04	0.00E+00
2.00E+01	-1.203866E-03	-1.203866E-03	0.00E+00
3.00E+01	-2.609842E-03	-2.609842E-03	0.00E+00
4.00E+01	-4.463972E-03	-4.463972E-03	0.00E+00
5.00E+01	-6.700352E-03	-6.700352E-03	0.00E+00
6.00E+01	-9.253076E-03	-9.253076E-03	0.00E+00
7.00E+01	-1.205624E-02	-1.205624E-02	0.00E+00
8.00E+01	-1.504394E-02	-1.504394E-02	0.00E+00
9.00E+01	-1.815026E-02	-1.815026E-02	0.00E+00
1.00E+02	-2.130932E-02	-2.130932E-02	0.00E+00

††Equation used in calculation: $v = -\frac{(P\cos\theta_P)x^2}{6EI_z}(x-3l) - \frac{(M\sin\theta_M)x^2}{2EI_z}$

Table 4.11: Analytical and 2DBEAM results of moment in the *y*-direction.

Axial Location (in)	†Calculated *y* -Moment (lb-in)	2DBEAM *y* -Moment (lb-in)	Percent Difference
0.00E+00	7.212489E+03	7.212489E+03	0.00E+00
1.00E+01	6.505382E+03	6.505382E+03	0.00E+00
2.00E+01	5.798276E+03	5.798276E+03	0.00E+00
3.00E+01	5.091169E+03	5.091169E+03	0.00E+00
4.00E+01	4.384062E+03	4.384062E+03	0.00E+00
5.00E+01	3.676955E+03	3.676955E+03	0.00E+00
6.00E+01	2.969848E+03	2.969848E+03	0.00E+00
7.00E+01	2.262742E+03	2.262742E+03	0.00E+00
8.00E+01	1.555635E+03	1.555635E+03	0.00E+00
9.00E+01	8.485281E+02	8.485281E+02	0.00E+00
1.00E+02	1.414214E+02	1.414214E+02	0.00E+00

†Equation used in calculation: $M_y = P\sin\theta_P(x-l) + M\cos\theta_M$

Table 4.12: Analytical and 2DBEAM results of moment in the *z*-direction.

Axial Location (m)	††Calculated *z* -Moment (lb-in)	2DBEAM *z* -Moment (lb-in)	Percent Difference
0.00E+00	-6.929646E+03	-6.929646E+03	0.00E+00
1.00E+01	-6.222540E+03	-6.222540E+03	0.00E+00
2.00E+01	-5.515433E+03	-5.515433E+03	0.00E+00
3.00E+01	-4.808326E+03	-4.808326E+03	0.00E+00
4.00E+01	-4.101219E+03	-4.101219E+03	0.00E+00
5.00E+01	-3.394113E+03	-3.394113E+03	0.00E+00
6.00E+01	-2.687006E+03	-2.687006E+03	0.00E+00
7.00E+01	-1.979899E+03	-1.979899E+03	0.00E+00
8.00E+01	-1.272792E+03	-1.272792E+03	0.00E+00
9.00E+01	-5.656854E+02	-5.656854E+02	0.00E+00
1.00E+02	1.414214E+02	1.414214E+02	0.00E+00

††Equation used in calculation: $M_z = -P\cos\theta_P(x-l) + M\sin\theta_M$

Table 4.13: Analytical and 2DBEAM results of shear in the *z*-direction.

Axial Location (m)	†Calculated *z*-Shear (lb)	2DBEAM *z*-Shear (lb)	Percent Difference
0.00E+00	-7.071068E+01	-7.071068E+01	0.00E+00
1.00E+01	-7.071068E+01	-7.071068E+01	0.00E+00
2.00E+01	-7.071068E+01	-7.071068E+01	0.00E+00
3.00E+01	-7.071068E+01	-7.071068E+01	0.00E+00
4.00E+01	-7.071068E+01	-7.071068E+01	0.00E+00
5.00E+01	-7.071068E+01	-7.071068E+01	0.00E+00
6.00E+01	-7.071068E+01	-7.071068E+01	0.00E+00
7.00E+01	-7.071068E+01	-7.071068E+01	0.00E+00
8.00E+01	-7.071068E+01	-7.071068E+01	0.00E+00
9.00E+01	-7.071068E+01	-7.071068E+01	0.00E+00
1.00E+02	-7.071068E+01	-7.071068E+01	0.00E+00

†Equation used in calculation: $V_z = P\sin\theta_P$

Table 4.14: Analytical and 2DBEAM results of shear in the *y*-direction.

Axial Location (m)	†† Calculated *y*-Shear (lb)	2DBEAM *y*-Shear (lb)	Percent Difference
0.00E+00	-7.071068E+01	-7.071068E+01	0.00E+00
1.00E+01	-7.071068E+01	-7.071068E+01	0.00E+00
2.00E+01	-7.071068E+01	-7.071068E+01	0.00E+00
3.00E+01	-7.071068E+01	-7.071068E+01	0.00E+00
4.00E+01	-7.071068E+01	-7.071068E+01	0.00E+00
5.00E+01	-7.071068E+01	-7.071068E+01	0.00E+00
6.00E+01	-7.071068E+01	-7.071068E+01	0.00E+00
7.00E+01	-7.071068E+01	-7.071068E+01	0.00E+00
8.00E+01	-7.071068E+01	-7.071068E+01	0.00E+00
9.00E+01	-7.071068E+01	-7.071068E+01	0.00E+00
1.00E+02	-7.071068E+01	-7.071068E+01	0.00E+00

††Equation used in calculation: $V_y = P\cos\theta_P$

The stress output from 2DBEAM is compared to the analytical results in Table 4.15 and 4.16. The hand calculations were performed using the same method and equations as were used in the Static Case I found in Section 4.1.1. From the tabulated results below, the 2DBEAM output is again shown to match the calculated values.

Table 4.15: Analytical and 2DBEAM results for maximum tensile stress.

Axial Location (in)	Calculated Max. Tensile Stress (kpsi)	2DBEAM Max. Tensile Stress (kpsi)	Percent Difference
0.00E+00	2.528614E-01	2.528614E-01	0.00E+00
1.00E+01	2.274055E-01	2.274055E-01	0.00E+00
2.00E+01	2.019497E-01	2.019497E-01	0.00E+00
3.00E+01	1.764939E-01	1.764939E-01	0.00E+00
4.00E+01	1.510380E-01	1.510380E-01	0.00E+00
5.00E+01	1.255822E-01	1.255822E-01	0.00E+00
6.00E+01	1.001263E-01	1.001263E-01	0.00E+00
7.00E+01	7.467048E-02	7.467048E-02	0.00E+00
8.00E+01	4.921463E-02	4.921463E-02	0.00E+00
9.00E+01	2.375879E-02	2.375879E-02	0.00E+00
1.00E+02	-1.697056E-03	-1.697056E-03	0.00E+00

Table 4.16: Analytical and 2DBEAM results for maximum shear stress.

Axial Location (in)	Calculated Max. Shear Stress (kpsi)	Calculated Max. Shear Stress (kpsi)	Percent Difference
0.00E+00	3.000000E-03	3.000000E-03	0.00E+00
1.00E+01	3.000000E-03	3.000000E-03	0.00E+00
2.00E+01	3.000000E-03	3.000000E-03	0.00E+00
3.00E+01	3.000000E-03	3.000000E-03	0.00E+00
4.00E+01	3.000000E-03	3.000000E-03	0.00E+00
5.00E+01	3.000000E-03	3.000000E-03	0.00E+00
6.00E+01	3.000000E-03	3.000000E-03	0.00E+00
7.00E+01	3.000000E-03	3.000000E-03	0.00E+00
8.00E+01	3.000000E-03	3.000000E-03	0.00E+00
9.00E+01	3.000000E-03	3.000000E-03	0.00E+00
1.00E+02	3.000000E-03	3.000000E-03	0.00E+00

4.1.3 Forces and Moment at Different Axial Positions along a Massless Beam

In this example, three forces and a moment act on the carbon steel cantilever at two different locations along the length of the beam. At a distance of 100in from the fixed end of the beam, the external forces of P_1 act at an angle θ_{P1} of 30° and P_2 at an angle θ_{P2} of 300°. The force P_3 at an angle θ_{P3} of 100° and moment M_1 at an angle θ_M of 200° are located at the free end of the cantilever. The magnitude of the forces and moment are shown in Figure 4.3. The thin-walled rectangular cross-section with a height of 8in, width of 10in, and thickness of 1in give different values for the area moment of inertias about the about the *y* and *z*-axes.

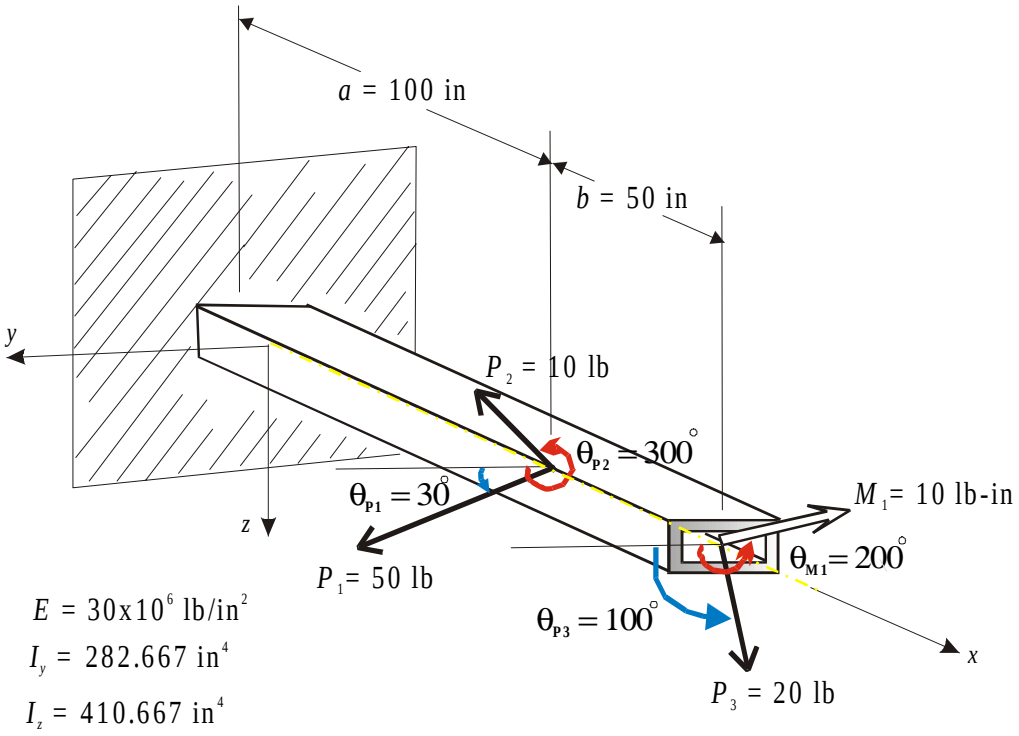

Figure 4.3: Cantilever acted upon by external forces (P_1, P_2, and P_3) and moment (M_1).

The static response of Figure 4.2 was calculated using equations from Shigley and Mitchell. After resolving the loads into *y* and *z* components, the response from each load was superpositioned to obtain the overall response of the system in the two directions.

As seen in the tables that follow the results from 2DBEAM match those computed analytically.

Table 4.17: Analytical and 2DBEAM results of deflection in the *z*-direction.

Axial Location (in)	†Calculated *z* -Deflection (in)	2DBEAM *z* -Deflection (in)	Percent Difference
0.00E+00	0.000000E+00	0.000000E+00	0.00E+00
2.00E+01	1.027725E-04	1.027725E-04	0.00E+00
4.00E+01	3.884260E-04	3.884260E-04	0.00E+00
6.00E+01	8.229644E-04	8.229644E-04	0.00E+00
8.00E+01	1.372391E-03	1.372391E-03	0.00E+00
1.00E+02	2.002711E-03	2.002711E-03	0.00E+00
1.10E+02	2.337903E-03	2.337903E-03	0.00E+00
1.20E+02	2.682496E-03	2.682496E-03	0.00E+00
1.30E+02	3.034169E-03	3.034169E-03	0.00E+00
1.40E+02	3.390597E-03	3.390597E-03	0.00E+00
1.50E+02	3.749459E-03	3.749459E-03	0.00E+00

†Equation used in calculation:

(for $0 \le x < 100$)

$$w = -\frac{(P_1 \sin\theta_{P1})x^2}{6EI_y}(x-3a) - \frac{(P_2 \sin\theta_{P2})x^2}{6EI_y}(x-3a) - \frac{(P_3 \sin\theta_{P3})x^2}{6EI_y}(x-3l) - \frac{(M_1 \cos\theta_{M1})x^2}{2EI_y}$$

(for $100 \le x \le 150$)

$$w = -\frac{(P_1 \sin\theta_{P1})a^2}{6EI_y}(a-3x) - \frac{(P_2 \sin\theta_{P2})a^2}{6EI_y}(a-3x) - \frac{(P_3 \sin\theta_{P3})x^2}{6EI_y}(x-3l) - \frac{(M_1 \cos\theta_{M1})x^2}{2EI_y}$$

Table 4.18: Analytical and 2DBEAM results of deflection in the *y*-direction.

Axial Location (in)	†Calculated *y*- Deflection (in)	2DBEAM *y* -Deflection (in)	Percent Difference
0.00E+00	0.000000E+00	0.000000E+00	0.00E+00
2.00E+01	6.504719E-05	6.504719E-05	0.00E+00
4.00E+01	2.407826E-04	2.407826E-04	0.00E+00
6.00E+01	4.980968E-04	4.980968E-04	0.00E+00
8.00E+01	8.078807E-04	8.078807E-04	0.00E+00
1.00E+02	1.141025E-03	1.141025E-03	0.00E+00
1.10E+02	1.307914E-03	1.307914E-03	0.00E+00
1.20E+02	1.473648E-03	1.473648E-03	0.00E+00
1.30E+02	1.638508E-03	1.638508E-03	0.00E+00
1.40E+02	1.802776E-03	1.802776E-03	0.00E+00
1.50E+02	1.966735E-03	1.966735E-03	0.00E+00

†Equation used in calculation:

(for $0 \le x < 100$)

$$v = -\frac{(P_1 \cos\theta_{P1})x^2}{6EI_z}(x-3a) - \frac{(P_2 \cos\theta_{P2})x^2}{6EI_z}(x-3a) - \frac{(P_3 \cos\theta_{P3})x^2}{6EI_z}(x-3l) - \frac{(M_1 \sin\theta_{M1})x^2}{2EI_z}$$

(for $100 \le x \le 150$)

$$v = -\frac{(P_1 \cos\theta_{P1})a^2}{6EI_z}(a-3x) - \frac{(P_2 \cos\theta_{P2})a^2}{6EI_z}(a-3x) - \frac{(P_3 \cos\theta_{P3})x^2}{6EI_z}(x-3l) - \frac{(M_1 \sin\theta_{M1})x^2}{2EI_z}$$

Table 4.19: Analytical and 2DBEAM results of moment in the *y*-direction.

Axial Location (in)	†Calculated *y* -Moment (lb-in)	2DBEAM *y* -Moment (lb-in)	Percent Difference
0.00E+00	-4.597795E+03	-4.597795E+03	0.00E+00
2.00E+01	-3.877077E+03	-3.877077E+03	0.00E+00
4.00E+01	-3.156359E+03	-3.156359E+03	0.00E+00
6.00E+01	-2.435641E+03	-2.435641E+03	0.00E+00
8.00E+01	-1.714923E+03	-1.714923E+03	0.00E+00
1.00E+02	-9.942047E+02	-9.942047E+02	0.00E+00
1.10E+02	-7.972431E+02	-7.972431E+02	0.00E+00
1.20E+02	-6.002816E+02	-6.002816E+02	0.00E+00
1.30E+02	-4.033200E+02	-4.033200E+02	0.00E+00
1.40E+02	-2.063585E+02	-2.063585E+02	0.00E+00
1.50E+02	-9.396926E+00	-9.396926E+00	0.00E+00

†Equation used in calculation:

(for $0 \le x < 100$)

$$M_y = P_1 \sin\theta_{P1}(x-a) + P_2 \sin\theta_{P2}(x-a) + P_3 \sin\theta_{P3}(x-l) + M_1 \cos\theta_{M1}$$

(for $100 \le x \le 150$)

$$M_y = P_3 \sin\theta_{P3}(x-l) + M_1 \cos\theta_{M1}$$

Table 4.20: Analytical and 2DBEAM results of moment in the *z*-direction.

Axial Location (m)	† Calculated *z* -Moment (lb-in)	2DBEAM *z* -Moment (lb-in)	Percent Difference
0.00E+00	4.305762E+03	4.305762E+03	0.00E+00
2.00E+01	3.409196E+03	3.409196E+03	0.00E+00
4.00E+01	2.512630E+03	2.512630E+03	0.00E+00
6.00E+01	1.616064E+03	1.616064E+03	0.00E+00
8.00E+01	7.194978E+02	7.194978E+02	0.00E+00
1.00E+02	-1.770684E+02	-1.770684E+02	0.00E+00
1.10E+02	-1.423387E+02	-1.423387E+02	0.00E+00
1.20E+02	-1.076091E+02	-1.076091E+02	0.00E+00
1.30E+02	-7.287947E+01	-7.287947E+01	0.00E+00
1.40E+02	-3.814984E+01	-3.814984E+01	0.00E+00
1.50E+02	-3.420201E+00	-3.420201E+00	0.00E+00

†Equation used in calculation:

(for $0 \leq x < 100$)

$$M_z = -P_1 \cos\theta_{P1}(x-a) - P_2 \cos\theta_{P2}(x-a) - P_3 \cos\theta_{P3}(x-l) + M_1 \sin\theta_{M1}$$

(for $100 \leq x \leq 150$)

$$M_z = -P_3 \cos\theta_{P3}(x-l) + M_1 \sin\theta_{M1}$$

Table 4.21: Analytical and 2DBEAM results of shear in the *z*-direction.

Axial Location (m)	†Calculated *z* -Shear (lb)	2DBEAM *z* -Shear (lb)	Percent Difference
0.00E+00	3.603590E+01	3.603590E+01	0.00E+00
2.00E+01	3.603590E+01	3.603590E+01	0.00E+00
4.00E+01	3.603590E+01	3.603590E+01	0.00E+00
6.00E+01	3.603590E+01	3.603590E+01	0.00E+00
8.00E+01	3.603590E+01	3.603590E+01	0.00E+00
1.00E+02	1.969616E+01	1.969616E+01	0.00E+00
1.10E+02	1.969616E+01	1.969616E+01	0.00E+00
1.20E+02	1.969616E+01	1.969616E+01	0.00E+00
1.30E+02	1.969616E+01	1.969616E+01	0.00E+00
1.40E+02	1.969616E+01	1.969616E+01	0.00E+00
1.50E+02	1.969616E+01	1.969616E+01	0.00E+00

†Equation used in calculation: $V_z = P_1 \sin\theta_{P1} + P_2 \sin\theta_{P2} + P_3 \sin\theta_{P3}$

Table 4.22: Analytical and 2DBEAM results of shear in the *z*-direction.

Axial Location (m)	††Calculated *y* -Shear (lb)	2DBEAM *y* -Shear (lb)	Percent Difference
0.00E+00	4.482831E+01	4.482831E+01	0.00E+00
2.00E+01	4.482831E+01	4.482831E+01	0.00E+00
4.00E+01	4.482831E+01	4.482831E+01	0.00E+00
6.00E+01	4.482831E+01	4.482831E+01	0.00E+00
8.00E+01	4.482831E+01	4.482831E+01	0.00E+00
1.00E+02	-3.472964E+00	-3.472964E+00	0.00E+00
1.10E+02	-3.472964E+00	-3.472964E+00	0.00E+00
1.20E+02	-3.472964E+00	-3.472964E+00	0.00E+00
1.30E+02	-3.472964E+00	-3.472964E+00	0.00E+00
1.40E+02	-3.472964E+00	-3.472964E+00	0.00E+00
1.50E+02	-3.472964E+00	-3.472964E+00	0.00E+00

††Equation used in calculation: $V_y = P_1 \cos\theta_{P1} + P_2 \cos\theta_{P2} + P_3 \cos\theta_{P3}$

The stress output from 2DBEAM is compared to the analytical results below. The hand calculations were performed using the same method and equations as explained for Static Case I. From the results below, the 2DBEAM output matches the calculated values.

Table 4.23: Analytical and 2DBEAM results for maximum tensile stress.

Axial Location (in)	Calculated Max. Tensile Stress (kpsi)	2DBEAM Max. Tensile Stress (kpsi)	Percent Difference
0.00E+00	-1.174872E-01	-1.174872E-01	0.00E+00
2.00E+01	-9.637236E-02	-9.637236E-02	0.00E+00
4.00E+01	-7.525754E-02	-7.525754E-02	0.00E+00
6.00E+01	-5.414272E-02	-5.414272E-02	0.00E+00
8.00E+01	-3.302789E-02	-3.302789E-02	0.00E+00
1.00E+02	-1.191307E-02	-1.191307E-02	0.00E+00
1.10E+02	-9.548722E-03	-9.548722E-03	0.00E+00
1.20E+02	-7.184375E-03	-7.184375E-03	0.00E+00
1.30E+02	-4.820028E-03	-4.820028E-03	0.00E+00
1.40E+02	-2.455680E-03	-2.455680E-03	0.00E+00
1.50E+02	-9.133331E-05	-9.133331E-05	0.00E+00

Table 4.23: Analytical and 2DBEAM results for maximum shear stress.

Axial Location (in)	Calculated Max. Shear Stress (kpsi)	2DBEAM Max. Shear Stress (kpsi)	Percent Difference
0.00E+00	3.990158E-03	3.990158E-03	0.00E+00
2.00E+01	3.990158E-03	3.990158E-03	0.00E+00
4.00E+01	3.990158E-03	3.990158E-03	0.00E+00
6.00E+01	3.990158E-03	3.990158E-03	0.00E+00
8.00E+01	3.990158E-03	3.990158E-03	0.00E+00
1.00E+02	1.548644E-03	1.548644E-03	0.00E+00
1.10E+02	1.548644E-03	1.548644E-03	0.00E+00
1.20E+02	1.548644E-03	1.548644E-03	0.00E+00
1.30E+02	1.548644E-03	1.548644E-03	0.00E+00
1.40E+02	1.548644E-03	1.548644E-03	0.00E+00
1.50E+02	1.548644E-03	1.548644E-03	0.00E+00

4.2 Free Vibration Response of an Elastic Beam with Distributed Mass

To verify the free-vibration response of the code, the output from the 2DBEAM is compared to the analytically solved problem.

The test example involves an elastic beam with continuously distributed mass of length (l). It has a height (h) of 10in and a width (w) of 5 in. The beam is made of carbon steel with modulus of elasticity (E) and weight density (γ) shown in Figure 4.3.

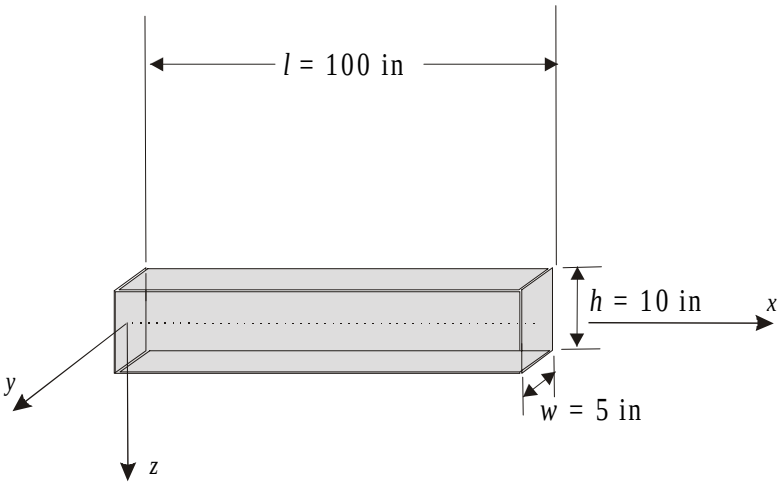

Material Properties:
$E = 30x10^6$ lb/in^2
$\gamma = 0.282$ lb/in^3

Geometry Properties:
$I_y = 416.6667$ in^4
$I_z = 104.1667$ in^4

Figure 4.3: Continuum Beam.

The beam is analytically solved using the Equation (4.1) from Harris and Crede [22].

$$\text{Angular Natural Frequency } \omega_n = A\sqrt{\frac{EI}{\mu l^4}} \text{ rad/sec} \qquad (4.1)$$

where E = Young's modulus, lb/in^2.

I = area moment of inertia of beam cross section, in^4.

l = length of beam, in.

μ = mass per unit length of beam, lb-sec^2/in^2.

A = Coefficient (characteristic number).

The value of the coefficient *A* for Equation (4.1) depends upon the boundary conditions of the beam. Since the values of *A* in Harris and Crede's table is only given to one decimal place, the number is obtained from an additional source by Young and Felgar [23] where it is provided, more accurately, to seven decimal places.

The following sections involve varying the boundary conditions of the continuum beam of Figure 4.1 and obtaining the first ten eigenvalues and their corresponding eigenvectors that occur in the *y* and *z*-directions. Three boundary conditions are considered, namely fixed-free, pinned-pinned and fixed-pinned.

4.2.1 Fixed-Free Boundary Condition

Natural Frequency

The eigenvalues for the beam of Figure 4.1 with a fixed left boundary condition and free right boundary condition are analyzed. The results from the 2DBEAM program are compared to those calculated from Equation (4.1). The *A* values to six decimal places are from the text by Young and Felgar.

Table 4.24: Analytical and 2DBEAM results of eigenvalues for fixed-free boundary.

Root	*A* value used in calculation	Calculated Frequency (Hz)	2DBEAM Frequency (Hz)	Percent Difference
1y	3.5160154	1.63692773E+01	1.63692767E+01	3.67E-06
1z	3.5160154	3.27385547E+01	3.27385534E+01	3.97E-06
2y	22.034492	1.02584508E+02	1.02584506E+02	1.95E-06
2z	22.034492	2.05169016E+02	2.05169012E+02	1.95E-06
3y	61.697214	2.87239586E+02	2.87239587E+02	3.48E-07
3z	61.697214	5.74479171E+02	5.74479175E+02	6.96E-07
4y	120.901916	5.62874950E+02	5.62874950E+02	0.00E+00
4z	120.901916	1.12574990E+03	1.12574990E+03	0.00E+00
5y	199.859530	9.30472623E+02	9.30472624E+02	1.07E-07
5z	199.859530	1.86094525E+03	1.86094525E+03	0.00E+00

A selective number of eigenvalues have been shown in Table 4.24 from the 2DBEAM output. This has been done to compare the 2DBEAM eigenvalue result to those that were available through hand calculations. In studying these values it is evident that the eigenvalues from 2DBEAM are close to the calculated ones. If you look at the eigenvalue and exclude the exponential portion, the frequency's digits are identical to at least six decimal digits. In some cases the accuracy is greater. It should be noted that there are limitations of the root-searching algorithm in use.

Mode Shape

The corresponding eigenvectors from 2DBEAM have been plotted in Figure 4.4 for the first five eigenvalues occurring in the *y*-direction and the first five eigenvalues occurring in the *z*-direction. The deflection portion of the mode shape output is shown.

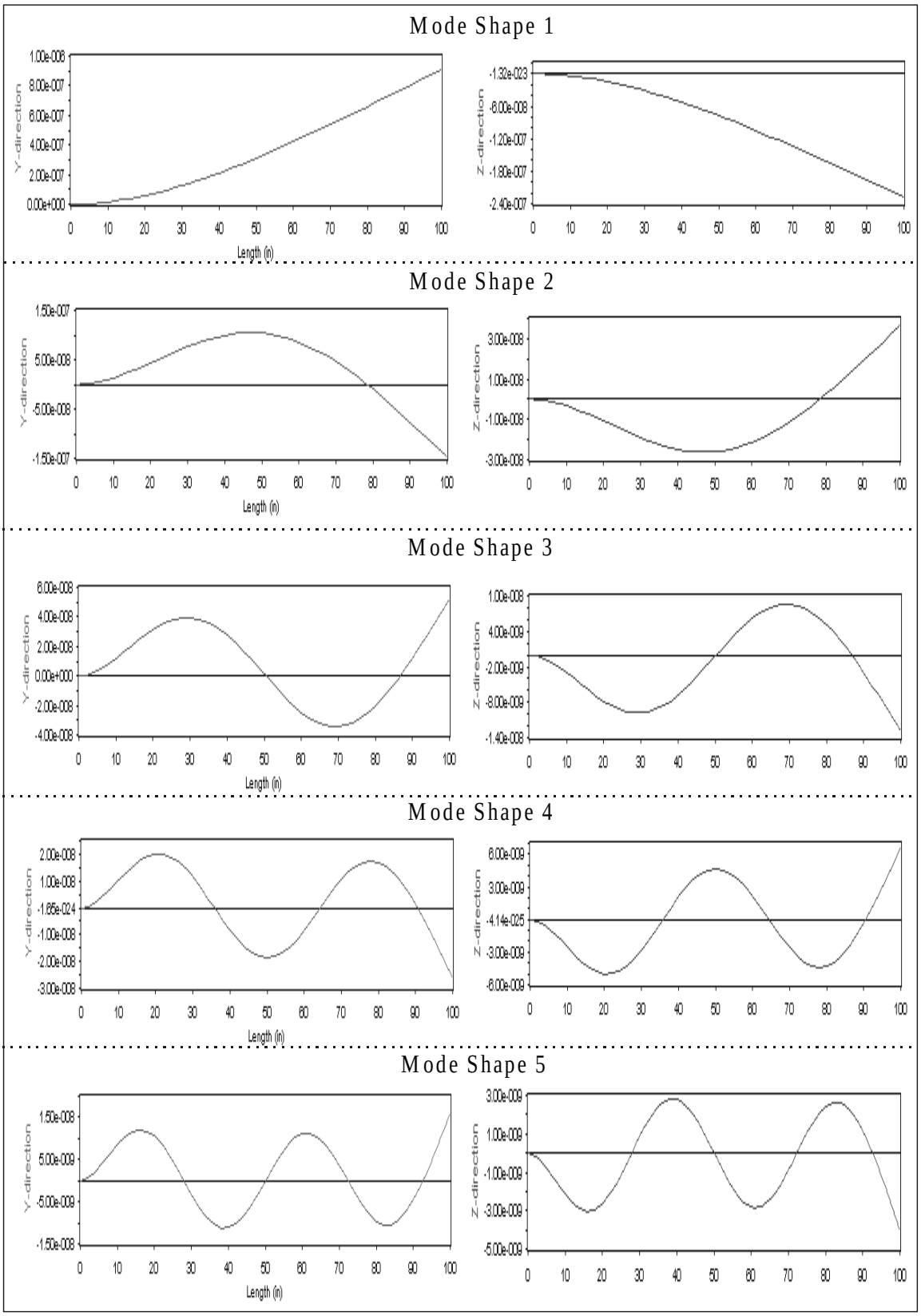

Figure 4.4: Eigenvectors for fixed-free boundary condition.

To evaluate the accuracy of the eigenvectors, the nodes of the shapes are examined with the table from Young and Felgar, which give the axial location to length of beam ratio (x/L) at which nodes are to occur. Ranges of the ratio in which the node occurred were provided and Table 4.25 is a summary of the information obtained.

Table 4.25: Node occurrences in first ten eigenvectors for fixed-free boundary.

	Natural	Node 1		Node 2		Node 3		Node 4	
Root	Frequency (Hz)	YF (x/L)	2DBEAM (x/L)	YF (x/L)	2DBEAM (x/L)	YF (x/L)	2DBEAM (x/L)	YF (x/L)	2DBEAM (x/L)
1y	1.6369E+01								
1z	3.2739E+01								
2y	1.0258E+02	0.78 - 0.80	0.784						
2z	2.0517E+02	0.78 - 0.80	0.784						
3y	2.8724E+02	0.50 - 0.52	0.504	0.86 - 0.88	0.868				
3z	5.7448E+02	0.50 - 0.52	0.504	0.86 - 0.88	0.868				
4y	5.6287E+02	0.34 - 0.36	0.358	0.64 - 0.66	0.644	0.90 - 0.92	0.906		
4z	1.1257E+03	0.34 - 0.36	0.358	0.64 - 0.66	0.644	0.90 - 0.92	0.906		
5y	9.3047E+02	0.26 - 0.28	0.279	0.48 - 0.50	0.500	0.72 - 0.74	0.723	0.92 - 0.94	0.927
5z	1.8610E+03	0.26 - 0.28	0.279	0.48 - 0.50	0.500	0.72 - 0.74	0.723	0.92 - 0.94	0.927

Note: YF in Table 4.25 denotes Young and Felgar (reference where data was obtained).

As seen in Table 4.25, the output from 2DBEAM of the location of nodes falls in the range given by Young and Felgar. This illustrates the accuracy of the mode shape results from the 2DBEAM program.

4.2.2 Pinned-Pinned Boundary Condition

Natural Frequency

2DBEAM provided the eigenvalues for the beam with the pinned-pinned boundary condition. The results are compared to those calculated from Equation (4.1). The A values in this case are from the Harris and Crede table as this boundary condition was not dealt with in the Young and Felgar reference.

Table 4.26: Analytical and 2DBEAM results of eigenvalues for pinned-pinned boundary.

Root	*A* value used in calculation	Calculated Frequency (Hz)	2DBEAM Frequency (Hz)	Percent Difference
1y	9.87	4.59510977E+01	4.59492559E+01	4.01E-03
1z	9.87	9.19021954E+01	9.18985119E+01	4.01E-03
2y	39.5	1.83897504E+02	1.83797024E+02	5.47E-02
2z	39.5	3.67795007E+02	3.67594048E+02	5.47E-02
3y	88.9	4.13885774E+02	4.13543304E+02	8.28E-02
3z	88.9	8.27771547E+02	8.27086607E+02	8.28E-02
4y	158	7.35590014E+02	7.35188095E+02	5.47E-02
4z	158	1.47118003E+03	1.47037619E+03	5.47E-02
5y	247	1.14994135E+03	1.14873140E+03	1.05E-01
5z	247	2.29988270E+03	2.29746280E+03	1.05E-01

The eigenvalues for this case do not match the calculated ones as closely as they did for the fixed-free boundary condition case of Section 4.2.1. The discrepancy can be explained from the fact that the *A* number used for the calculations for this case were available to at most two decimal places. In other words the expected accuracy of the calculated frequencies are:

Root 1y and 1z is ± 0.10%,

Root 2y and 2z is ± 0.25%,

Root 3y and 3z is ± 0.11%,

Root 4y and 4z is ± 0.63%,

and Root 5y and 5z is ± 0.40%.

Mode Shape

The corresponding eigenvectors from 2DBEAM have been collectively plotted in Figure 4.5 for all ten eigenvalues.

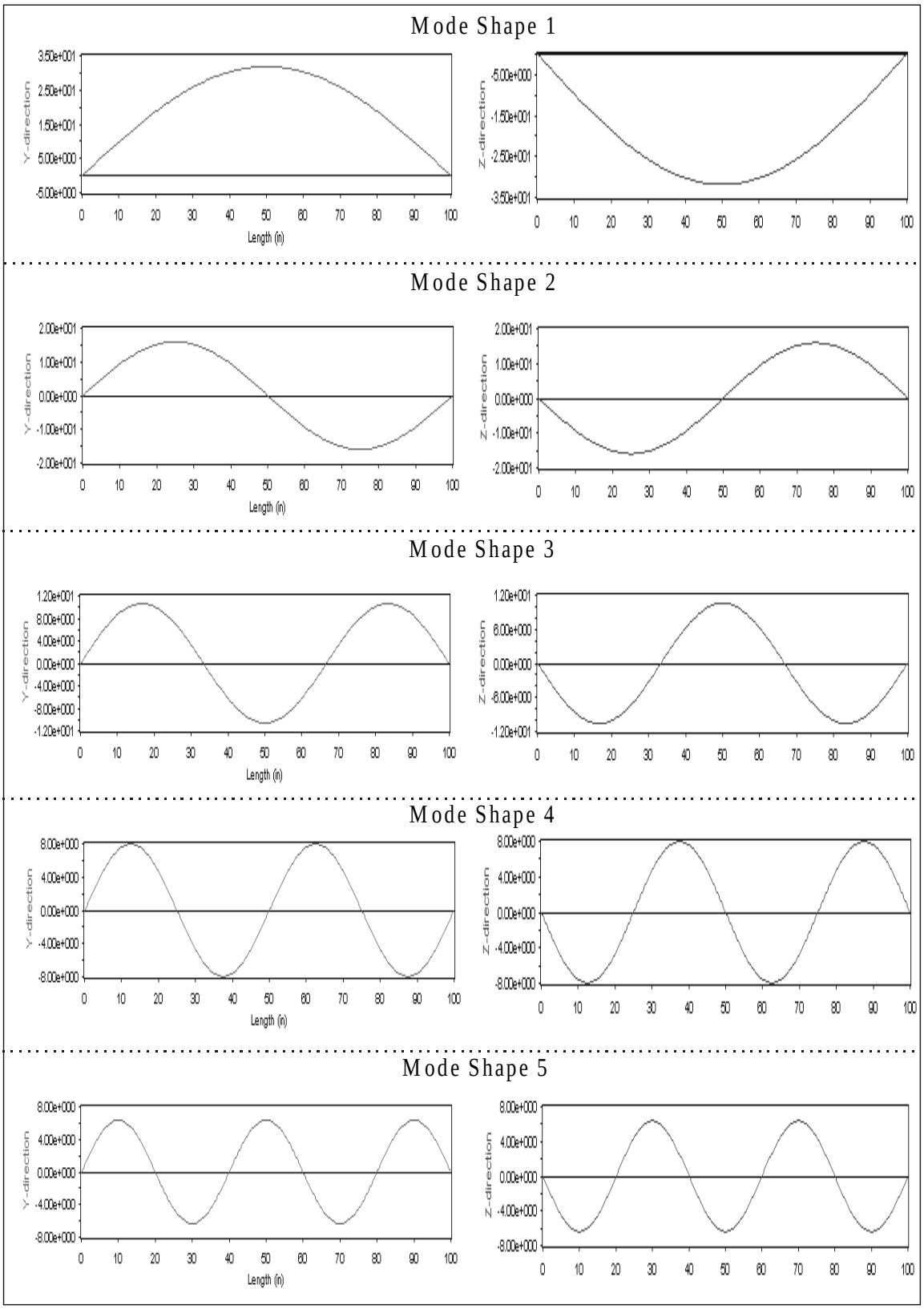

Figure 4.5: Eigenvectors for pinned-pinned boundary condition.

To determine the accuracy of the eigenvectors, the nodes of the shapes are compared to the axial location to length of beam ratio (x/L) given in Harris and Crede.

Table 4.27: Node occurrences in first ten eigenvectors for pinned-pinned boundary.

Root	Natural Frequency (Hz)	Node 1		Node 2		Node 3		Node 4	
		HC (x/L)	2DBEAM (x/L)	HC (x/L)	2DBEAM (x/L)	HC (x/L)	2DBEAM (x/L)	HC (x/L)	2DBEAM (x/L)
1y	4.5949E+01								
1z	9.1899E+01								
2y	1.8380E+02	0.500	0.500						
2z	3.6759E+02	0.500	0.500						
3y	4.1354E+02	0.333	0.333	0.667	0.667				
3z	8.2709E+02	0.333	0.333	0.667	0.667				
4y	7.3519E+02	0.250	0.250	0.500	0.500	0.750	0.750		
4z	1.4704E+03	0.250	0.250	0.500	0.500	0.750	0.750		
5y	1.1487E+03	0.200	0.200	0.400	0.400	0.600	0.600	0.800	0.800
5z	2.2975E+03	0.200	0.200	0.400	0.400	0.600	0.600	0.800	0.800

Note: HC in Table 4.27 denotes Harris and Crede (reference where data was obtained).

The results of the node occurrences for the pinned-pinned boundary condition case exactly match those given in the reference.

4.2.3 Fixed-Pinned Boundary Condition

Natural Frequency

The eigenvalues for the beam of Figure 4.1 with a left fixed boundary condition and a right pinned condition are considered in this section. The results from the 2DBEAM program are compared to those calculated from Equation (4.1). For this boundary condition, the A values are taken from Young and Felgar with six decimal points of precision.

Table 4.28: Analytical and 2DBEAM results of eigenvalues for fixed-pinned boundary.

Root	*A* value used in calculation	Calculated Frequency (Hz)	2DBEAM Frequency (Hz)	Percent Difference
1y	15.4182060	7.17815087E+01	7.17815073E+01	1.95E-06
1z	15.4182060	1.43563017E+02	1.43563015E+02	1.39E-06
2y	49.964862	2.32618060E+02	2.32618054E+02	2.58E-06
2z	49.964862	4.65236121E+02	4.65236010E+02	2.39E-05
3y	104.247697	4.85339018E+02	4.85339016E+02	4.12E-07
3z	104.247697	9.70678037E+02	9.70678032E+02	5.15E-07
4y	178.269730	8.29958438E+02	8.29958436E+02	2.41E-07
4z	178.269730	1.65991688E+03	1.65991687E+03	6.02E-07
5y	272.030971	1.26647637E+03	1.26647637E+03	0.00E+00
5z	272.030971	2.53295273E+03	2.53295273E+03	0.00E+00

The eigenvalues obtained from 2DBEAM are a close match to the calculated ones, but seen again is the limitation of the root-search calculation method.

Mode Shape

The mode shapes of the ten roots from 2DBEAM were combined into Figure 4.6.

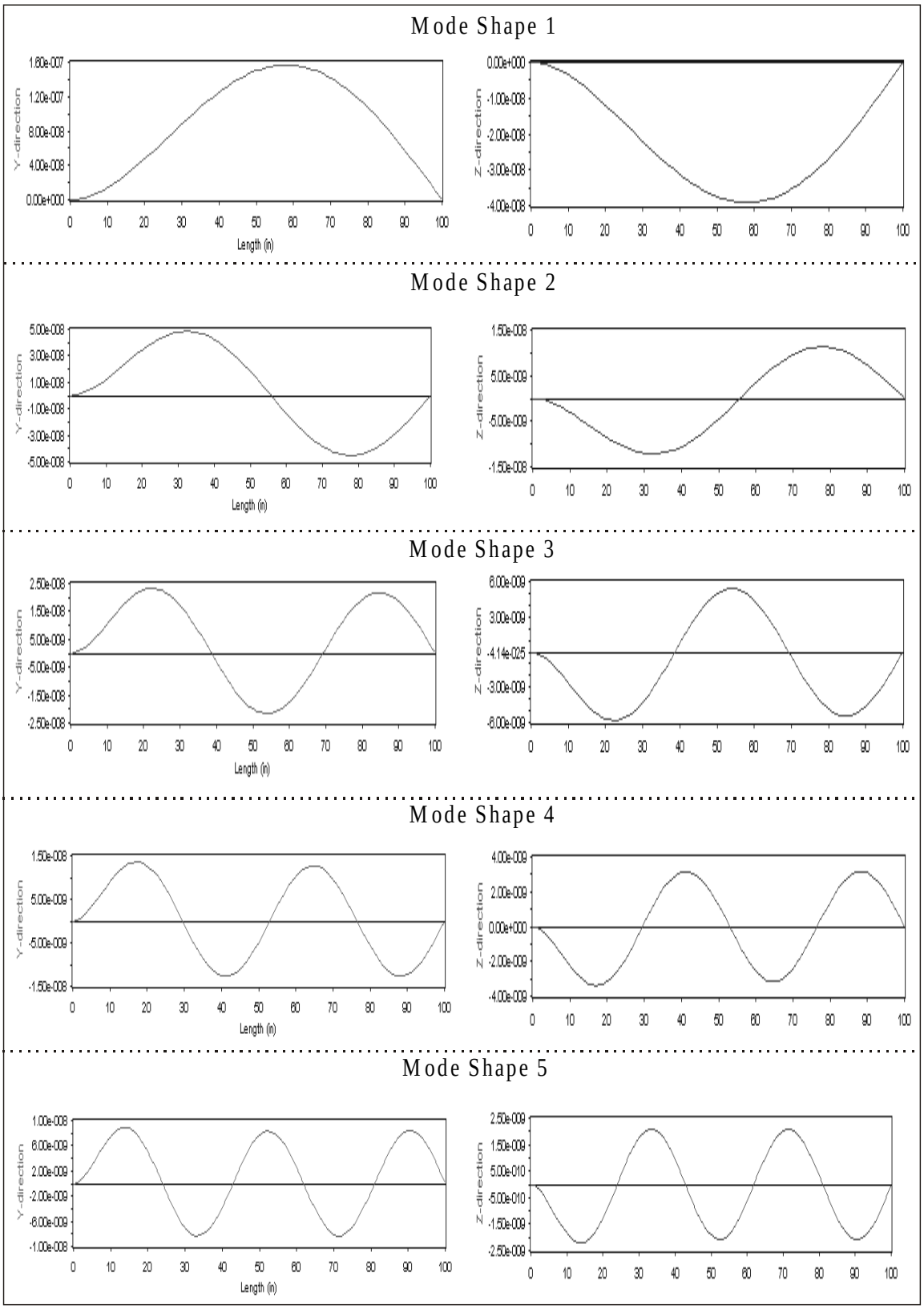

Figure 4.6: Eigenvectors for fixed-pinned boundary condition.

To determine the accuracy of the eigenvectors, the nodes of the shapes are compared to the axial location to length of beam ratio (*x/L*) given in Young and Felgar. The results are tabulated below.

Table 4.29: Node occurrences in first ten eigenvectors for fixed-pinned boundary.

Root	Natural Frequency (Hz)	Node 1		Node 2		Node 3		Node 4	
		YF (*x/L*)	2DBEAM (*x/L*)	YF (*x/L*)	2DBEAM (*x/L*)	YF (*x/L*)	2DBEAM (*x/L*)	YF (*x/L*)	2DBEAM (*x/L*)
1y	7.1782E+01								
1z	1.4356E+02								
2y	2.3262E+02	0.54 - 0.56	0.558						
2z	4.6524E+02	0.54 - 0.56	0.558						
3y	4.8534E+02	0.38 - 0.40	0.386	0.68 - 0.70	0.693				
3z	9.7068E+02	0.38 - 0.40	0.386	0.68 - 0.70	0.693				
4y	8.2996E+02	0.28 - 0.30	0.296	0.52 - 0.54	0.529	0.76 - 0.78	0.765		
4z	1.6599E+03	0.28 - 0.30	0.296	0.52 - 0.54	0.529	0.76 - 0.78	0.765		
5y	1.2665E+03	0.22 - 0.24	0.239	0.42 - 0.44	0.429	0.60 - 0.62	0.619	0.80 - 0.82	0.810
5z	2.5330E+03	0.22 - 0.24	0.239	0.42 - 0.44	0.429	0.60 - 0.62	0.619	0.80 - 0.82	0.810

Note: YF in Table 4.29 denotes Young and Felgar (reference where data was obtained).

As seen in Table 4.29, the axial location of where nodes occur from 2DBEAM fall within the range given and are, therefore, considered accurate.

4.3 Free Vibration, Forced Dynamic, and Frequency Responses of an Uncoupled and Coupled Massless Elastic Beam.

The eigenvalue-eigenvector analysis, forced dynamic analysis, and frequency response analysis output from the 2DBEAM code is verified with the analytical solution of the problems.

4.3.1 Uncoupled Massless Elastic Beam Example

The test case shown in Figure 4.7 has been taken from Young and Mitchell [24]. The area moment of inertia about the *y*-axis has been added and the harmonic excitation ($F\sin(\omega t)$) has been changed to act at an angle θ_F as shown in the figure.

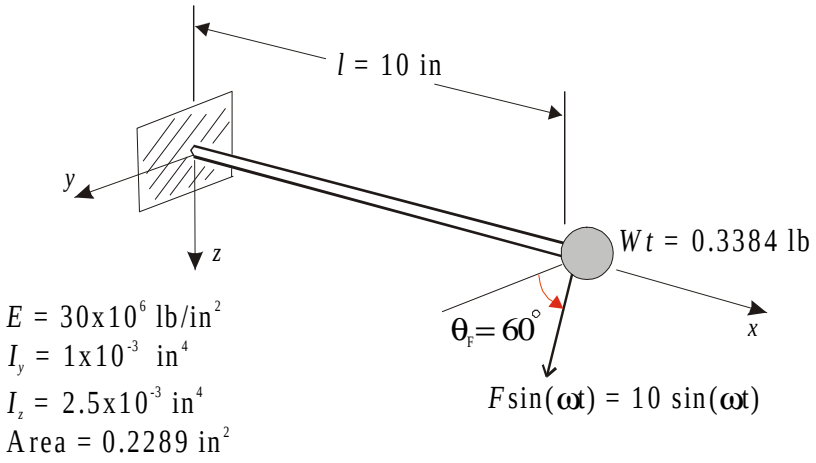

Figure 4.7: Cantilever with end mass acted upon by harmonic excitation.

An equivalent single degree of freedom model to that of Figure 4.7 is constructed and shown in Figure 4.8.

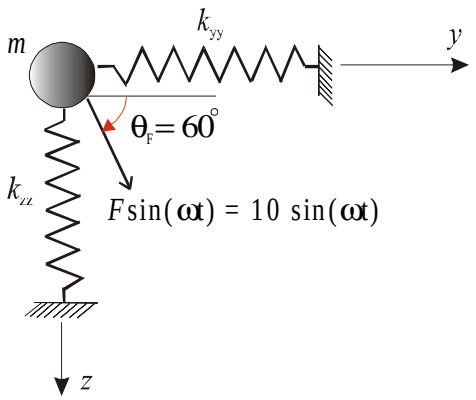

Figure 4.8: Single degree of freedom mass-spring model.

As the system is uncoupled the equation of motion in the *y* and *z* directions are,

$$m\ddot{y} + k_{yy}y = F\sin(\omega t)\cos(\theta_F) \tag{4.2}$$

$$m\ddot{z} + k_{zz}z = F\sin(\omega t)\sin(\theta_F) \tag{4.3}$$

The values for stiffness coefficients in Equations (4.2) and (4.3), obtained from the beam properties of the cantilever model of Figure 4.7, are as follow

$$k_{yy} = \frac{3EI_z}{l^3} \tag{4.4}$$

$$k_{zz} = \frac{3EI_y}{l^3} \tag{4.5}$$

Solving Equations (4.2) and (4.3) for the steady-state frequency response function gives

$$Y = \frac{F\cos(\theta_F)}{k_{yy} - m\omega^2} \tag{4.6}$$

$$Z = \frac{F\sin(\theta_F)}{k_{zz} - m\omega^2} \tag{4.7}$$

Free Vibration Response

Using the natural frequency equation for a single degree of freedom spring-mass system $\left(\omega_n = \sqrt{k/m}\right)$, the eigenvalues in the *y* and *z* directions when compared to output from 2DBEAM are:

Table 4.30: Analytical and 2DBEAM eigenvalue results for the uncoupled system.

Root	Calculated Frequency (Hz)	2DBEAM Frequency (Hz)
1y	8.06379290E+01	8.06379290E+01
1z	5.09999043E+01	5.09999043E+01

The resulting mode shape of the two eigenvalues is found in Figure 4.9 and Figure 4.10.

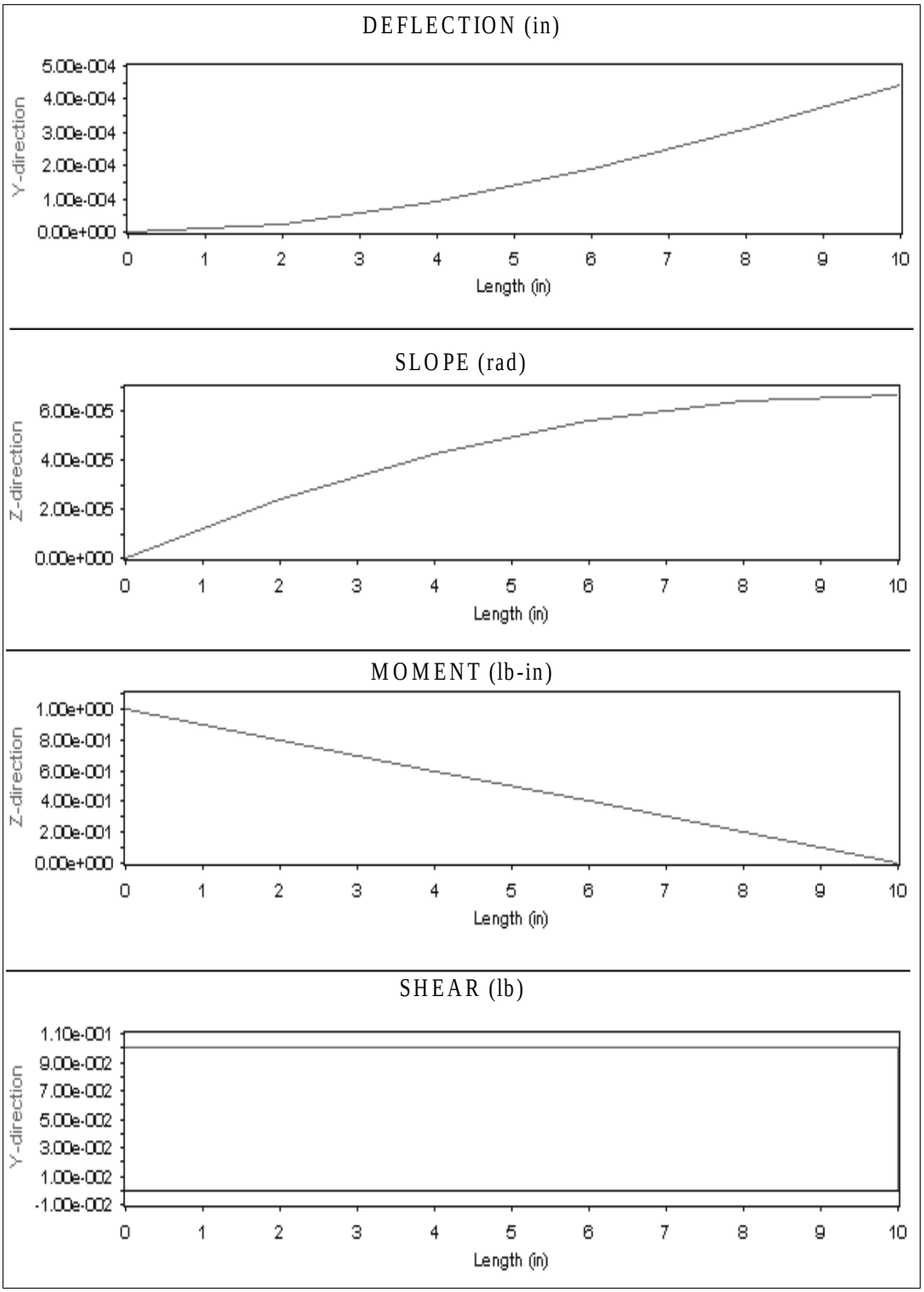

Figure 4.9: Mode shape corresponding to natural frequency of 80.638 Hz (Root 1y)

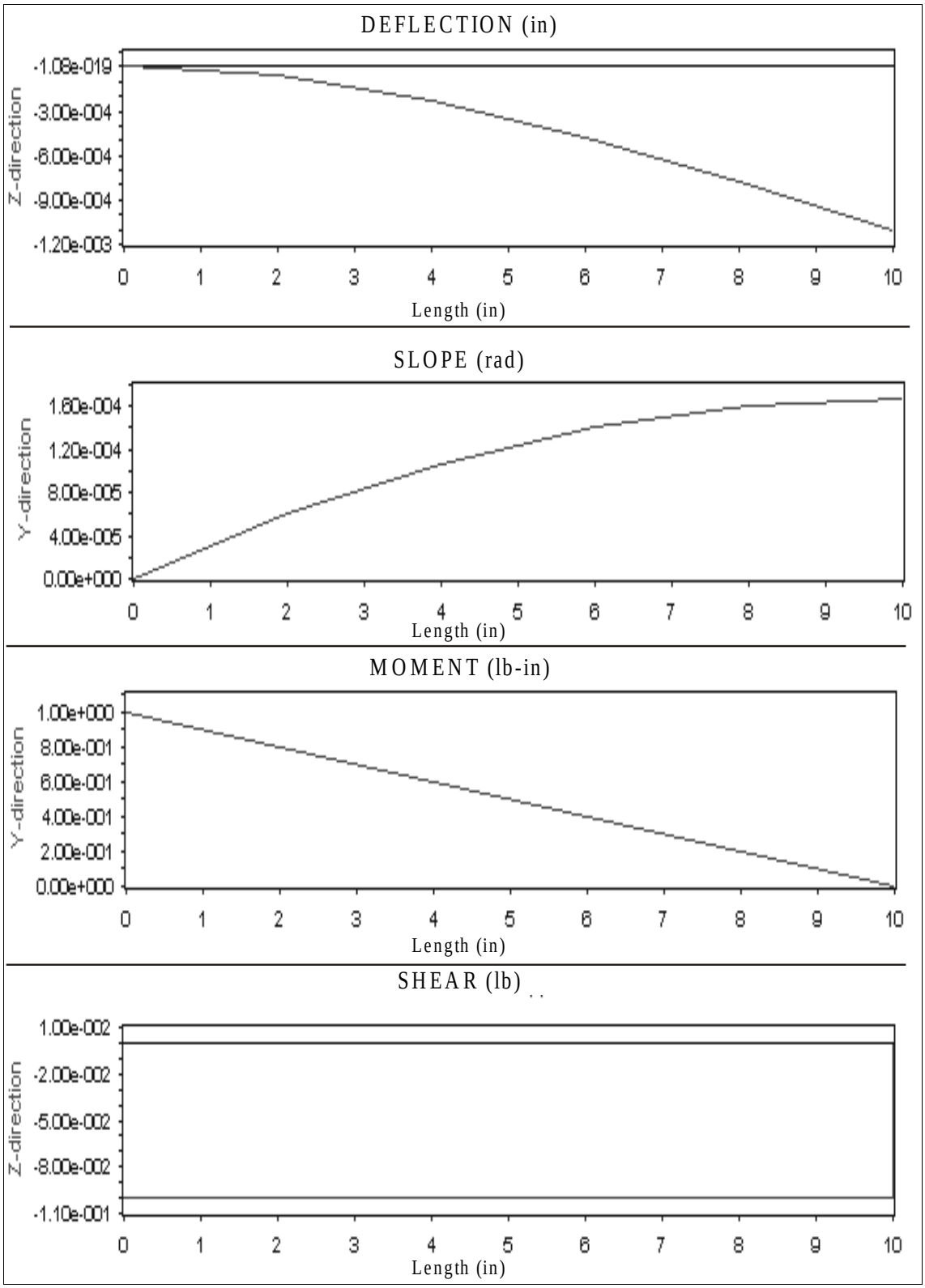

Figure 4.10: Mode shape corresponding to natural frequency of 51 Hz (Root 1z).

Forced Dynamic Response

On substituting numerical values for the parameters of Equations (4.6) and (4.7), the maximum amplitudes of oscillation for the forcing frequency of 30 Hz are,

$$Y_{max} = 2.5792072\text{E-}02 \text{ in}$$

$$Z_{max} = 1.47138059\text{E-}01 \text{ in.}$$

The forced response deflection results from 2DBEAM for the cantilever of Figure 4.7 have been tabulated in Table 4.30.

Table 4.31: Uncoupled 2DBEAM forced response for forcing frequency of 30 Hz.

Axial Location (in)	**Deflection-y (in)**	**Deflection-z (in)**
0.00E+00	0.000000E+00	0.000000E+00
1.00E+00	3.739851E-04	2.133502E-03
2.00E+00	1.444356E-03	8.239731E-03
3.00E+00	3.133737E-03	1.787727E-02
4.00E+00	5.364751E-03	3.060472E-02
5.00E+00	8.060023E-03	4.598064E-02
6.00E+00	1.114218E-02	6.356364E-02
7.00E+00	1.453383E-02	8.291230E-02
8.00E+00	1.815762E-02	1.035852E-01
9.00E+00	2.193616E-02	1.251409E-01
1.00E+01	**2.579207E-02**	**1.471381E-01**

In Table 4.30 the maximum deflections in the *y* and *z* direction, occurring at the axial location of 10 in, correspond to the Y_{max} and Z_{max} values obtained through analytical Equations (4.6) and (4.7).

Frequency Response

To perform a frequency response analysis of the system of Figure 4.7, the far right end point (axial location of 10 in) is evaluated analytically using Equations (4.6) and (4.7). The maximum oscillation amplitudes, Y_{max} and Z_{max}, are evaluated for a range of

frequencies. Chosen here is the frequency range around the natural frequencies of uncoupled system.

The frequency response output from 2DBEAM and the analytical solution are plotted for the *y*-direction in Figure 4.9 and for the *z*-direction in Figure 4.10.

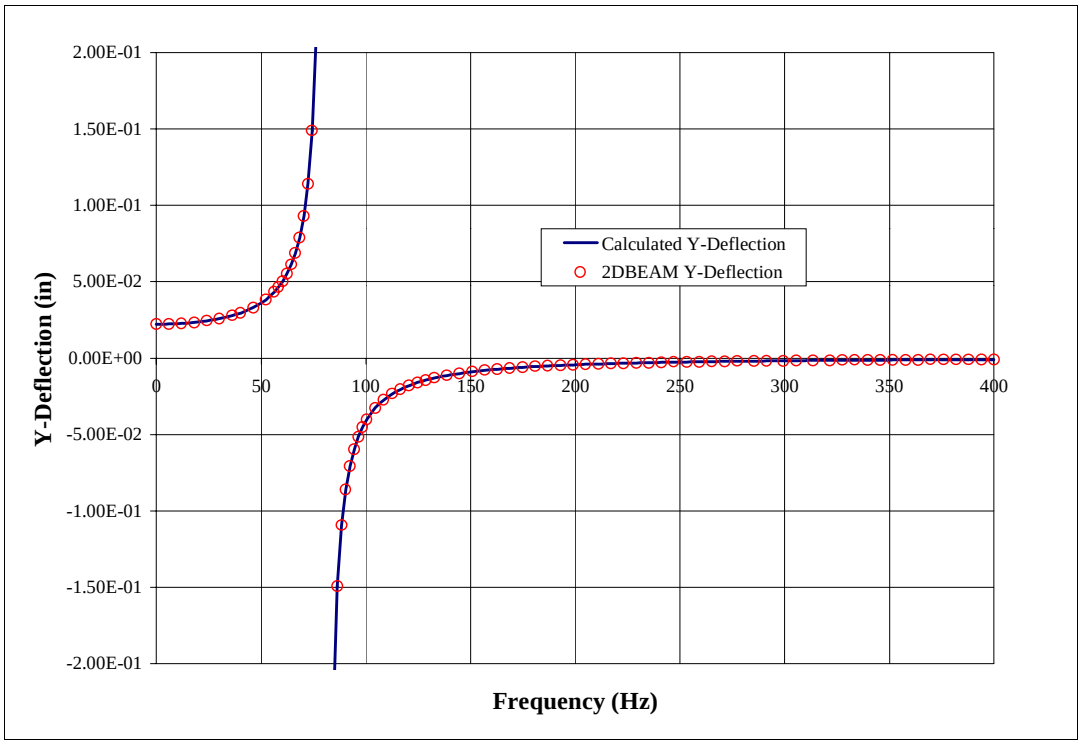

Figure 4.9: Analytically calculated and 2DBEAM frequency response in *y*-direction.

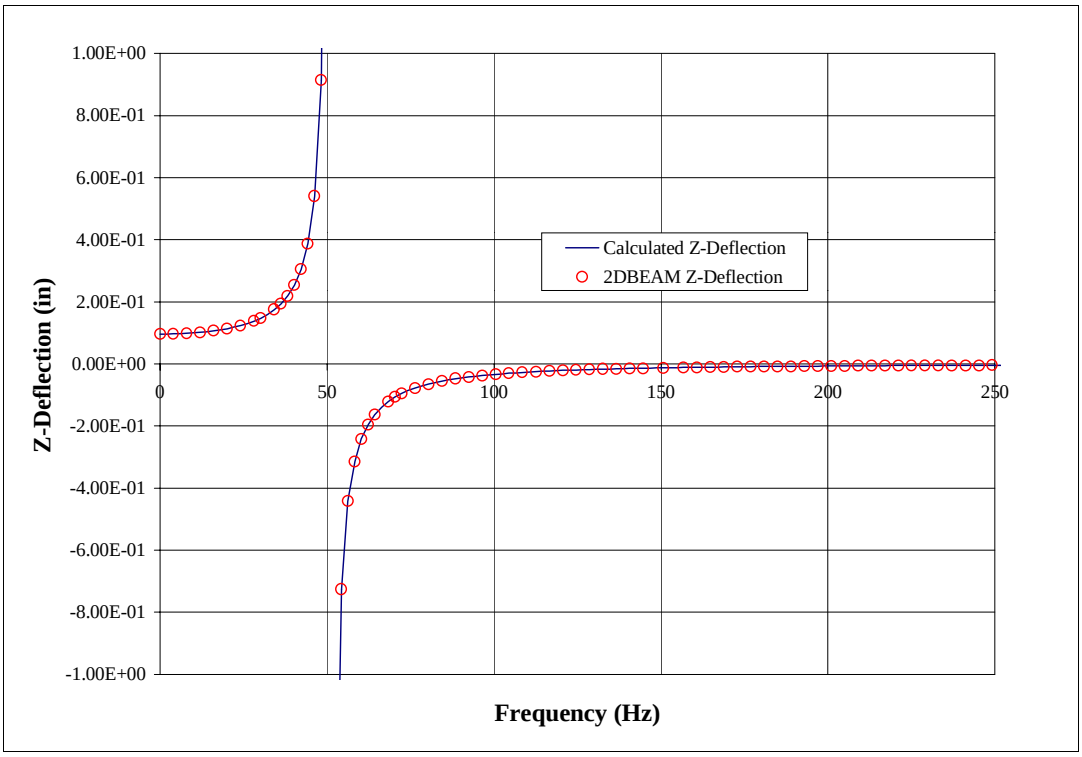

Figure 4.10: Analytically calculated and 2DBEAM frequency response in *z*-direction.

As seen in Figures 4.9 and 4.10, the output data points from the 2DBEAM program closely match the calculated curves obtained from the analytical equations.

4.3.2 Coupled Massless Elastic Beam Example

To verify a coupled forced response and frequency response analyses of 2DBEAM, the model of Figure 4.7 has been modified to include the cross coupled stiffness coefficients, k_{yz} and k_{zy}. To perform hand calculation for the responses, the equivalent system model shown in Figure 4.10 is used. The numerical values for the constant cross coupling stiffness are depicted in the figure.

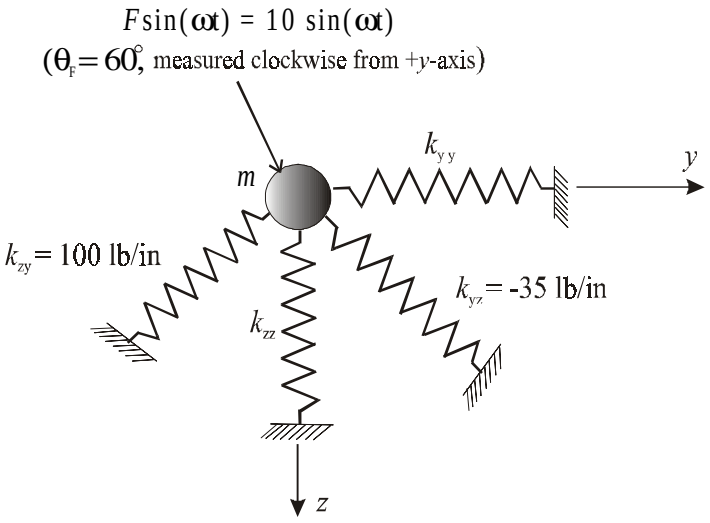

Figure 4.11: Mass-springs model.

To simplify the hand calculation, the harmonic excitation in Figure 4.10 is resolved into its y and z components giving,

$$F_y \sin(\omega t) = F \sin(\omega t)\cos(\theta_F) \tag{4.8a}$$

$$F_z \sin(\omega t) = F \sin(\omega t)\sin(\theta_F) \tag{4.8b}$$

The equations of motion for the system are,

$$m\ddot{y} + k_{yy}y + k_{yz}z = F_y \sin(\omega t) \tag{4.9}$$

$$m\ddot{z} + k_{zz}z + k_{zy}y = F_z \sin(\omega t) \tag{4.10}$$

Assembling Equations (4.9) and (4.10) into a matrix format, for easier manipulation, gives

$$\begin{bmatrix} m & 0 \\ 0 & m \end{bmatrix}\begin{Bmatrix} \ddot{y} \\ \ddot{z} \end{Bmatrix} + \begin{bmatrix} k_{yy} & k_{yz} \\ k_{zy} & k_{zz} \end{bmatrix}\begin{Bmatrix} y \\ z \end{Bmatrix} = \begin{Bmatrix} F_y \sin(\omega t) \\ F_z \sin(\omega t) \end{Bmatrix} \tag{4.11}$$

The solution for this undamped system can be assumed to be

$$\begin{Bmatrix} y \\ z \end{Bmatrix} = \begin{Bmatrix} Y \\ Z \end{Bmatrix} \sin(\omega t) \tag{4.12}$$

After performing relevant substitutions and matrix evaluations, the resulting equations obtained are

$$Y = \frac{-F_z k_{yz} + F_y (k_{zz} - m\omega^2)}{m^2(\omega_z^2 - \omega^2)(\omega_y^2 - \omega^2) - k_{zy} k_{yz}} \tag{4.13}$$

$$Z = \frac{F_z (k_{yy} - m\omega^2) - F_y k_{zy}}{m^2(\omega_z^2 - \omega^2)(\omega_y^2 - \omega^2) - k_{zy} k_{yz}} \tag{4.14}$$

where ω_y and ω_z are the natural frequencies (obtained from the direct stiffness) in the *y* and *z* directions, respectively.

Free Vibration Response

With the external excitation playing no part in obtaining the natural frequencies and mode shapes of the system of Figure 4.11, premultiplying the equation of motion by the inverse of the mass matrix and assuming harmonic motion ($\ddot{y} = -\omega^2 y$ and $\ddot{z} = -\omega^2 z$) gives the matrix equation

$$\begin{bmatrix} k_{yy} - m\omega^2 & k_{yz} \\ k_{zy} & k_{zz} - m\omega^2 \end{bmatrix} \begin{Bmatrix} y \\ z \end{Bmatrix} = \begin{Bmatrix} 0 \\ 0 \end{Bmatrix} \tag{4.15}$$

The *characteristic equation* from Equation (4.15) can re-written as Equation (4.16).

$$\left(1 - \frac{\omega^2}{\omega_z^2}\right)\left(1 - \frac{\omega^2}{\omega_y^2}\right) - k_{zy} k_{yz} = 0 \tag{4.16}$$

Solving for Equation (4.16) gives

$$\omega_{n\,1,2}^2 = \frac{\omega_z^2 + \omega_y^2}{2} \pm \sqrt{\left(\frac{\omega_z^2 - \omega_y^2}{2}\right)^2 + \left(\frac{k_{zy}k_{yz}}{k_{zz}k_{yy}}\right)\omega_z^2\omega_y^2} \tag{4.17}$$

In Table 4.32 the output from 2DBEAM is compared to roots from Equation (4.17).

Table 4.32: Analytical and 2DBEAM eigenvalue results for the coupled system.

Root	Calculated Frequency (Hz)	2DBEAM Frequency (Hz)
1	6.01039636E+01	6.01039636E+01
2	7.41011430E+01	7.41011430E+01

The mode shapes of the system are evaluated from the adjoint matrix of Equation (4.15) in which the eigenvalues are substituted. The amplitude ratios were normalized to one and gave,

$$\phi_1 = \begin{Bmatrix} 0.35 \\ 1.00 \end{Bmatrix} \text{ and } \phi_2 = \begin{Bmatrix} 1.00 \\ 1.00 \end{Bmatrix}$$

where ϕ_1 is the normal mode for the first eigenvalue

and ϕ_2 is the normal mode for the second eigenvalue.

The output from 2DBEAM has been tabulated in Table 4.33 and the mode shape deflection curves of the two eigenvalues are graphically illustrated in Figures 4.14 and Figure 4.15. Note that the *y* to *z* ratios of the deflection of each eigenvalue, at the end mass location (bold face typed in Table 4.33), when normalized to unity gives the normal modes that were calculated by hand.

Table 4.33: Mode shape data for natural frequencies of 60.104 Hz and 74.101 Hz.

Axial Location (in)	Root 1 = 60.104 Hz		Root 2 = 74.101 Hz	
	Deflection-y (in)	Deflection-z (in)	Deflection-y (in)	Deflection-z (in)
0.00E+00	0.000000E+00	0.000000E+00	0.000000E+00	0.000000E+00
2.00E+00	-2.177778E-05	-6.222222E-05	-6.222222E-05	-6.222222E-05
4.00E+00	-8.088889E-05	-2.311111E-04	-2.311111E-04	-2.311111E-04
6.00E+00	-1.680000E-04	-4.800000E-04	-4.800000E-04	-4.800000E-04
8.00E+00	-2.737778E-04	-7.822222E-04	-7.822222E-04	-7.822222E-04
1.00E+01	**-3.888889E-04**	**-1.111111E-03**	**-1.111111E-03**	**-1.111111E-03**

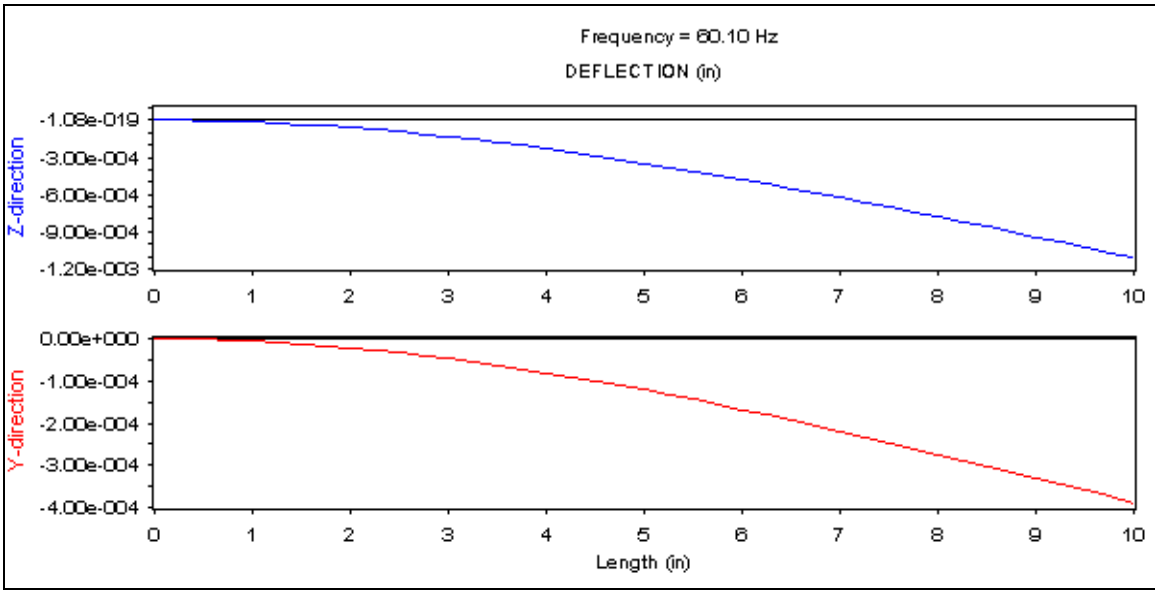

Figure 4.14: Mode shape of the natural frequency of 60.104 Hz.

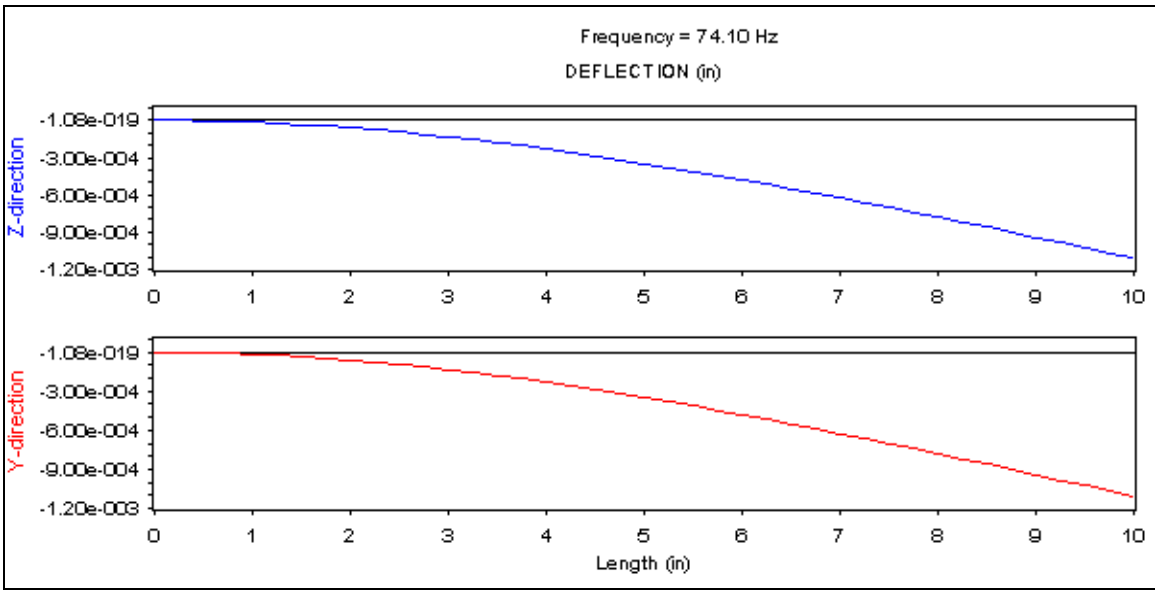

Figure 4.15: Mode shape of the natural frequency of 74.101 Hz.

Forced Dynamic Response

Evaluating Equations (4.13) and (4.14) for the forcing frequency of 30 Hz give

$$Y_{max} = 4.00667367\text{E-}02 \text{ in}$$

$$Z_{max} = 7.90645154\text{E-}02 \text{ in.}$$

The forced response *y* and *z*-deflection results from 2DBEAM for the coupled model of Figure 4.7 are located in Table 4.34.

Table 4.34: Coupled 2DBEAM forced response for forcing frequency of 30 Hz.

Axial Location (in)	Deflection-y (in)	Deflection-z (in)
0.00E+00	0.000000E+00	0.000000E+00
1.00E+00	5.809677E-04	1.146435E-03
2.00E+00	2.243737E-03	4.427613E-03
3.00E+00	4.868109E-03	9.606339E-03
4.00E+00	8.333881E-03	1.644542E-02
5.00E+00	1.252086E-02	2.470766E-02
6.00E+00	1.730883E-02	3.415587E-02
7.00E+00	2.257761E-02	4.455285E-02
8.00E+00	2.820698E-02	5.566142E-02
9.00E+00	3.407676E-02	6.724437E-02
1.00E+01	**4.006674E-02**	**7.906451E-02**

The bold face type in Table 4.34 highlights the maximum deflections in the *y* and *z* directions obtained using 2DBEAM. These values correspond to the Y_{max} and Z_{max} values obtained through analytical Equations (4.13) and (4.14).

Frequency Response

The frequency response of the coupled test example of Figure 4.10 is first calculated using Equations (4.13) and (4.14). The results from the equations are then compared to the output from 2DBEAM. The frequency range used in the evaluation is around the natural frequencies of coupled system. The frequency response output from 2DBEAM and the analytical solution are plotted in Figure 4.16 and in Figure 4.17.

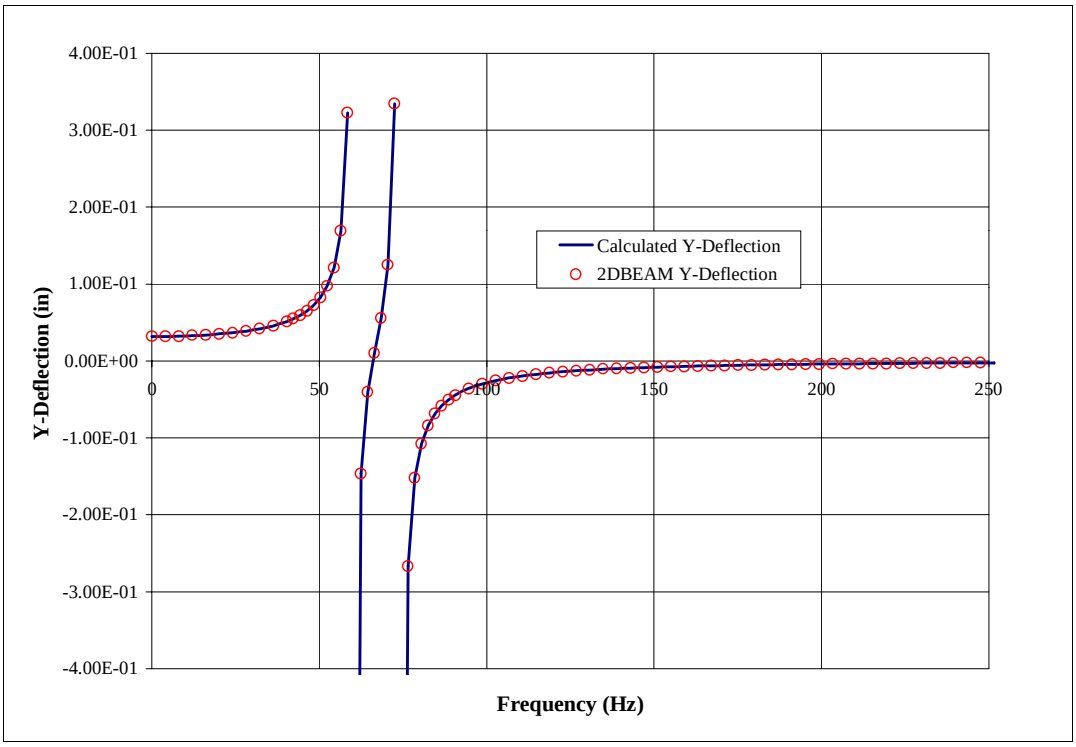

Figure 4.16: Analytically calculated and 2DBEAM frequency response in *y*-direction.

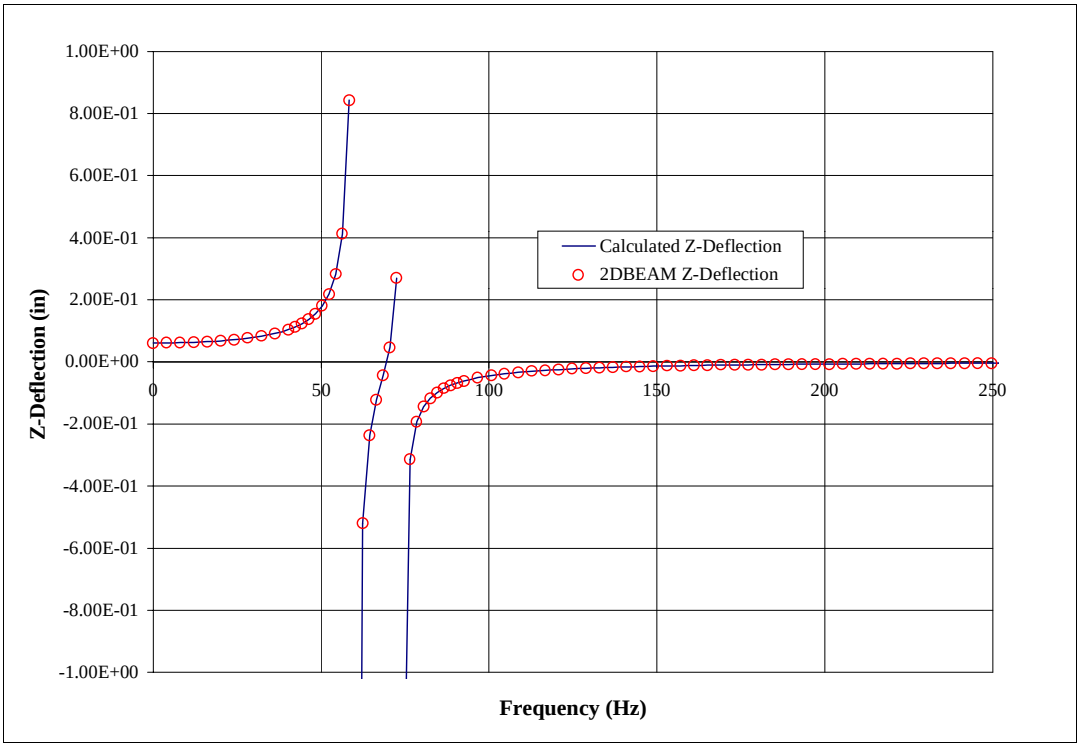

Figure 4.17: Analytically calculated and 2DBEAM frequency response in *z*-direction.

Figures 4.16 and 4.17 show the output data points from 2DBEAM lie on the curves from the analytical equations. This demonstrates the accuracy of the frequency response results obtained from the 2DBEAM program.

In the signed undamped frequency response curves of Figures 4.16 and 4.17, as frequency increases from zero to the first resonance frequency the response increases toward positive infinity. As frequency increases further, the response wraps from positive infinity around to negative infinity. This is the 180 degree phase shift seen in the conventional magnitude and phase representation of the same response (see Harris and Crede [25]). Beyond the first resonance the response moves from negative infinity toward zero where it reaches anti-resonance. Even further increase in frequency causes a positive increase in response until the second resonance frequency is reached with a response that approaches positive infinity, wraps around to negative infinity, and then comes negatively toward an asymptotic approach to zero.

4.4 Forced Dynamic and Frequency Responses of a Rotor

To illustrate the coupled rotor capability of 2DBEAM, the following example has been taken from Rao [25]. A visual model of this rotor is shown in Figure 4.14. The rotor is mounted on two 4 axial groove bearings. The bearings are 2.54 cm in diameter and 1.27 cm long. They have a radial clearance of 0.00254 cm and the viscosity at the operating temperature is 0.0242 N-sec/m^2. The rotors shaft stiffness at the point the mass is lumped (mid span of the shaft) was given as 1.387E+07 N/m. The stiffness of the shaft at this point (mid span of the shaft) is

$$K_{yy} = \frac{48EI_z}{l^3} \tag{4.15}$$

$$K_{zz} = \frac{48EI_y}{l^3} \tag{4.16}$$

From Equations (4.15) and (4.16) the geometry and material parameters to input into 2DBEAM were obtained and these values are shown in Figure 4.14.

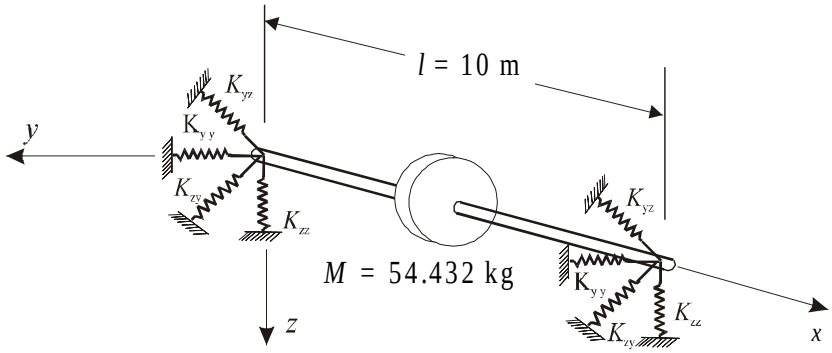

Figure 4.14: Rotor on fluid film bearings, adapted from Rao [26].

The direct and cross-coupled stiffness coefficients for the bearing at a speed of 4500 rpm as given by Rao are:

K_{zz} = 4.16E+07 N/m; K_{yy} = 1.01E+07 N/m

K_{zy} = 3.12E+07 N/m; K_{yz} = 4.16E+05 N/m.

Equation (4.17) found in Rao [27] is used in evaluating the analytical eigenvalues of the system.

$$p_{1,2}^2 = \frac{\omega_1^2 + \omega_2^2}{2} \pm \sqrt{\left(\frac{\omega_1^2 - \omega_2^2}{2}\right)^2 + \mu_1 \mu_2 \omega_1^2 \omega_2^2} \tag{4.17}$$

where the parameters of the equation are given by the following equations,

$$\omega_1^2 = \frac{K_1}{M} \tag{4.18}$$

$$\omega_{21}^2 = \frac{K_2}{M} \tag{4.19}$$

$$\mu_1 = \frac{K_{12}}{K_1} \tag{4.20}$$

$$\mu_2 = \frac{K_{21}}{K_2} \tag{4.21}$$

$$K_1 = \frac{K[2K_{zz}(2K_{yy}+K)-4K_{zy}K_{yz}]}{(2K_{zz}+K)(2K_{yy}+K)-4K_{zy}K_{yz}} \tag{4.22}$$

$$K_2 = \frac{K[2K_{yy}(2K_{zz}+K)-4K_{zy}K_{yz}]}{(2K_{zz}+K)(2K_{yy}+K)-4K_{zy}K_{yz}} \tag{4.23}$$

$$K_{12} = \frac{2K_{zy}K^2}{(2K_{zz}+K)(2K_{yy}+K)-4K_{zy}K_{yz}} \tag{4.24}$$

$$K_{21} = \frac{2K_{yz}K^2}{(2K_{zz}+K)(2K_{yy}+K)-4K_{zy}K_{yz}} \tag{4.25}$$

The results obtained from the Equation (4.17), from 2DBEAM, and from those given by Rao (in which he also uses Equation (4.17) for calculating the eigenvalues) are found in Table 4.32.

Table 4.32: Eigenvalues from calculations, Rao text, and 2DBEAM.

Root	Calculated Frequency (Hz)	Rao Frequency (Hz)	2DBEAM Frequency (Hz)
1	61.340	61.587	61.340
2	74.431	74.602	74.431

The discrepancy between the results given in Rao's text, those obtained through the analytical equation, and from 2DBEAM could originate in the stiffness coefficients used. The stiffness coefficients used by Rao in his calculations may have been taken at a higher degree of accuracy than the one he provided in the text. The Rao coefficients were reported to 3 digits or about 1:416 while the results are off by at most 2:746. The slightly high error may be caused by accumulated numeric inaccuracies during successive multiplications.

Forced Dynamic Response

To perform the forced response, an unbalance (*Me*) of 54.432 kg-m is introduced in the model of Figure 4.14 at an angle θ of 45 degrees measures counter-clockwise from the positive *y*-axis.

The disc deflection, response of the rotor at mid span or at the axial location of 5 m, for a forcing frequency of 50 Hz is analytically calculated using Equations (4.27) and (4.28) adapted from Rao [27].

$$Y = \frac{-K_{21}Me\omega^2 \sin(\theta) + Me\omega^2 \cos(\theta)(K_1 - M\omega^2)}{(K_1 - M\omega^2)(K_2 - M\omega^2) - K_{12}K_{21}} \tag{4.27}$$

$$Z = \frac{Me\omega^2 \sin(\theta)(K_2 - M\omega^2)) + -K_{12}Me\omega^2 \cos(\theta)}{(K_1 - M\omega^2)(K_2 - M\omega^2) - K_{12}K_{21}} \tag{4.28}$$

The equations for the deflection of the shaft in the journal are functions of the disc deflection, the shaft stiffness at mid span, and bearing stiffnesses. These are provided by Rao [28] as

$$y_0 = K\frac{(2K_{zz} + K)Y - 2K_{yz}Z}{(2K_{zz} + K)(2K_{yy} + K) - 4K_{zy}K_{yz}} \tag{4.29}$$

$$z_0 = K\frac{(2K_{yy} + K)Z - 2K_{zy}Y}{(2K_{zz} + K)(2K_{yy} + K) - 4K_{zy}K_{yz}} \tag{4.30}$$

Evaluating Equations (4.27), (4.28), (4.29), and (4.30) gives *y* and *z* disc deflections as

Y = 1.379289E+00 m

Z = -1.985754E-01 m.

And the *y* and *z* shaft deflections in the journal as

y_0 = 5.711721E-01 m

z_0 = -3.955432E-01 m.

The 2DBEAM forced response output of deflection in *y* and *z* directions is found in Table 4.33

Table 4.33: 2DBEAM forced response for forcing frequency of 50 Hz.

Axial Location (m)	Deflection-y (m)	Deflection-z (m)
0.00E+00	**5.711721E-01**	**-3.955432E-01**
1.00E+00	8.103748E-01	-3.372408E-01
2.00E+00	1.030183E+00	-2.836655E-01
3.00E+00	1.211201E+00	-2.395447E-01
4.00E+00	1.334035E+00	-2.096056E-01
5.00E+00	**1.379289E+00**	**-1.985754E-01**
6.00E+00	1.334035E+00	-2.096056E-01
7.00E+00	1.211201E+00	-2.395447E-01
8.00E+00	1.030183E+00	-2.836655E-01
9.00E+00	8.103748E-01	-3.372408E-01
1.00E+01	**5.711721E-01**	**-3.955432E-01**

The bold face type of the axial locations of 0 m and 10 m match the analytically computed shaft deflections in the journal and the disc deflection at the axial location of 5 m corresponds to the hand calculated values.

Frequency Response

The analytically calculated frequency response from Equations (4.27) and (4.28) are compared to the 2DBEAM output by plotting the equations and program results. These results are shown in Figures 4.15 and 4.16.

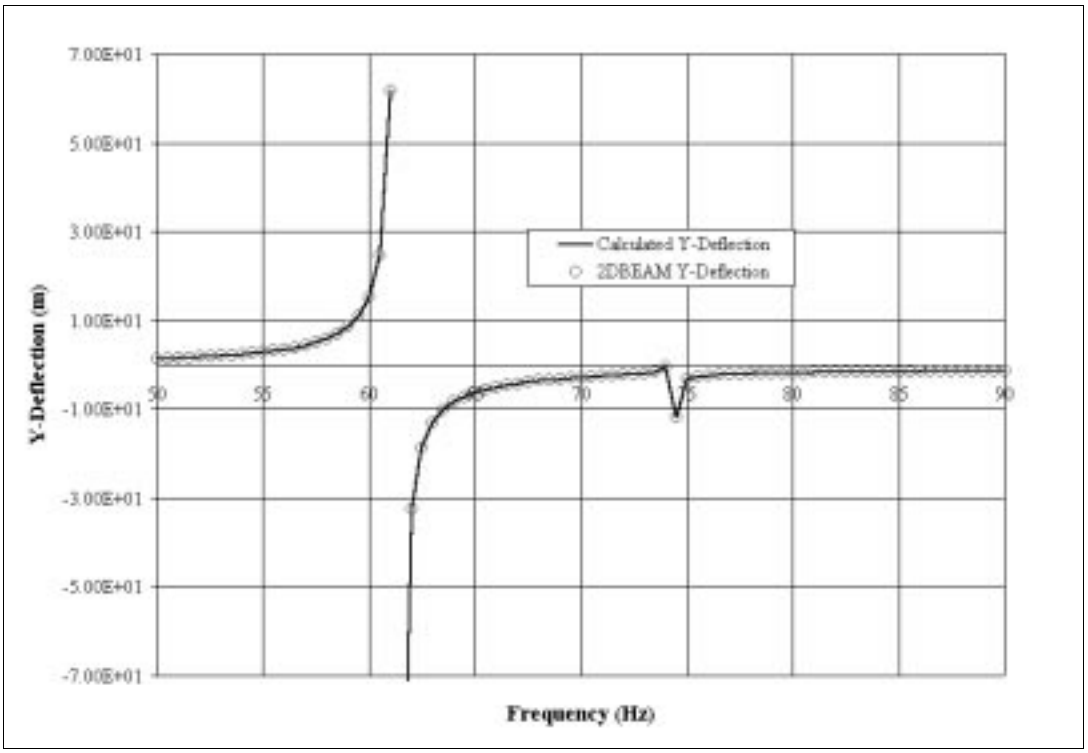

Figure 4.15: Analytically calculated and 2DBEAM frequency response in *y*-direction.

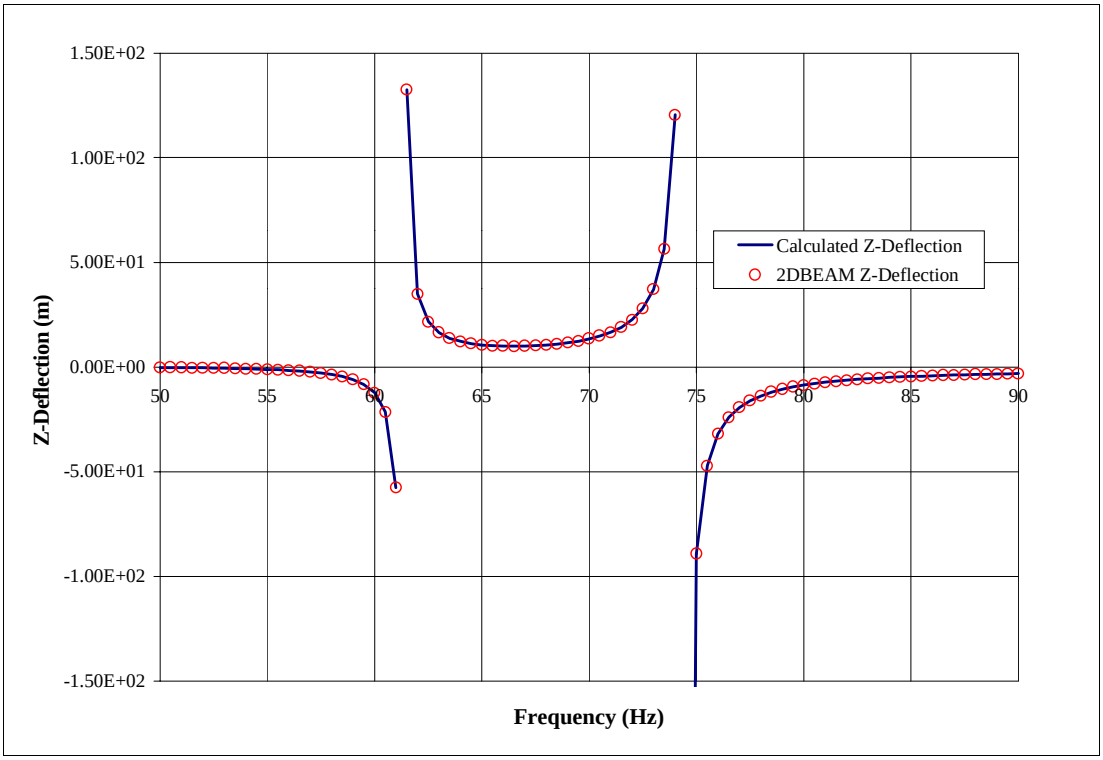

Figure 4.16: Analytically calculated and 2DBEAM frequency response in *z*-direction.

Figures 4.15 and 4.16 show a consistent match between the output from 2DBEAM and that of the analytical equations. Seen again in the figures is the infinity wraps explained earlier in Section 4.3.2. It is realized that some of the deflections shown are far in excess of the realistic linear elastic deflection of a shaft. This is an undamped result from a linear code and a linear model established by Rao. These type of results are expected when shaft running speeds approach system critical speeds. This occurs twice in the frequency range we are looking at here.

Chapter 5
Conclusions and Recommendations

5.1 Conclusions

A computer-aided analysis and design package, 2DBEAM, which performs the two-dimensional analyses of beams and rotors has been developed. 2DBEAM is capable of generating system eigenvalues automatically using the Muller root searching method, and of obtaining the corresponding eigenvectors. Also available in the package is the capability to perform static analysis, forced dynamic analysis, and frequency response analysis of a system. The analyses may be performed on models with and without cross-coupling stiffnesses. Responses are obtained for both the vertical and horizontal planes of motion. The code has been tested for all the types of analysis mentioned above and for uncoupled and coupled models. The results were consistent with the analytically and published solutions.

5.2 Recommendations

The following are suggestions for future work for this research:

- Only undamped systems can be modeled by 2DBEAM. In reality mechanical systems possess internal and external damping properties. Therefore, to model systems more accurately in dynamic situations, the capability of the user to input both structural and viscous damping should be added to the program.
- To increase the ability of the analysis of rotors, the feature of obtaining the critical speed map of a rotor system can be added.
- To enhance the rotor-bearing modeling capability, a subprogram can be included to provide users with the bearing stiffness coefficients over a range of running speeds.

The coefficients would be computed from the input information of the type of bearing desired (4 axial-groove, plain cylindrical, ball bearing, roller bearing, etc.) and properties such as length, diameter, radial clearance, viscosity at operating speed etc. of the bearing. It is realized that this effort alone would be a thesis unto itself.

- The forced dynamic response can be expanded to include phased harmonic forcing functions. The phased forcing functions are handled using complex number representation and arithmetic. This would be easy to include after the earlier suggested damping has been added to the program.
- The program can be extended to perform three-dimensional analyses of systems by adding the axial and torsional vibration computing capability. As this would enlarge the *transfer matrices* considerably, a major problem that would be encountered is the slow computation time of results.
- In expanding the *transfer matrices* to accommodate the three-dimensional analyses of systems, the additional modeling capability of allowing transverse loads to be applied in planes other than the principal planes of the body should be considered. Another consideration would be to allow the loads to act through points other than the shear center of the body. For a detailed look on such computations refer to Cook and Young [28]. Moreover, the program should be able to link beam sections with different orientations of principal axes.
- 2DBEAM has been developed using the Microsoft Visual Basic 4.0 language. Since Visual Basic 4.0 simply interprets the code on execution, it is recommended that future versions of 2DBEAM use the compiling capabilities of Visual Basic 5.0 or higher. This would improve the performance of the software package by significantly reducing the computation time.

Appendix A

Catalogue of Two-Dimensional Transfer Matrices used in 2DBEAM code

A.1 State Vector

The transfer matrices in this appendix correspond to the following *state vector*:

$$\{z\} = \begin{Bmatrix} w \\ \psi \\ M_y \\ V_z \\ \cdots \\ v \\ \vartheta \\ M_z \\ V_y \\ \cdots \\ 1 \end{Bmatrix} \tag{A.1}$$

Also used in following sections the symbol ω (angular displacement/time) which is the circular frequency of free vibration.

Note that matrices in this Appendix that were obtained from the Pestel and Leckie reference have changes in sign due to the difference in *state vectors* used.

A.2 Linear Support Stiffness and Cross-Coupled Support Stiffness

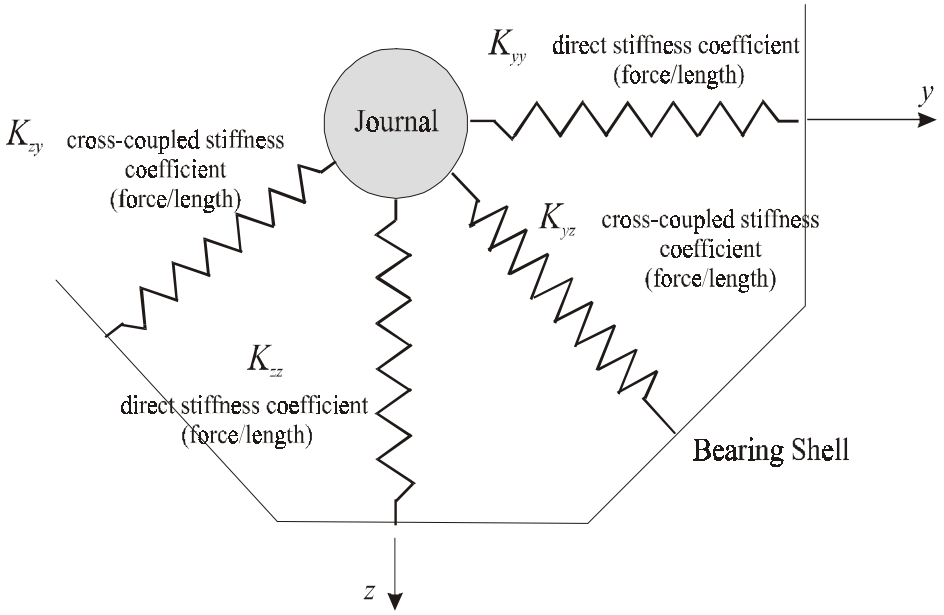

Figure A.1: Stiffness properties of fluid film in bearing, adapted from Rao [29].

The subscripts of the direct and cross-coupled stiffness coefficients mean the following:

K_{zz}: Force is in the *z*-direction and displacement is the *z*-direction

K_{yy}: Force is in the *y*-direction and displacement is the *y*-direction

K_{zy}: Force is in the *z*-direction and displacement is the *y*-direction

K_{yz}: Force is in the *y*-direction and displacement is the *z*-direction.

The *point transfer matrix* of Equation (A.2) has been compiled from equations found in Rao [30].

$$\{z\} = \left[\begin{array}{cccc:cccc:c} 1 & 0 & 0 & 0 & 0 & 0 & 0 & 0 & 0 \\ 0 & 1 & 0 & 0 & 0 & 0 & 0 & 0 & 0 \\ 0 & 0 & 1 & 0 & 0 & 0 & 0 & 0 & 0 \\ K_{zz} & 0 & 0 & 1 & K_{zy} & 0 & 0 & 0 & 0 \\ \hdashline 0 & 0 & 0 & 0 & 1 & 0 & 0 & 0 & 0 \\ 0 & 0 & 0 & 0 & 0 & 1 & 0 & 0 & 0 \\ 0 & 0 & 0 & 0 & 0 & 0 & 1 & 0 & 0 \\ K_{yz} & 0 & 0 & 0 & K_{yy} & 0 & 0 & 1 & 0 \\ \hdashline 0 & 0 & 0 & 0 & 0 & 0 & 0 & 0 & 1 \end{array}\right] \qquad \text{(A.2)}$$

A.3 Uncoupled two-dimensional Rotor-Housing-Ground Model

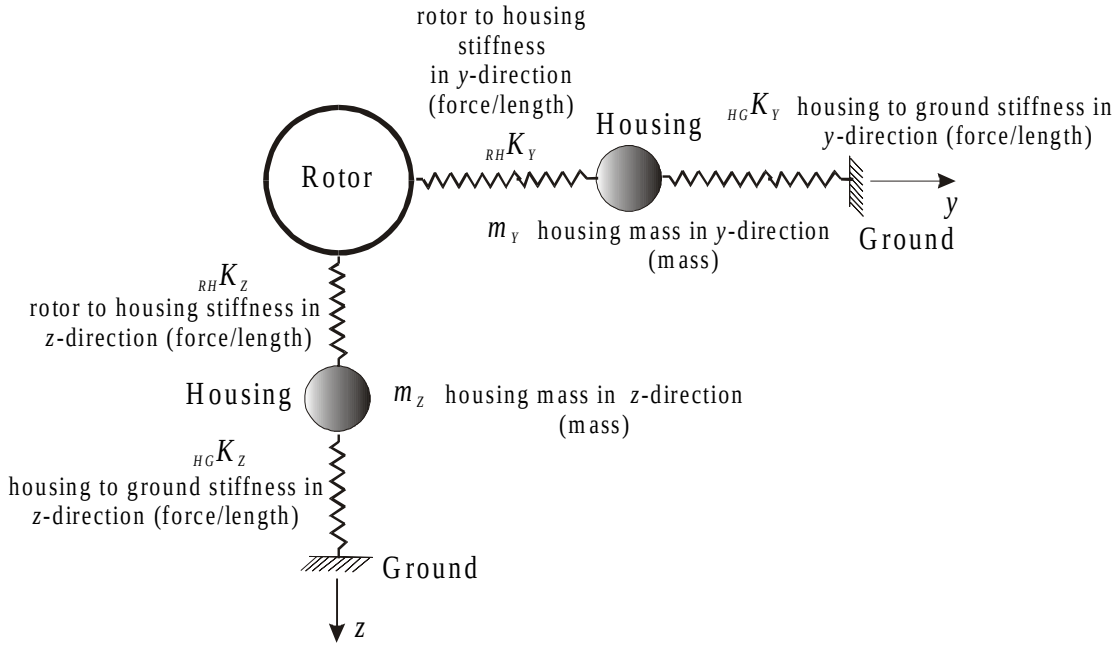

Figure A.2: Rotor-Housing-Ground Model.

The *point transfer matrix* of Equation (A.3) is an extended version of that found in Pestel and Leckie [31].

$$\{z\} = \left[\begin{array}{cccc:cccc:c} 1 & 0 & 0 & 0 & 0 & 0 & 0 & 0 & 0 \\ 0 & 1 & 0 & 0 & 0 & 0 & 0 & 0 & 0 \\ 0 & 0 & 1 & 0 & 0 & 0 & 0 & 0 & 0 \\ K_{Dz} & 0 & 0 & 1 & 0 & 0 & 0 & 0 & 0 \\ \hdashline 0 & 0 & 0 & 0 & 1 & 0 & 0 & 0 & 0 \\ 0 & 0 & 0 & 0 & 0 & 1 & 0 & 0 & 0 \\ 0 & 0 & 0 & 0 & 0 & 0 & 1 & 0 & 0 \\ 0 & 0 & 0 & 0 & K_{Dy} & 0 & 0 & 1 & 0 \\ \hdashline 0 & 0 & 0 & 0 & 0 & 0 & 0 & 0 & 1 \end{array}\right] \qquad \text{(A.3)}$$

where $$K_{Dz} = \frac{_{RH}K_Z(\,_{HG}K_Z - m_Z\omega^2)}{_{RH}K_Z + {}_{HG}K_Z - m_Z\omega^2} \text{ and } K_{Dy} = \frac{_{RH}K_Y(\,_{HG}K_Y - m_Y\omega^2)}{_{RH}K_Y + {}_{HG}K_Y - m_Y\omega^2} \qquad \text{(A.4)}$$

A.4 Massless Elastic Beam subjected to a Distributed Load at an Angle

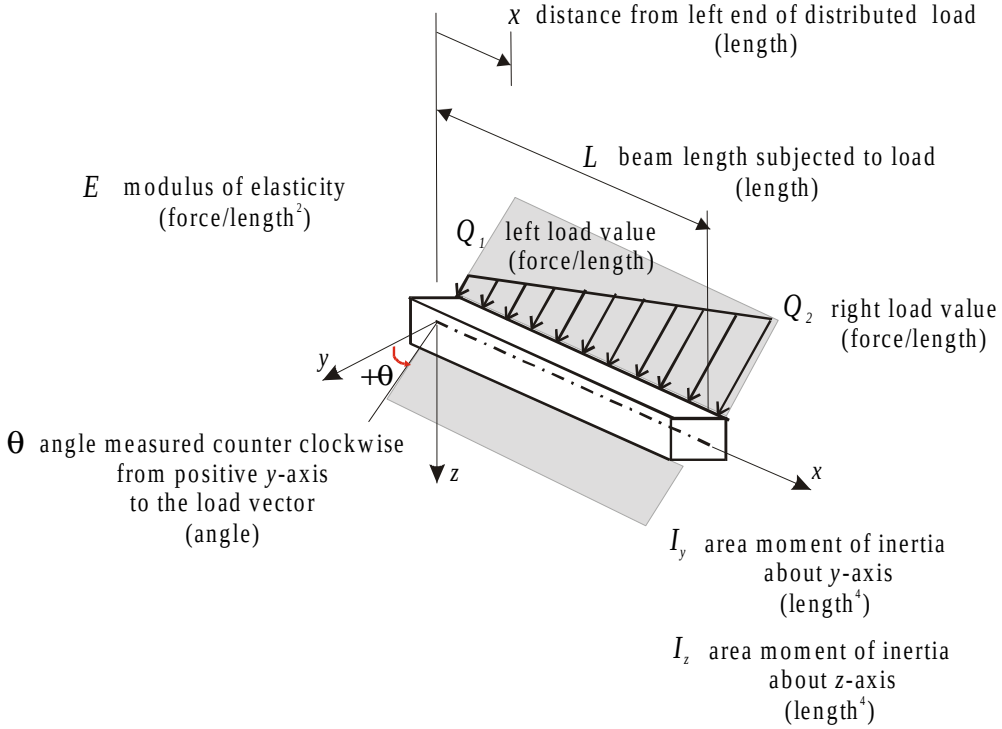

Figure A.3: Massless beam subjected to distributed load.

Pestel and Leckie [32] provide the *field transfer matrix* of Equation (A.5). The load components of the extension column are obtained from Pilkey [33].

$$\{z\} = \left[\begin{array}{cccc:cccc:c}
1 & -l & -\frac{l^2}{2EI_y} & -\frac{l^3}{6EI_y} & 0 & 0 & 0 & 0 & \frac{QZ*x^4}{24EI_y}+\frac{DQ_Z*x^5}{120EI_y} \\
0 & 1 & \frac{l}{EI_y} & \frac{l^2}{2EI_y} & 0 & 0 & 0 & 0 & -\frac{QZ*x^3}{6EI_y}-\frac{DQ_Z*x^4}{24EI_y} \\
0 & 0 & 1 & l & 0 & 0 & 0 & 0 & -\frac{QZ*x^2}{2}-\frac{DQ_Z*x^3}{6} \\
0 & 0 & 0 & 1 & 0 & 0 & 0 & 0 & -QZ*x-\frac{DQ_Z*x^2}{2} \\ \hdashline
0 & 0 & 0 & 0 & 1 & l & \frac{l^2}{2EI_z} & -\frac{l^3}{6EI_z} & \frac{QY*x^4}{24EI_z}+\frac{DQ_Y*x^5}{120EI_z} \\
0 & 0 & 0 & 0 & 0 & 1 & \frac{l}{EI_z} & -\frac{l^2}{2EI_z} & \frac{QY*x^3}{6EI_z}+\frac{DQ_Y*x^4}{24EI_z} \\
0 & 0 & 0 & 0 & 0 & 0 & 1 & -l & \frac{QY*x^2}{2}+\frac{DQ_Y*x^3}{6} \\
0 & 0 & 0 & 0 & 0 & 0 & 0 & 1 & -QY*x-\frac{DQ_Y*x^2}{2} \\ \hdashline
0 & 0 & 0 & 0 & 0 & 0 & 0 & 0 & 1
\end{array}\right] \quad \text{(A.5)}$$

where $$QZ = Q_1 \sin(\theta) \quad \text{and} \quad QY = Q_1 \cos(\theta) \quad \text{(A.6)}$$

$$DQ_Z = \frac{(Q_2 - Q_1)\sin(\theta)}{L} \quad \text{and} \quad DQ_Y = \frac{(Q_2 - Q_1)\cos(\theta)}{L} \quad \text{(A.7)}$$

A.5 Elastic Field with Distributed Mass on Elastic Foundation

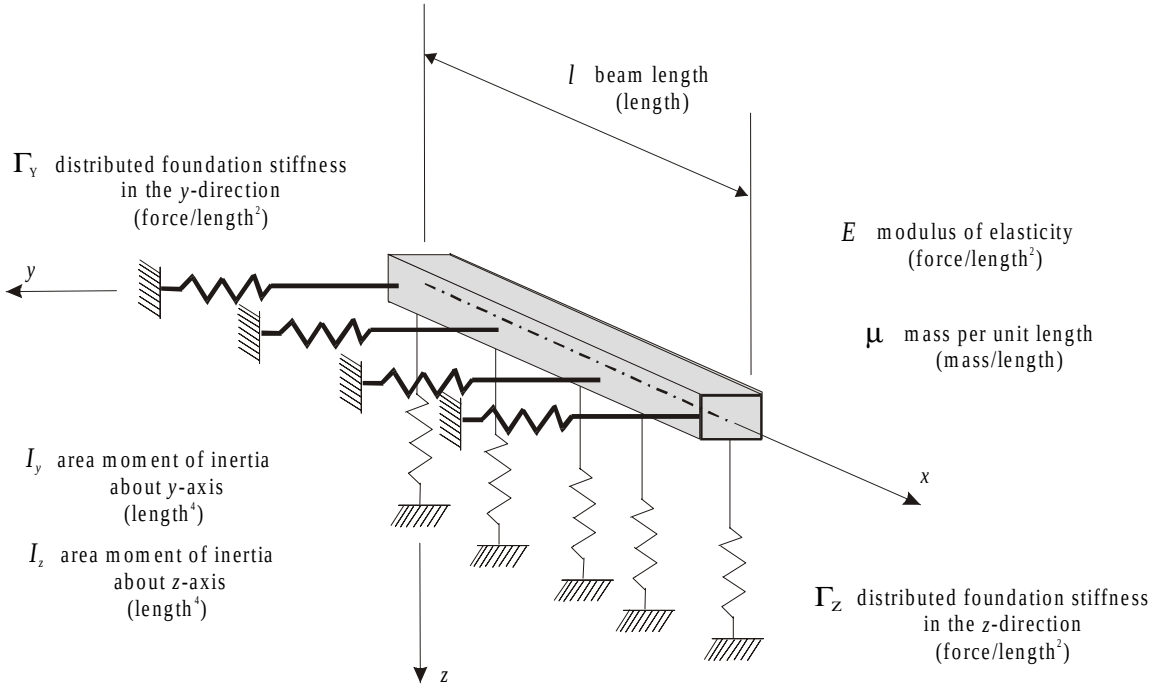

Figure A.4: Continuum beam on elastic foundation.

The *field transfer matrix* of Equation (A.8) has been extended from Pestel and Leckie [34].

$$\{z\}=\begin{bmatrix} -c_{0z} & -lc_{1z} & -a_z c_{2z} & -a_z l c_{3z} & 0 & 0 & 0 & 0 & 0 \\ -\frac{\beta_z^4}{l}c_{3z} & c_{0z} & \frac{a_z}{l}c_{1z} & a_z c_{2z} & 0 & 0 & 0 & 0 & 0 \\ -\frac{\beta_z^4}{a_z}c_{2z} & \frac{\beta_z^4 l}{a_z}c_{3z} & c_{0z} & lc_{1z} & 0 & 0 & 0 & 0 & 0 \\ -\frac{\beta_z^4}{a_z l}c_{1z} & \frac{\beta_z^4}{a_z}c_{2z} & \frac{\beta_z^4}{l}c_{3z} & c_{0z} & 0 & 0 & 0 & 0 & 0 \\ 0 & 0 & 0 & 0 & c_{0y} & lc_{1y} & a_y c_{2y} & -a_y l c_{3y} & 0 \\ 0 & 0 & 0 & 0 & \frac{\beta_y^4}{l}c_{3y} & c_{0z} & \frac{l}{EI_z} & -a_y c_{2y} & 0 \\ 0 & 0 & 0 & 0 & \frac{\beta_y^4}{a_y}c_{2y} & \frac{\beta_y^4 l}{a_y}c_{3y} & c_{0y} & -lc_{1y} & 0 \\ 0 & 0 & 0 & 0 & -\frac{\beta_y^4}{a_y l}c_{1y} & -\frac{\beta_y^4}{a_y}c_{2y} & -\frac{\beta_{yz}^4}{l}c_{3y} & -c_{0y} & 0 \\ 0 & 0 & 0 & 0 & 0 & 0 & 0 & 0 & 1 \end{bmatrix} \quad \text{(A.8)}$$

where

$$c_{0z}=\frac{1}{2}(\cosh\beta_z+\cos\beta_z) \qquad c_{0y}=\frac{1}{2}(\cosh\beta_y+\cos\beta_y)$$

$$c_{1z}=\frac{1}{2\beta_z}(\sinh\beta_z+\sin\beta_z) \qquad c_{1y}=\frac{1}{2\beta_y}(\sinh\beta_y+\sin\beta_y)$$

$$c_{2z}=\frac{1}{2\beta_z^2}(\cosh\beta_z-\cos\beta_z) \qquad c_{2y}=\frac{1}{2\beta_y^2}(\cosh\beta_y-\cos\beta_y)$$

$$c_{3z}=\frac{1}{2\beta_z^3}(\sinh\beta_z-\sin\beta_z) \qquad c_{3y}=\frac{1}{2\beta_y^3}(\sinh\beta_y-\sin\beta_y)$$

$$a_z=\frac{l^2}{EI_y} \qquad a_y=\frac{l^2}{EI_z}$$

$$\beta_z^4=\frac{\mu\omega^2-\Gamma_z}{EI_y}l^4 \qquad \beta_y^4=\frac{\mu\omega^2-\Gamma_y}{EI_z}l^4$$

A.6 Elastic Field with Distributed Mass, Shear Deformation, and Rotary Inertia

The *field transfer matrix* of Equation (A.9) is located in Pestel and Leckie [35]. For this matrix only the extension column has not been included.

Nomenclature:

E	Modulus of elasticity
G	Shear modulus
$GA_{S_y} = \frac{GA}{K_{S_y}}$	Shear stiffness in *y*-direction (K_{S_y} = form factor in *y*-direction)
$GA_{S_z} = \frac{GA}{K_{S_z}}$	Shear stiffness in *z*-direction (K_{S_z} = form factor in *z*-direction)
EI_y	Bending stiffness about *y*-axis
EI_z	Bending stiffness about *z*-axis
μ	Mass per unit length
i_y	Radius of gyration of cross-sectional area about *y*-axis
i_z	Radius of gyration of cross-sectional area about *z*-axis
U	Transfer matrix

$$h = \begin{cases} -1 & \text{for bending vibration} \\ +1 & \text{for rotating shaft (equal angular direction of whirl and rotation)} \\ -3 & \text{for rotating shaft (opposite angular direction of whirl and rotation)} \end{cases}$$

$$U = \left[\begin{array}{c:c} A & 0 \\ \hdashline 0 & B \end{array}\right] \tag{A.9}$$

The *A* and *B* components of Equation (A.9) are as follow:

$$A=\begin{bmatrix} -(c_0-\sigma_z c_2) & -l[c_1-(\sigma_z+\tau_z)c_3] & -a_z c_2 & -\frac{a_z l}{\beta_z^4}[-\sigma_z c_1+(\beta_z^4+\sigma_z^2)c_3] \\ -\frac{\beta_z^4}{l}c_3 & c_0-\tau_z c_2 & \frac{a_z}{l}(c_1-\tau_z c_3) & a_z c_2 \\ -\frac{\beta_z^4}{a_z}c_2 & \frac{l}{a_z}[-\tau_z c_1+(\beta_z^4+\tau_z^2)c_3] & (c_0-\tau_z c_2) & l[c_1-(\sigma_z+\tau_z)c_3] \\ -\frac{\beta_z^4}{a_z l}(c_1-\sigma_z c_3) & \frac{\beta_z^4}{a_z}c_2 & \frac{\beta_z^4}{l}c_3 & (c_0-\sigma_z c_2) \end{bmatrix}$$

$$B=\begin{bmatrix} (c_0-\sigma_y c_2) & l[c_1-(\sigma_y+\tau_y)c_3] & a_y c_2 & -\frac{a_y l}{\beta_y^4}[-\sigma_y c_1+(\beta_y^4+\sigma_y^2)c_3] \\ \frac{\beta_y^4}{l}c_3 & c_0-\tau_y c_2 & \frac{a_y}{l}(c_1-\tau_y c_3) & -a_y c_2 \\ \frac{\beta_y^4}{a_y}c_2 & \frac{l}{a_y}[-\tau_y c_1+(\beta_y^4+\tau_y^2)c_3] & (c_0-\tau_y c_2) & -l[c_1-(\sigma_y+\tau_y)c_3] \\ -\frac{\beta_y^4}{a_y l}(c_1-\sigma_y c_3) & -\frac{\beta_y^4}{a_y}c_2 & -\frac{\beta_y^4}{l}c_3 & -(c_0-\sigma_y c_2) \end{bmatrix}$$

where,

$$a_z=\frac{l^2}{EI_y} \qquad a_y=\frac{l^2}{EI_z}$$

$$\beta_z^4=\frac{\mu\omega^2}{EI_y}l^4 \qquad \beta_y^4=\frac{\mu\omega^2}{EI_z}l^4$$

$$\sigma_z=\frac{\mu\omega^2}{GA_{Sz}}l^2 \qquad \sigma_y=\frac{\mu\omega^2}{GA_{Sy}}l^2$$

$$\tau_z=-\frac{l^2}{EI_y}(h\mu i_y^2\omega^2) \qquad \tau_y=-\frac{l^2}{EI_z}(h\mu i_z^2\omega^2)$$

$$\lambda_{1,2}=+\sqrt{\sqrt{\beta_{(y,z)}^4+\frac{1}{4}(\sigma_{(y,z)}-\tau_{(y,z)})^2}\mp\frac{1}{2}(\sigma_{(y,z)}+\tau_{(y,z)})}$$

$$c_{0(y,z)}=\Lambda(\lambda_2^2\cosh\lambda_1+\lambda_1^2\cos\lambda_2)$$

$$c_{1(y,z)}=\Lambda\left(\frac{\lambda_2^2}{\lambda_1}\sinh\lambda_1+\frac{\lambda_1^2}{\lambda_2}\sin\lambda_2\right)$$

$$c_{2(y,z)}=\Lambda(\cosh\lambda_1-\cos\lambda_2)$$

$$c_{3(y,z)}=\Lambda\left(\frac{1}{\lambda_1}\sinh\lambda_1-\frac{1}{\lambda_2}\sin\lambda_2\right)$$

A.7 Eccentric Point Mass with Rotary Inertia

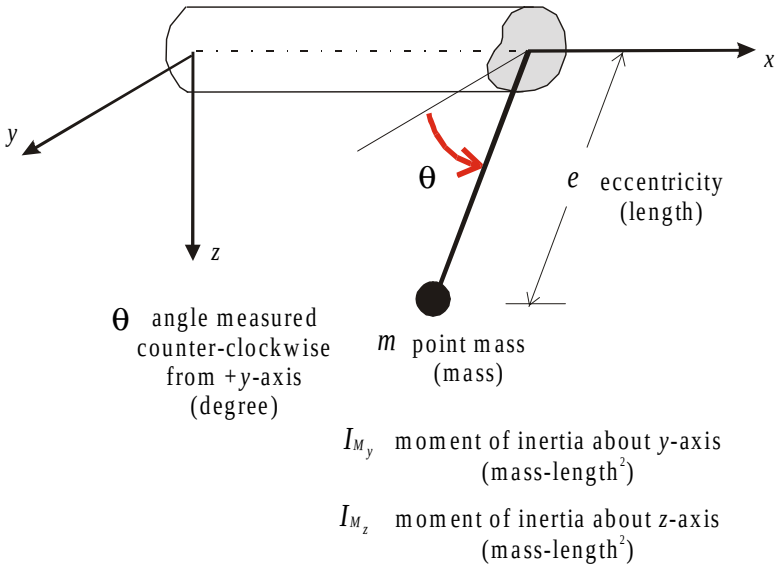

Figure A.6: Eccentric point mass with rotary inertia.

The *point transfer matrix* has been combined from matrices found in Pestel and Leckie [36].

$$\{z\} = \left[\begin{array}{cccc:cccc:c} 1 & 0 & 0 & 0 & 0 & 0 & 0 & 0 & 0 \\ 0 & 1 & 0 & 0 & 0 & 0 & 0 & 0 & 0 \\ 0 & hI_{M_y}\omega^2 & 1 & 0 & 0 & 0 & 0 & 0 & 0 \\ -m\omega^2 & 0 & 0 & 1 & 0 & 0 & 0 & 0 & -me\omega^2\sin(\theta) \\ \hdashline 0 & 0 & 0 & 0 & 1 & 0 & 0 & 0 & 0 \\ 0 & 0 & 0 & 0 & 0 & 1 & 0 & 0 & 0 \\ 0 & 0 & 0 & 0 & 0 & hI_{M_z}\omega^2 & 1 & 0 & 0 \\ 0 & 0 & 0 & 0 & -m\omega^2 & 0 & 0 & 1 & -me\omega^2\cos(\theta) \\ \hdashline 0 & 0 & 0 & 0 & 0 & 0 & 0 & 0 & 1 \end{array}\right] \quad \text{(A.10)}$$

where $h = \begin{cases} -1 & \text{for bending vibration} \\ +1 & \text{for rotating shaft (equal angular direction of whirl and rotation)} \\ -3 & \text{for rotating shaft (opposite angular direction of whirl and rotation)} \end{cases}$

A.8 Tuned Absorber

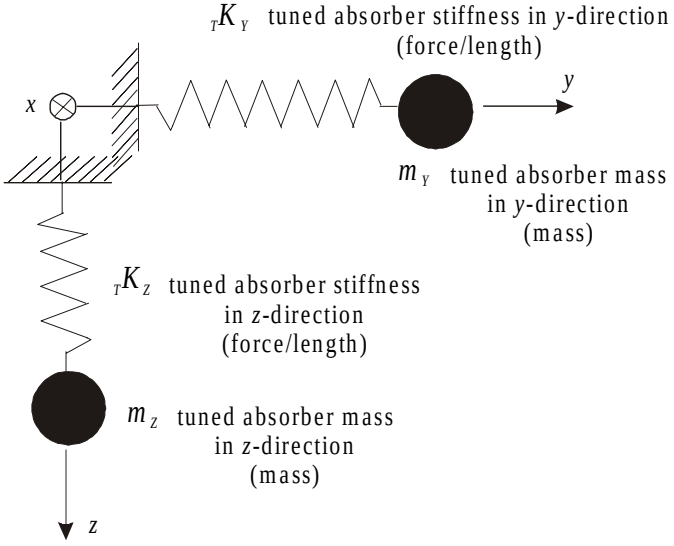

Figure A.7: Tuned absorber.

The *point transfer matrix* has been taken from Pestel and Leckie [37].

$$\{z\} = \left[\begin{array}{cccc:cccc:c} 1 & 0 & 0 & 0 & 0 & 0 & 0 & 0 & 0 \\ 0 & 1 & 0 & 0 & 0 & 0 & 0 & 0 & 0 \\ 0 & 0 & 1 & 0 & 0 & 0 & 0 & 0 & 0 \\ K_{dz} & 0 & 0 & 1 & 0 & 0 & 0 & 0 & 0 \\ \hdashline 0 & 0 & 0 & 0 & 1 & 0 & 0 & 0 & 0 \\ 0 & 0 & 0 & 0 & 0 & 1 & 0 & 0 & 0 \\ 0 & 0 & 0 & 0 & 0 & 0 & 1 & 0 & 0 \\ 0 & 0 & 0 & 0 & K_{dy} & 0 & 0 & 1 & 0 \\ \hdashline 0 & 0 & 0 & 0 & 0 & 0 & 0 & 0 & 1 \end{array}\right] \tag{A.11}$$

where $$K_{dz} = \frac{{}_T K_Z m_Z \omega^2}{{}_T K_Z - m_Z \omega^2} \quad \text{and} \quad K_{dy} = \frac{{}_T K_Y m_Y \omega^2}{{}_T K_Y - m_Y \omega^2} \tag{A.12}$$

A.9 Bent Rotor

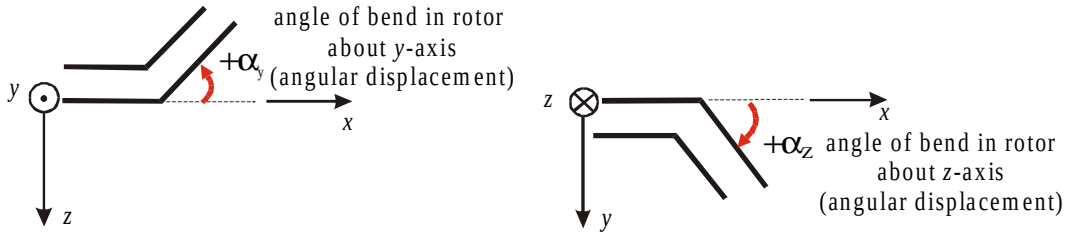

Figure A.8: Bent Rotor.

The extension column of Equation (A.13) is expanded from the *extended point transfer matrix* found in Pilkey [38].

$$\{z\} = \left[\begin{array}{cccc:cccc:c} 1 & 0 & 0 & 0 & 0 & 0 & 0 & 0 & 0 \\ 0 & 1 & 0 & 0 & 0 & 0 & 0 & 0 & -\alpha_Y \\ 0 & 0 & 1 & 0 & 0 & 0 & 0 & 0 & 0 \\ 0 & 0 & 0 & 1 & 0 & 0 & 0 & 0 & 0 \\ \hdashline 0 & 0 & 0 & 0 & 1 & 0 & 0 & 0 & 0 \\ 0 & 0 & 0 & 0 & 0 & 1 & 0 & 0 & -\alpha_Z \\ 0 & 0 & 0 & 0 & 0 & 0 & 1 & 0 & 0 \\ 0 & 0 & 0 & 0 & 0 & 0 & 0 & 1 & 0 \\ \hdashline 0 & 0 & 0 & 0 & 0 & 0 & 0 & 0 & 1 \end{array}\right] \qquad \textbf{(A.13)}$$

A.10 Prescribed Relative Transverse Motion

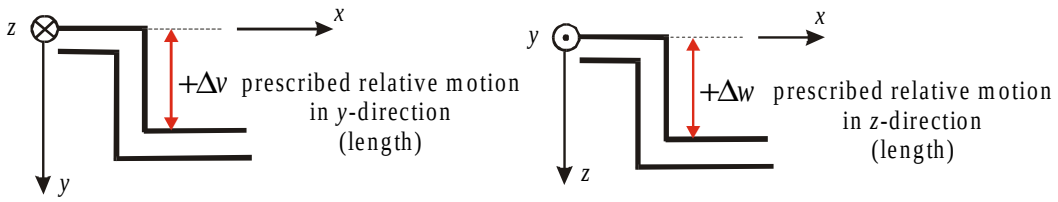

Figure A.9: Prescribed Relative Transverse Motion.

The extension column of Equation (A.14) is expanded from the *extended point transfer matrix* found in Pilkey [39].

$$\{z\} = \left[\begin{array}{cccc:cccc:c} 1 & 0 & 0 & 0 & 0 & 0 & 0 & 0 & \Delta w \\ 0 & 1 & 0 & 0 & 0 & 0 & 0 & 0 & 0 \\ 0 & 0 & 1 & 0 & 0 & 0 & 0 & 0 & 0 \\ 0 & 0 & 0 & 1 & 0 & 0 & 0 & 0 & 0 \\ \hdashline 0 & 0 & 0 & 0 & 1 & 0 & 0 & 0 & \Delta v \\ 0 & 0 & 0 & 0 & 0 & 1 & 0 & 0 & 0 \\ 0 & 0 & 0 & 0 & 0 & 0 & 1 & 0 & 0 \\ 0 & 0 & 0 & 0 & 0 & 0 & 0 & 1 & 0 \\ \hdashline 0 & 0 & 0 & 0 & 0 & 0 & 0 & 0 & 1 \end{array}\right] \tag{A.14}$$

Appendix B

Screen Shots from 2DBEAM

The figures in this appendix provide an overview of screen displays seen while using 2DBEAM. The following is a summary of the figures.

Figure B.1	Start up screen of the program
Figures B.2 – B.11	Input screens used build the model
Figure B.12	Illustration of the model built
Figures B.13 – B.17	Performing static analysis of model
Figures B.18 – B.23	Performing free vibration analysis of model
Figures B.24 – B.28	Performing forced dynamic analysis of model
Figures B.29 – B.33	Performing frequency response analysis of model

.

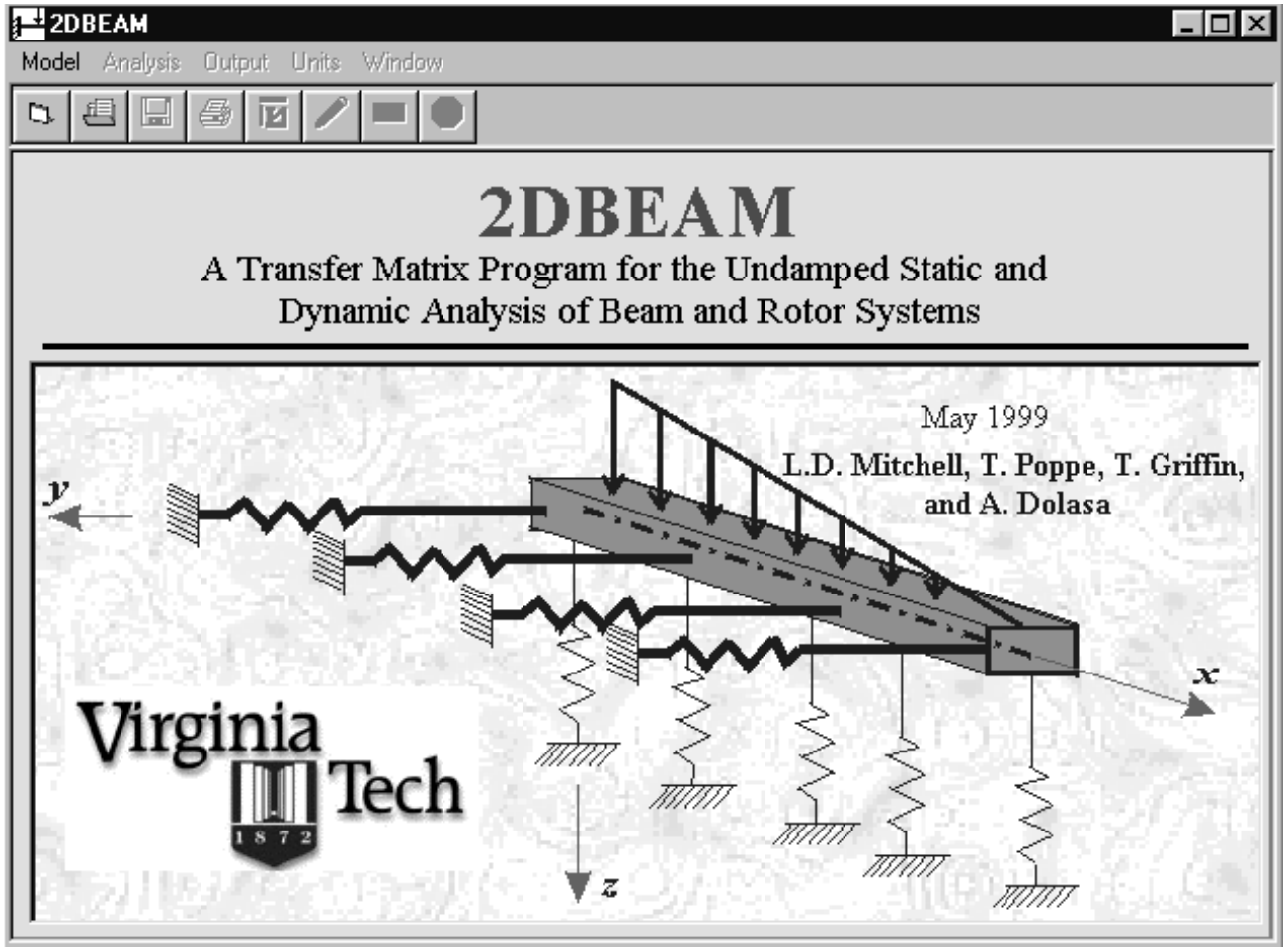

Figure B.1: Title page.

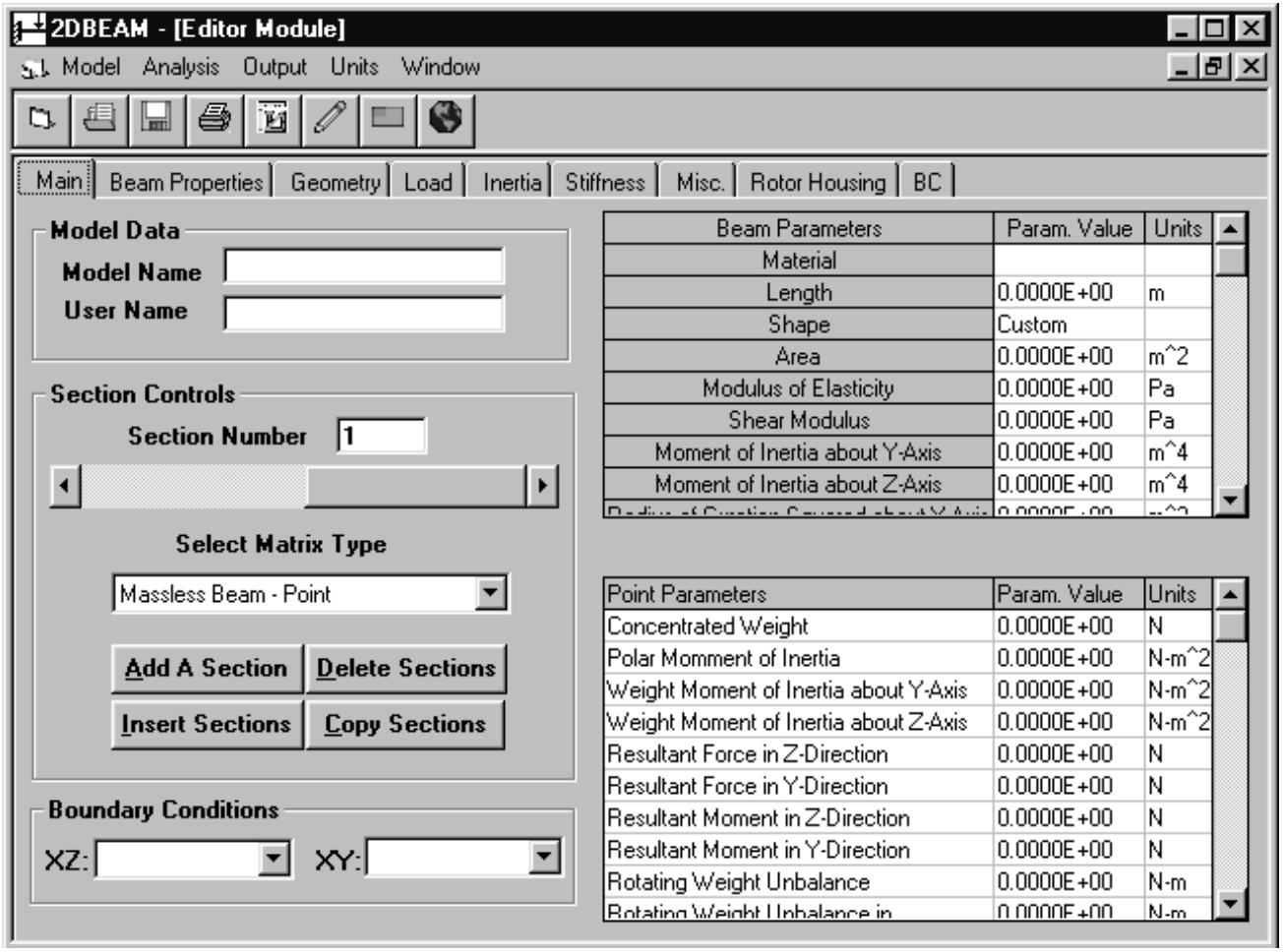

Figure B.2: Main menu tab providing summary of data entered.

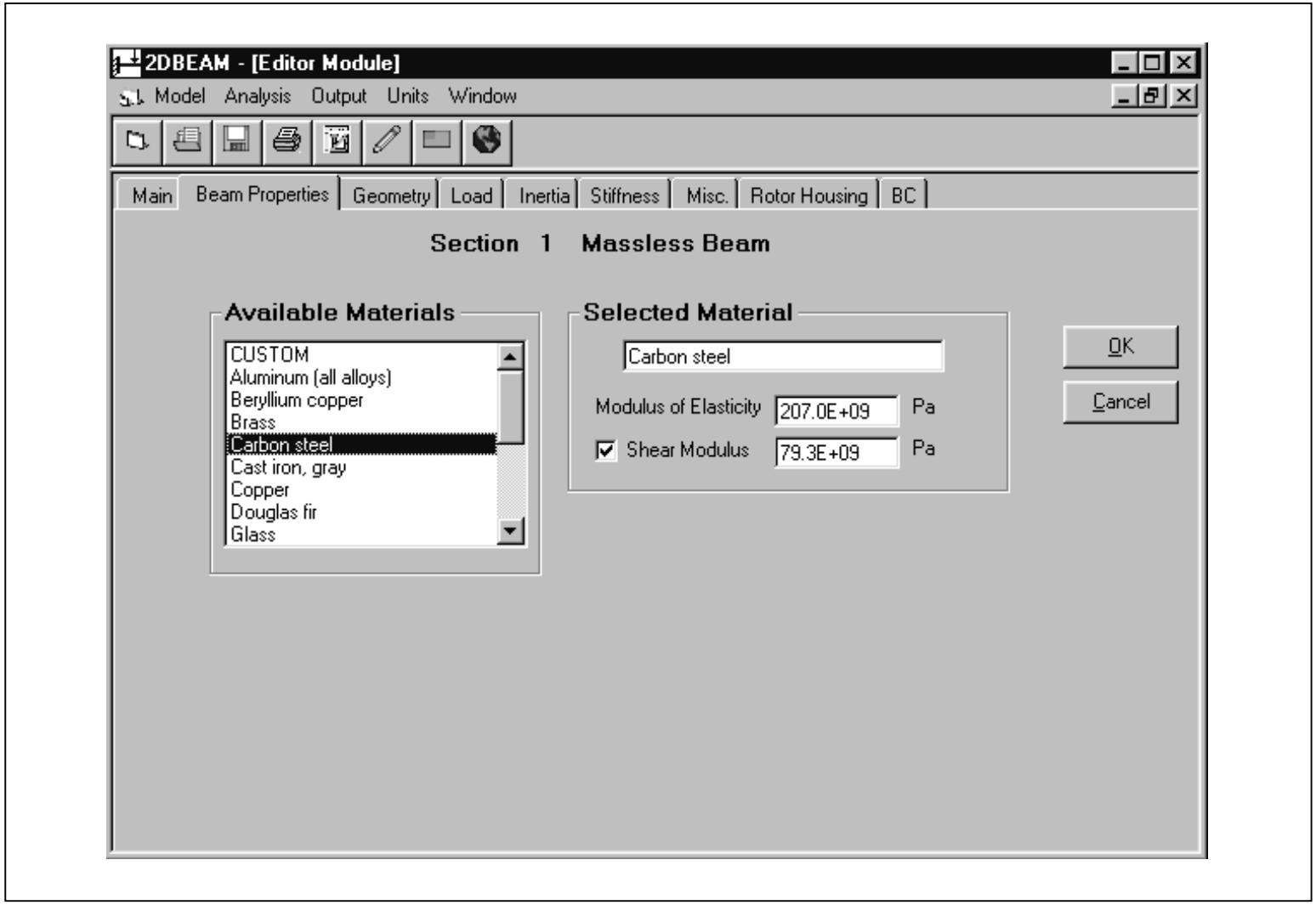

Figure B.3: Tab appearance to enter beam properties when massless or timoshenko beam sections selected.

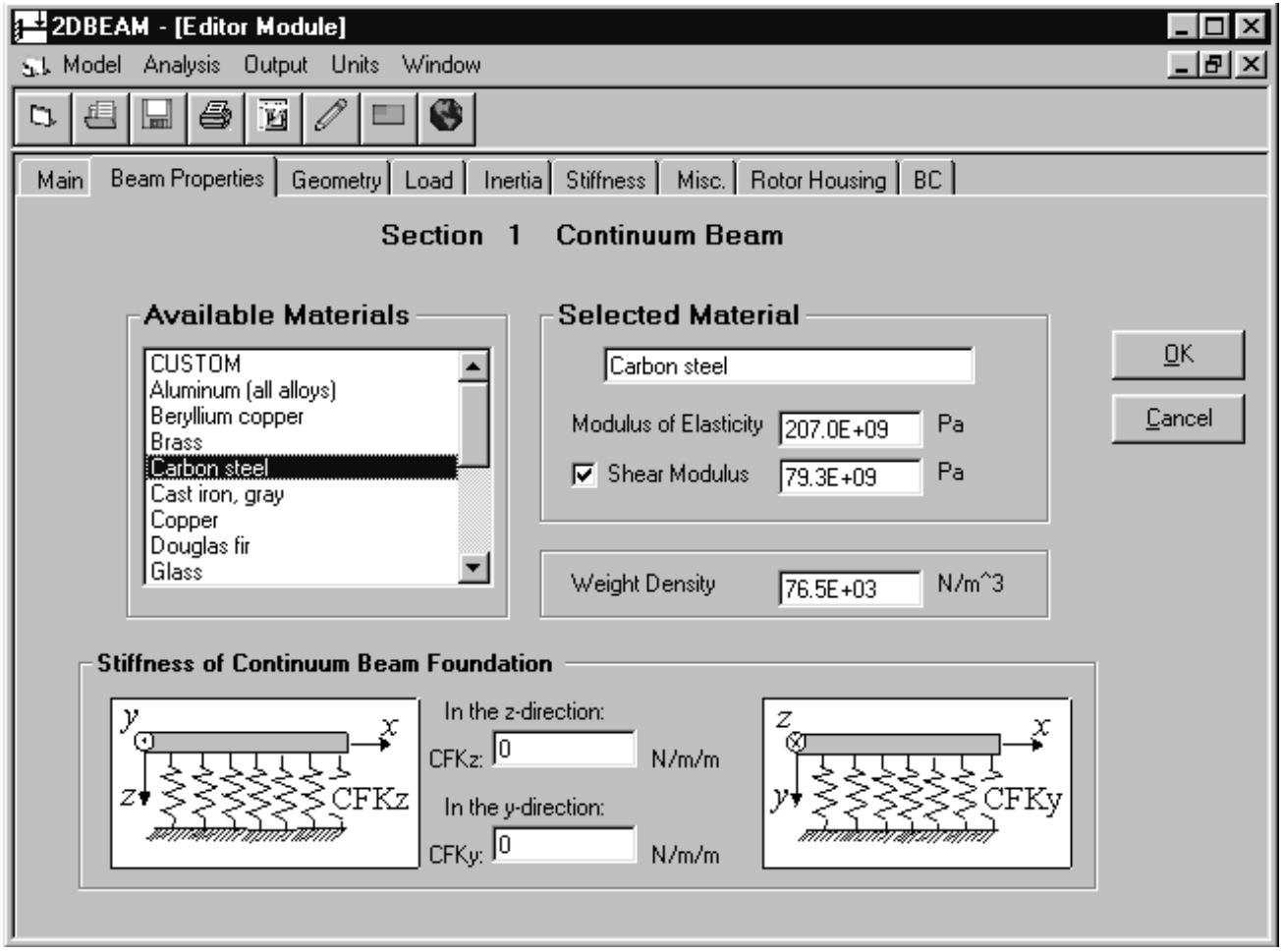

Figure B.4: Tab appearance to enter beam properties when continuum beam section selected.

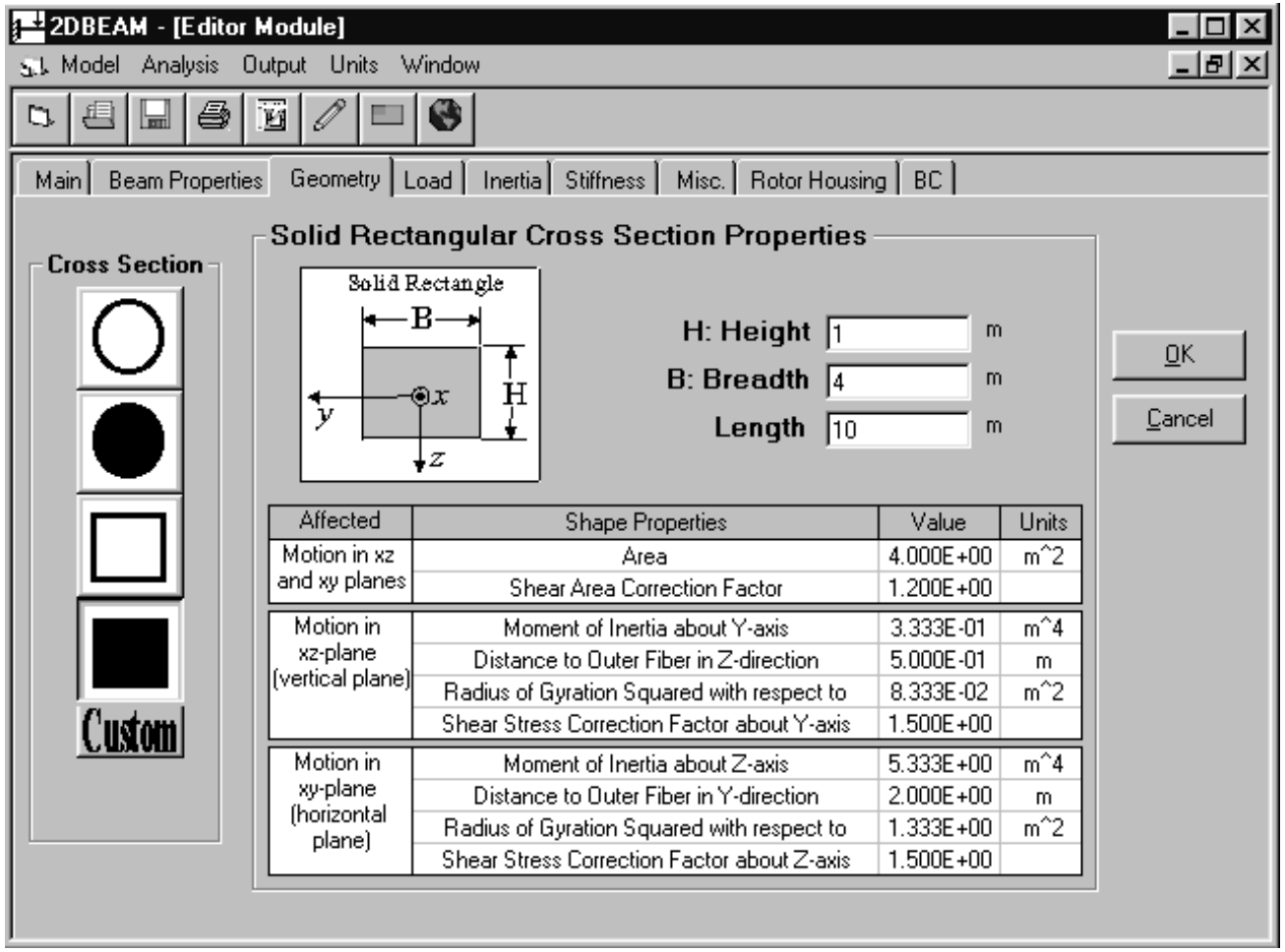

Figure B.5: Tab to enter geometry of beam section.

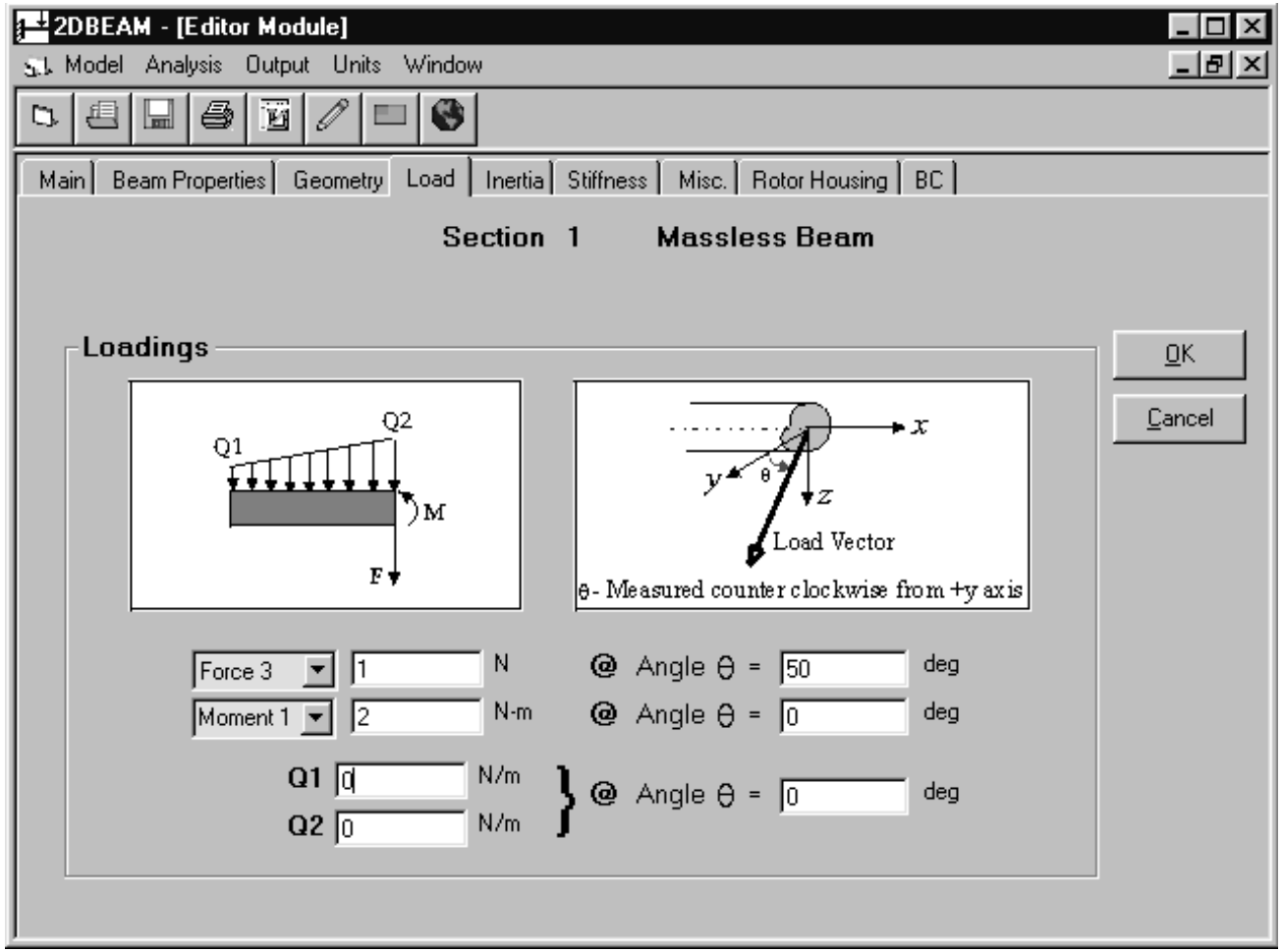

Figure B.6: Tab to enter loads acting on the beam section.

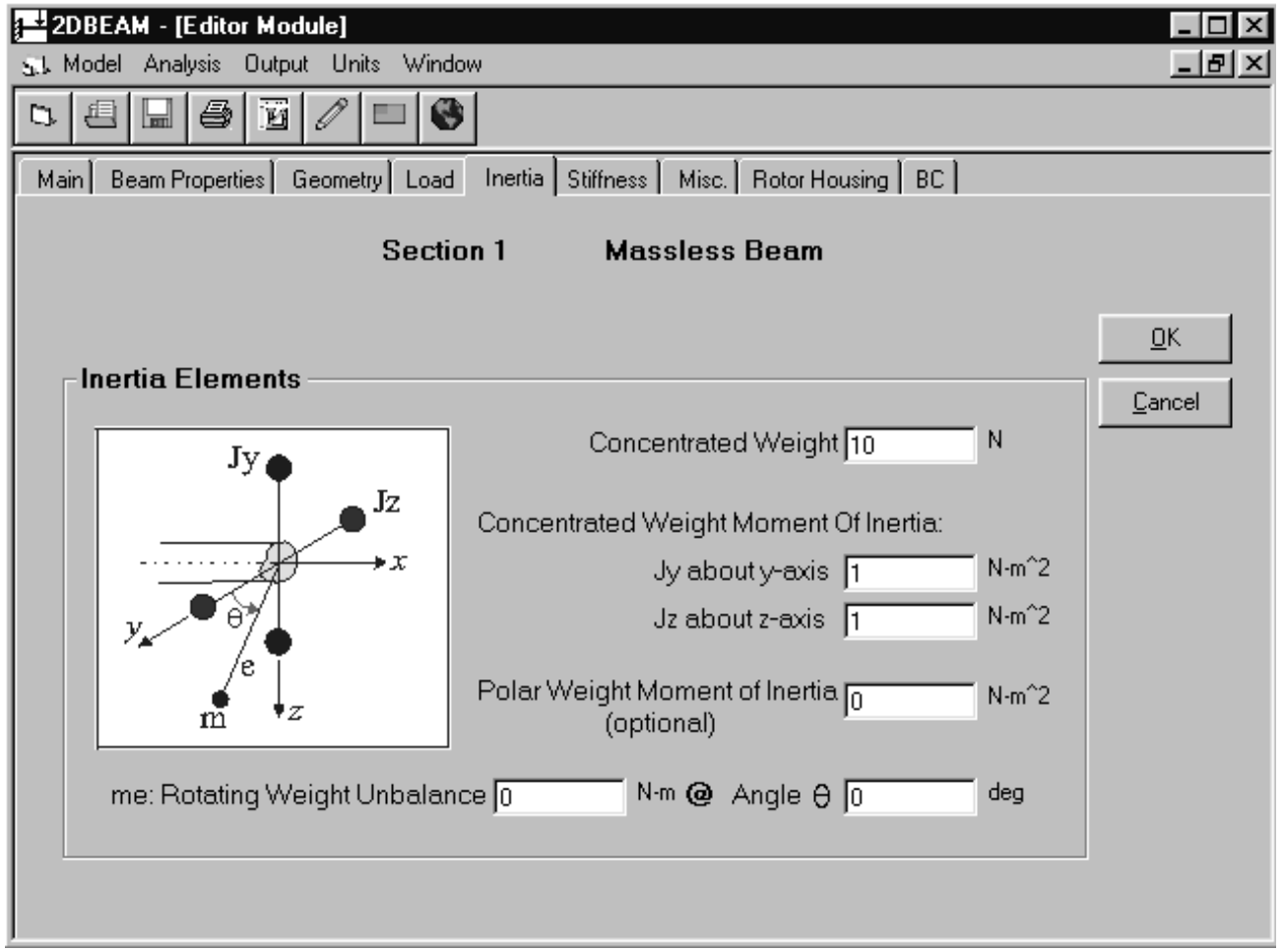

Figure B.7: Tab to enter inertia elements to the beam section.

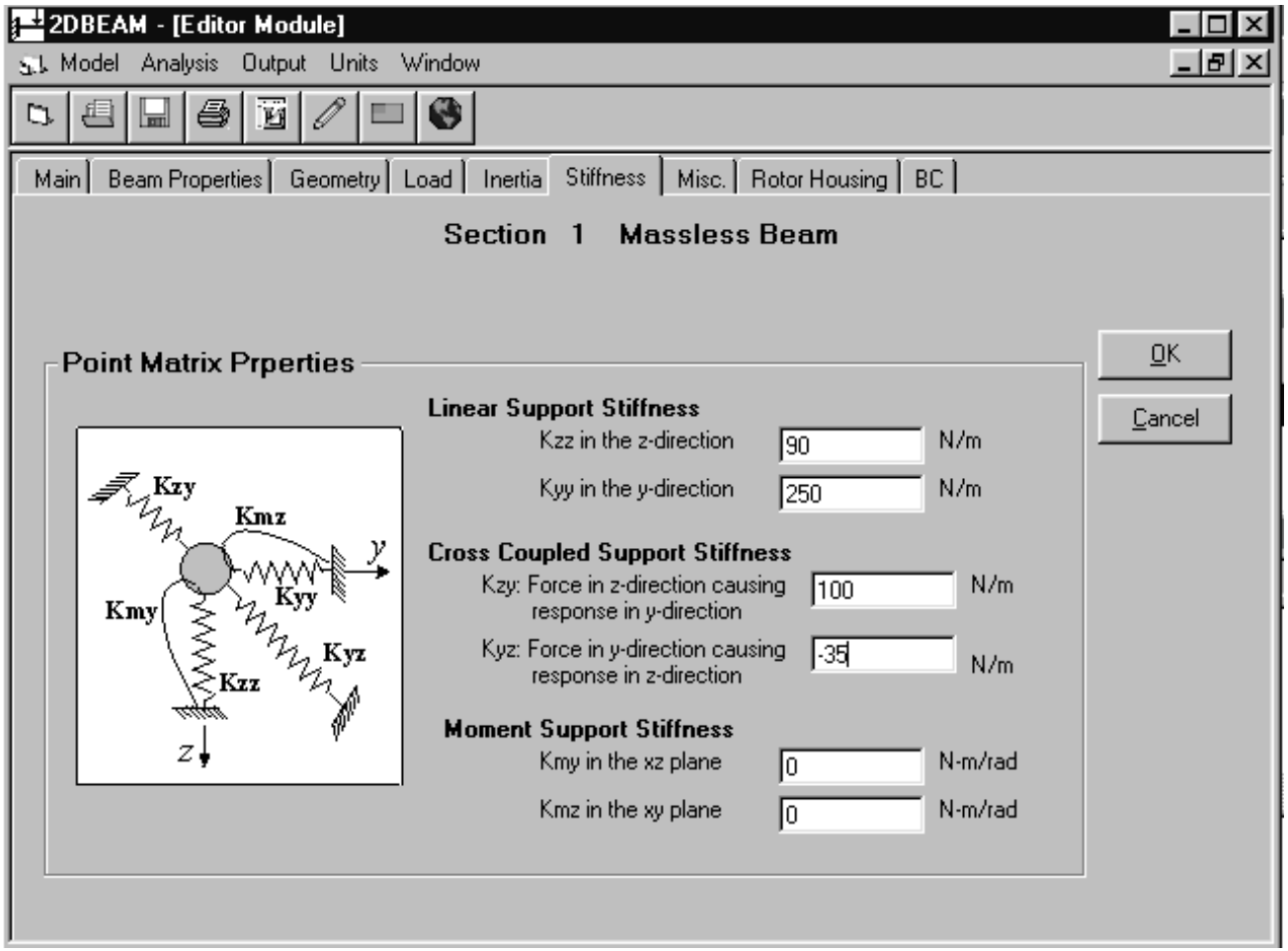

Figure B.8: Tab to enter stiffness elements to the beam section.

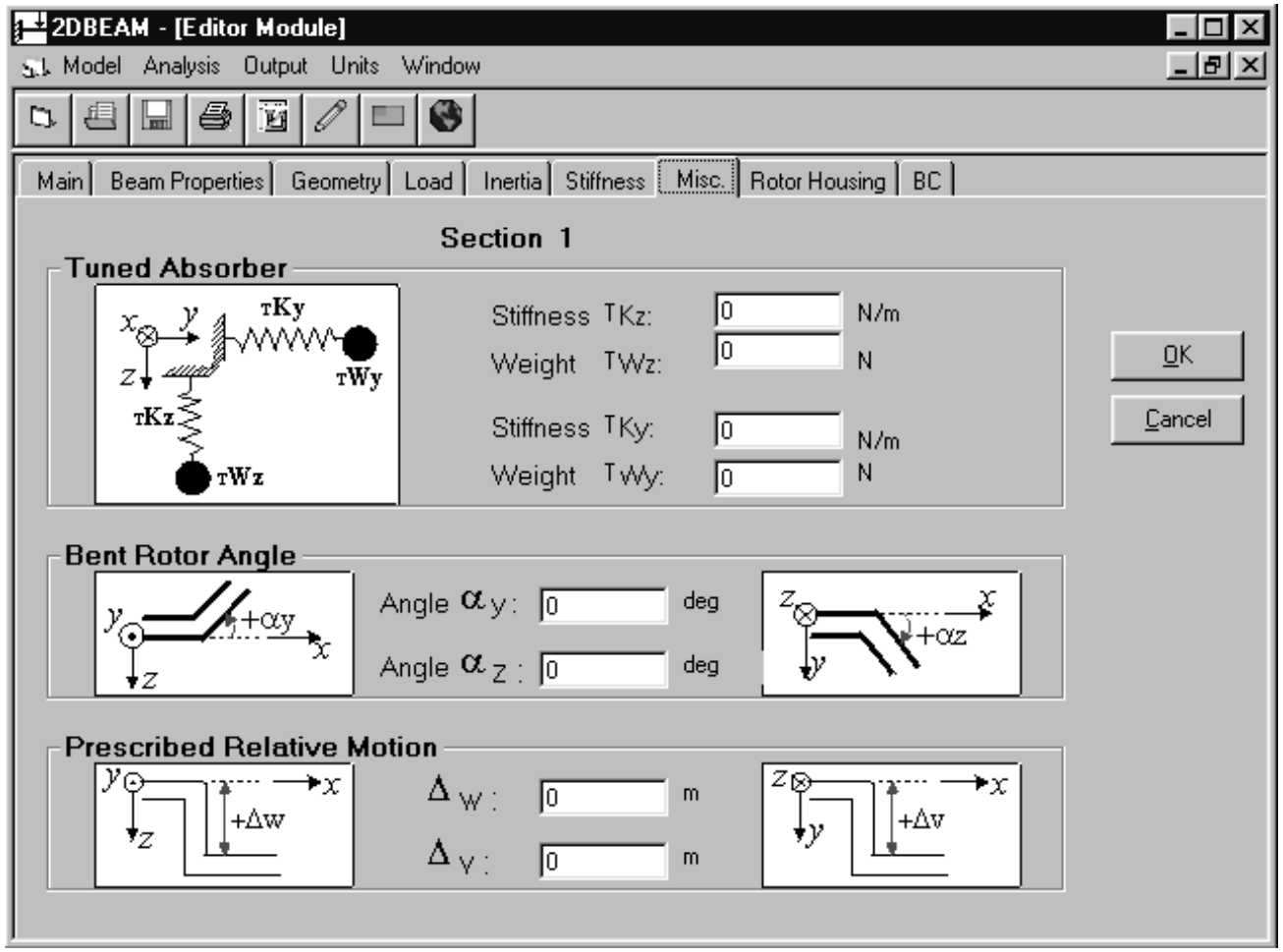

Figure B.9: Tab to enter miscellaneous elements to the beam.

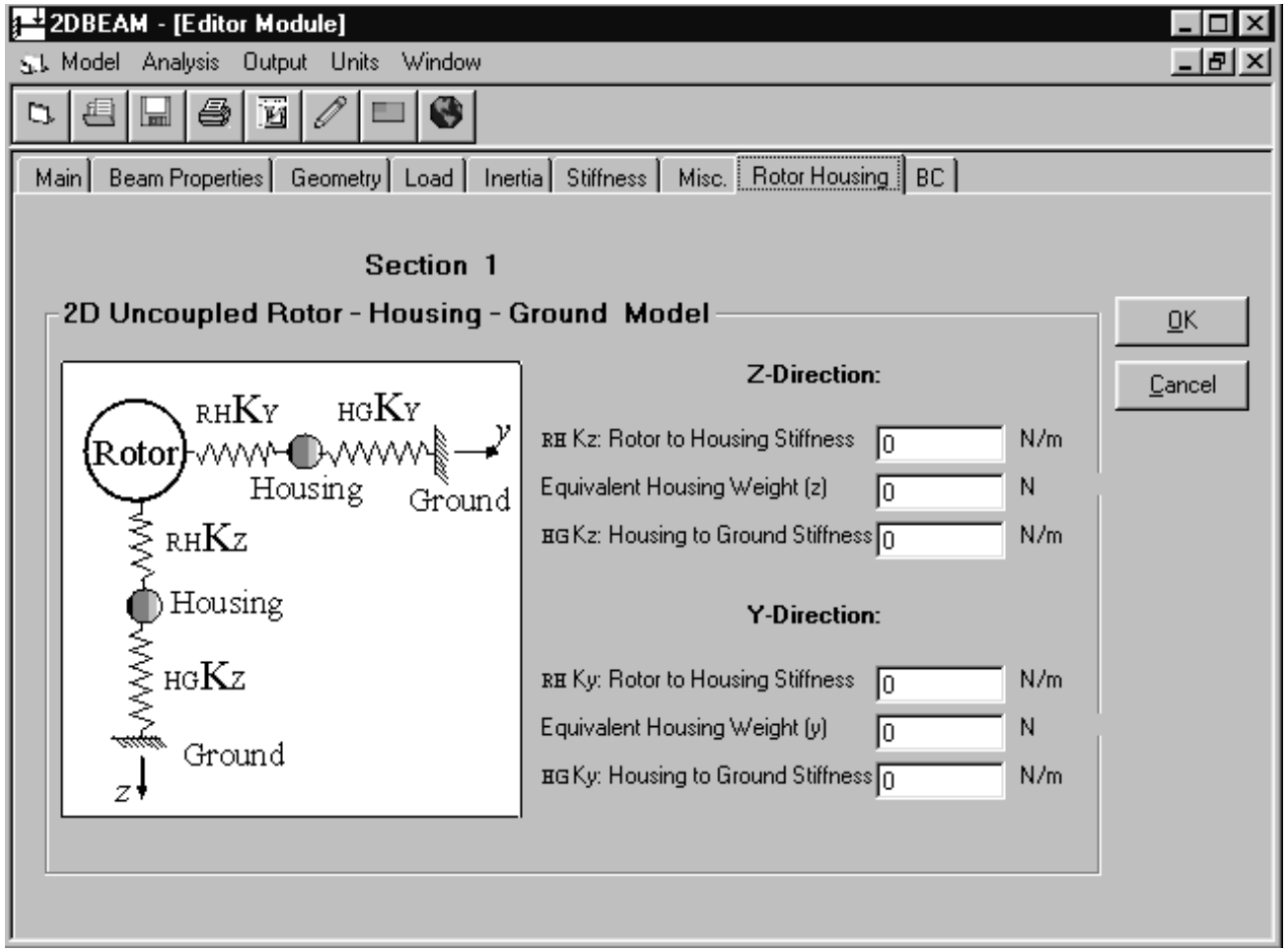

Figure B.10: Tab to uncoupled rotor-housing model to the beam.

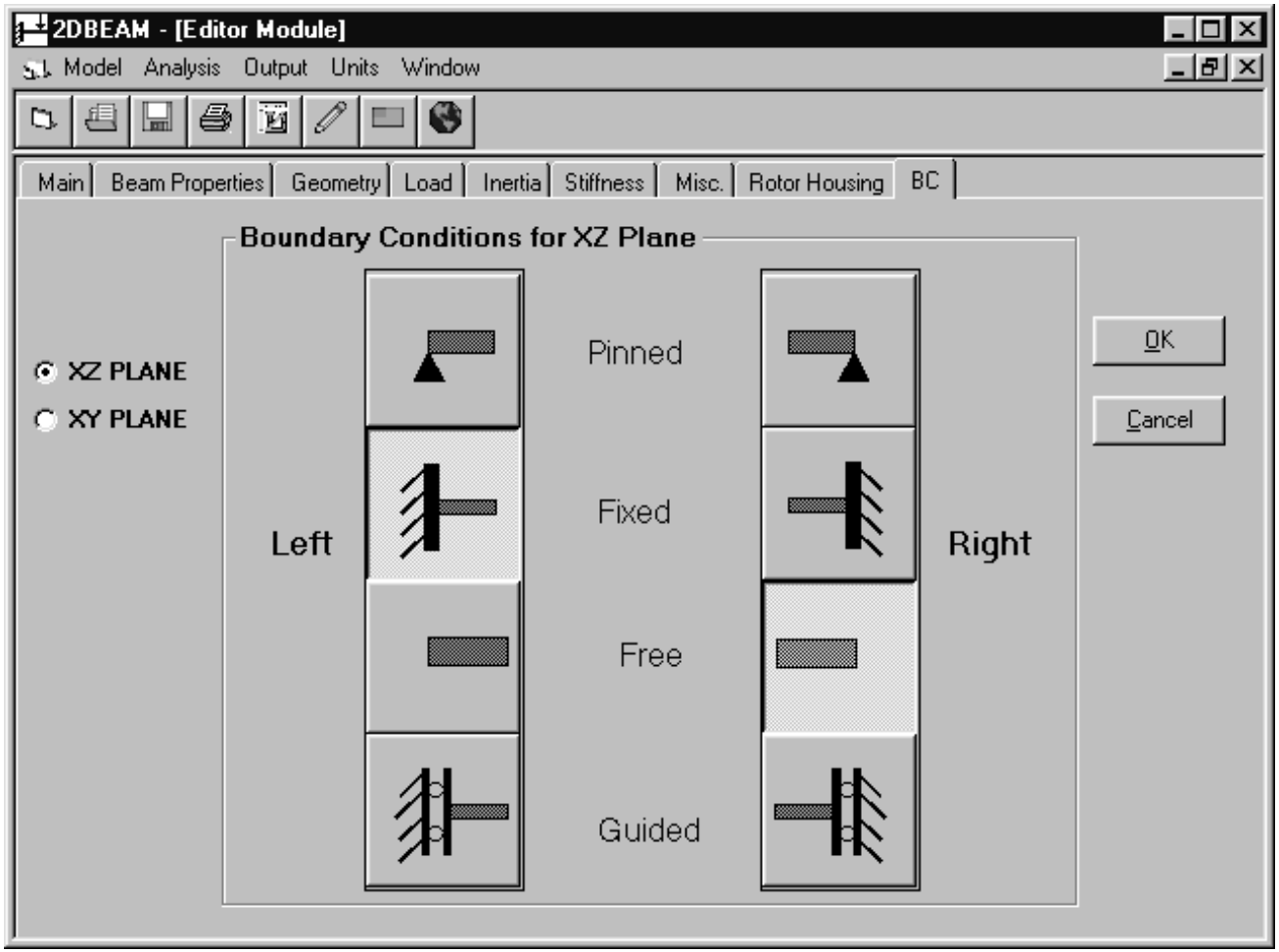

Figure B.11: Tab to enter boundary conditions of the beam in XZ and XY planes.

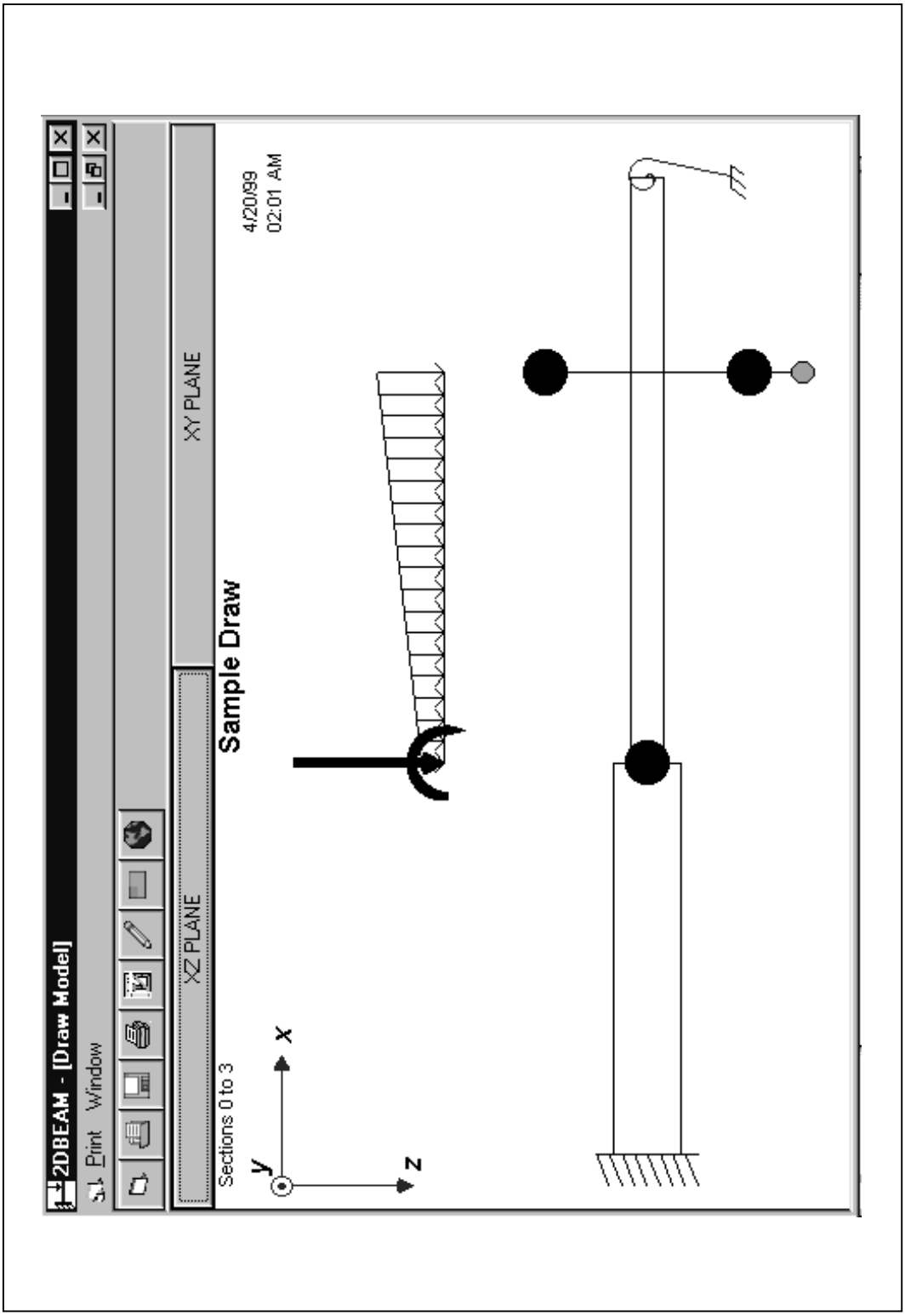

Figure B.12: Draw option displaying model as viewed in the XZ or XY plane.

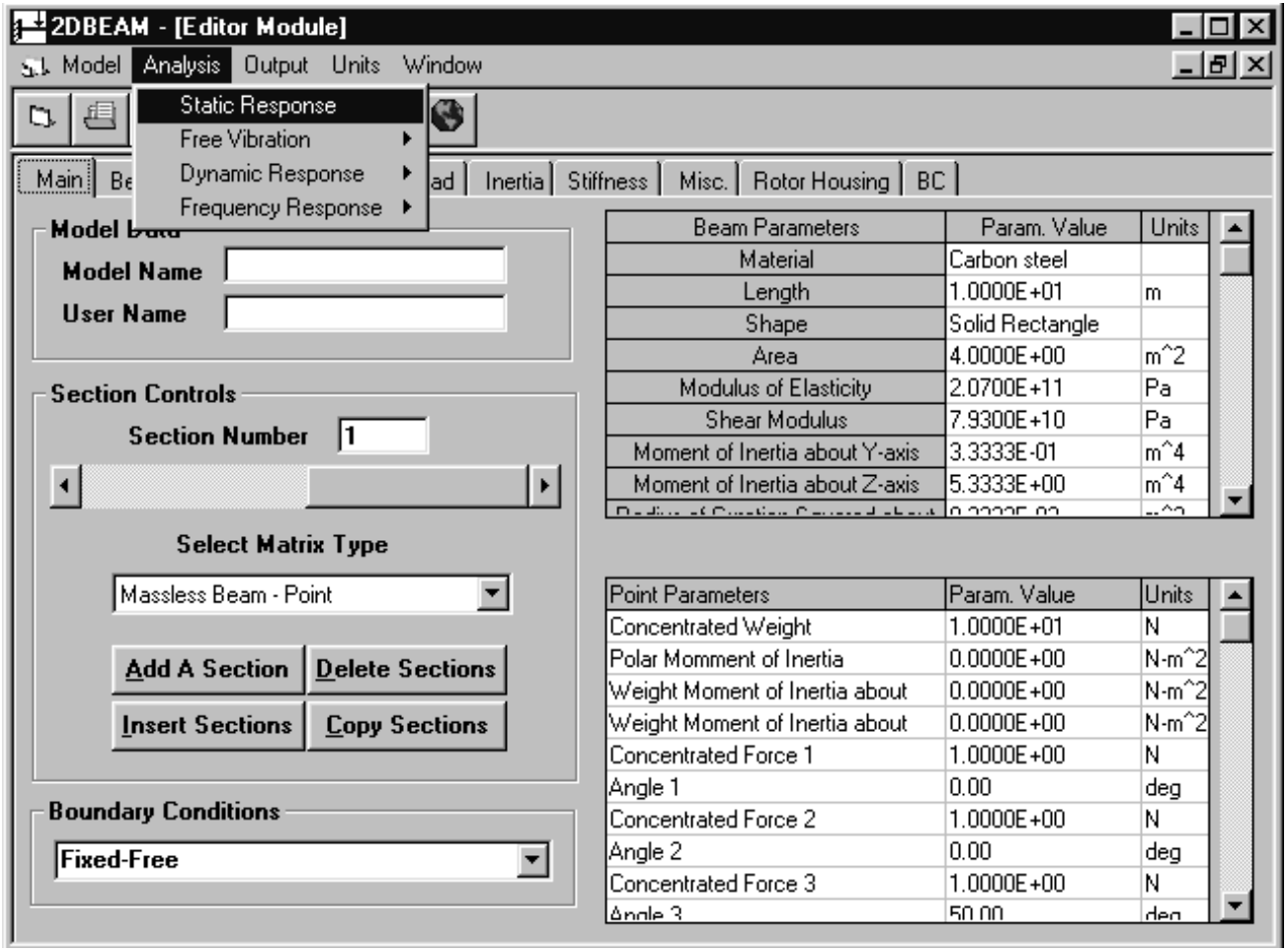

Figure B.13: Drop down menu selecting static response.

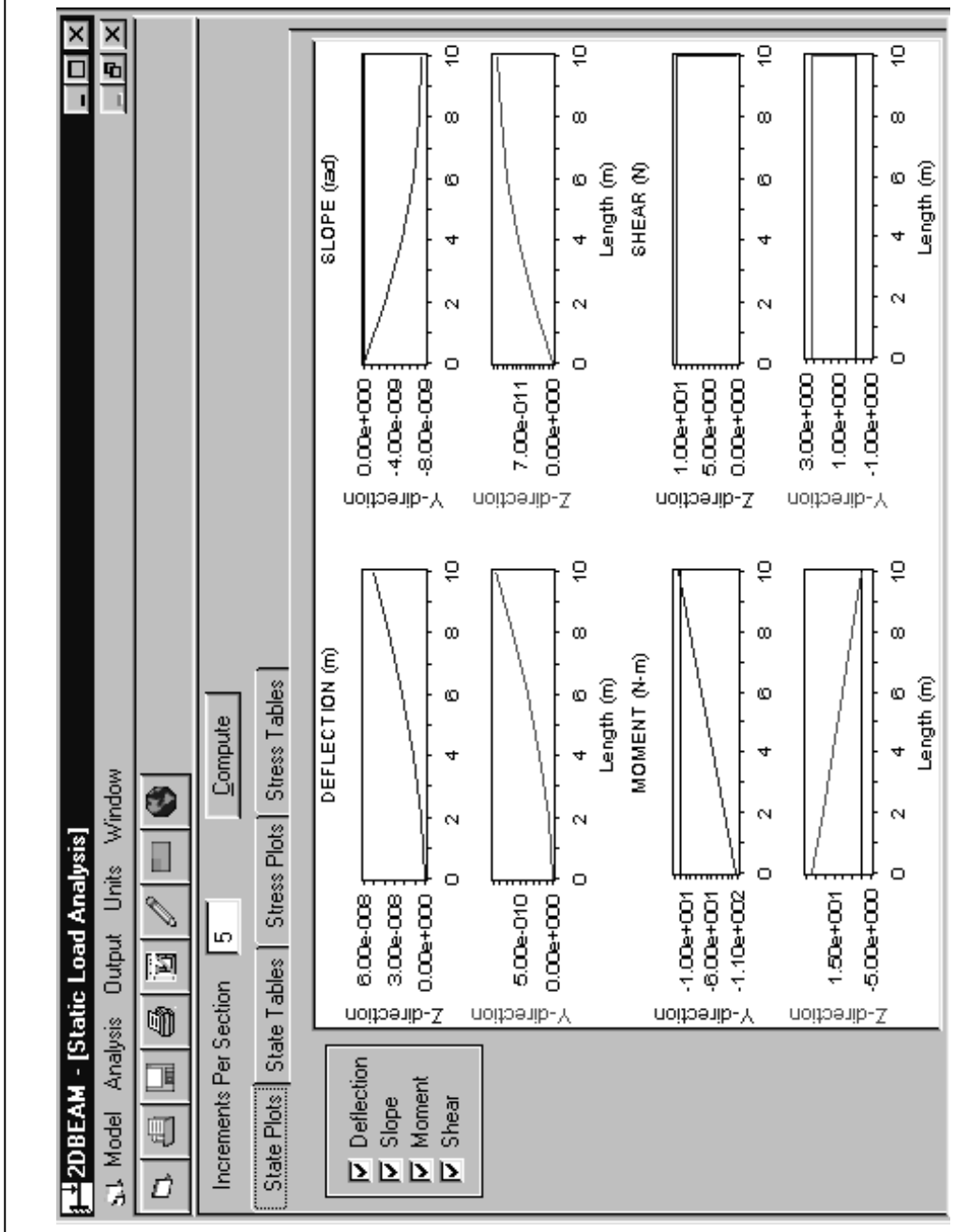

Figure B.14: Output screen displaying static response graphically.

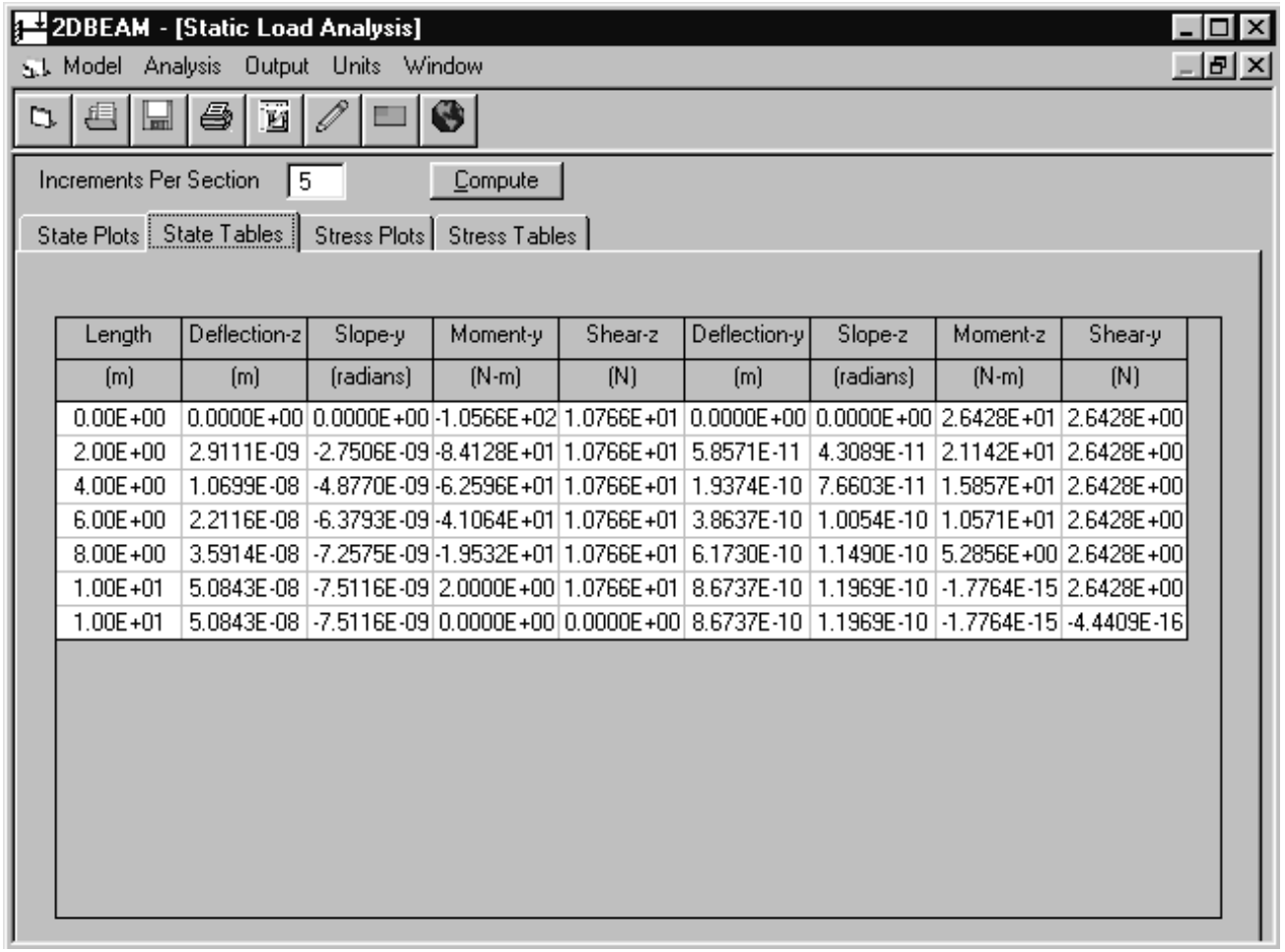

Length (m)	Deflection-z (m)	Slope-y (radians)	Moment-y (N-m)	Shear-z (N)	Deflection-y (m)	Slope-z (radians)	Moment-z (N-m)	Shear-y (N)
0.00E+00	0.0000E+00	0.0000E+00	-1.0566E+02	1.0766E+01	0.0000E+00	0.0000E+00	2.6428E+01	2.6428E+00
2.00E+00	2.9111E-09	-2.7506E-09	-8.4128E+01	1.0766E+01	5.8571E-11	4.3089E-11	2.1142E+01	2.6428E+00
4.00E+00	1.0699E-08	-4.8770E-09	-6.2596E+01	1.0766E+01	1.9374E-10	7.6603E-11	1.5857E+01	2.6428E+00
6.00E+00	2.2116E-08	-6.3793E-09	-4.1064E+01	1.0766E+01	3.8637E-10	1.0054E-10	1.0571E+01	2.6428E+00
8.00E+00	3.5914E-08	-7.2575E-09	-1.9532E+01	1.0766E+01	6.1730E-10	1.1490E-10	5.2856E+00	2.6428E+00
1.00E+01	5.0843E-08	-7.5116E-09	2.0000E+00	1.0766E+01	8.6737E-10	1.1969E-10	-1.7764E-15	2.6428E+00
1.00E+01	5.0843E-08	-7.5116E-09	0.0000E+00	0.0000E+00	8.6737E-10	1.1969E-10	-1.7764E-15	-4.4409E-16

Figure B.15: Output screen displaying static response in tabular format.

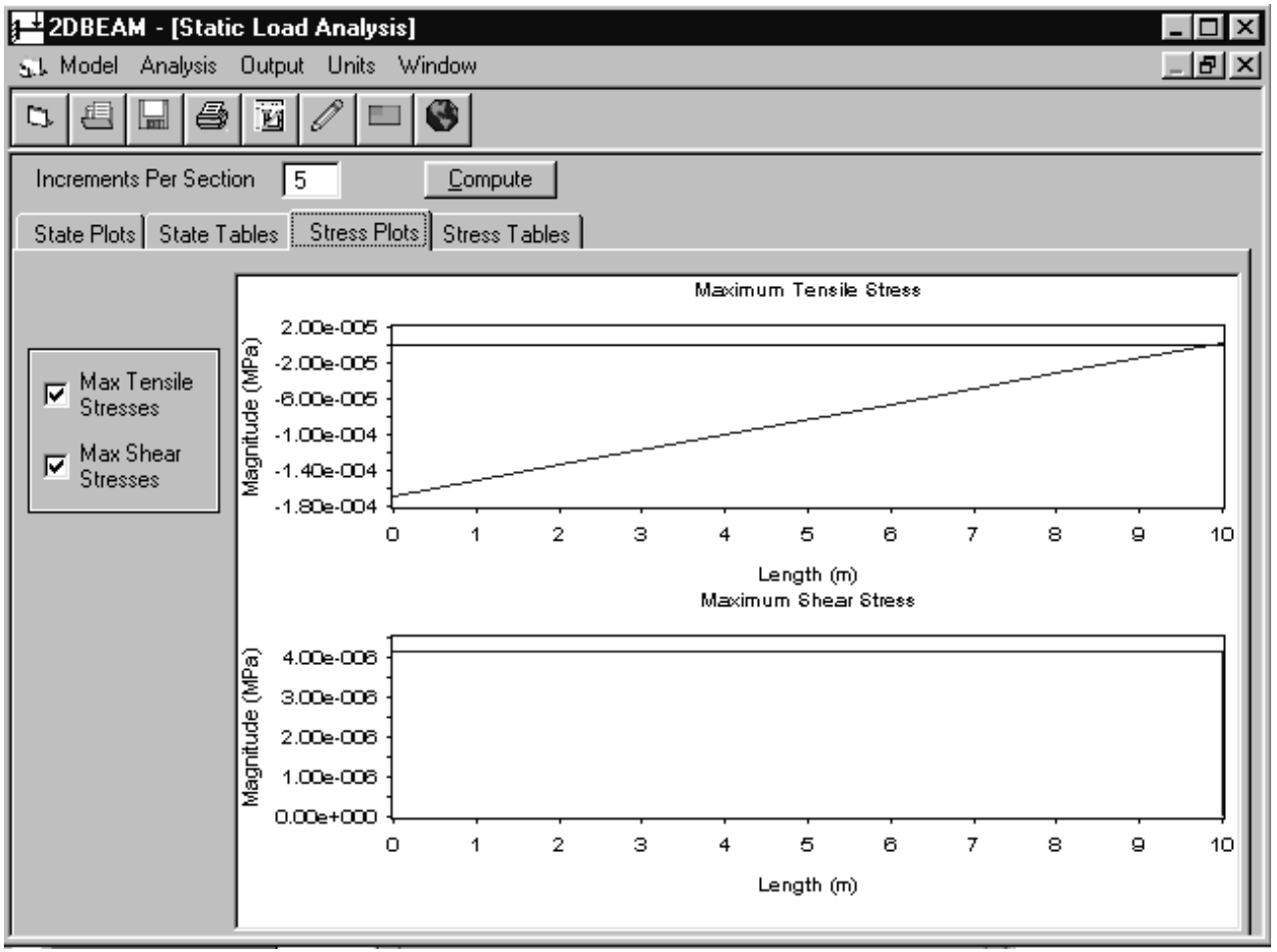

Figure B.16: Output screen displaying static stress response graphically.

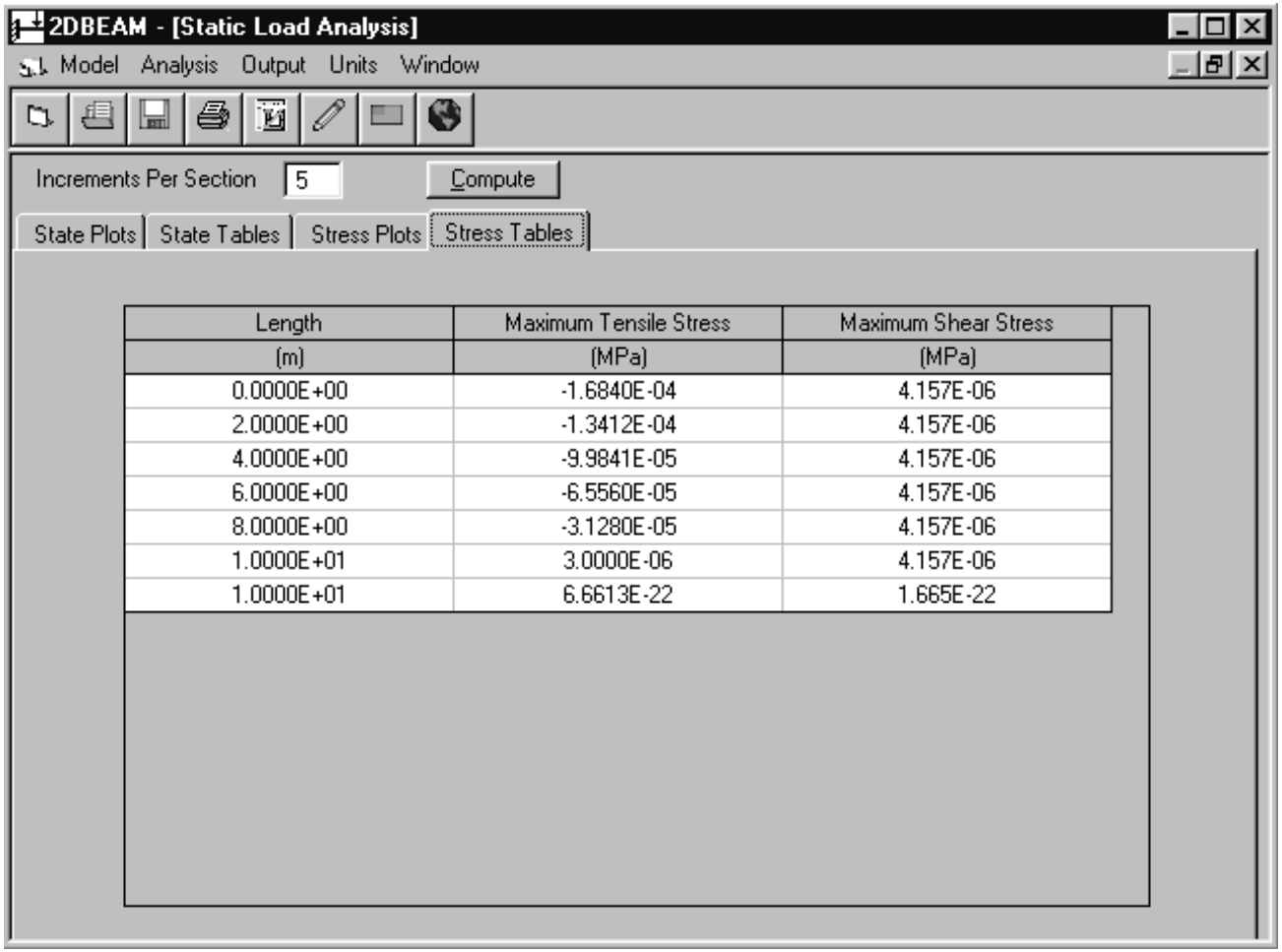

Length (m)	Maximum Tensile Stress (MPa)	Maximum Shear Stress (MPa)
0.0000E+00	-1.6840E-04	4.157E-06
2.0000E+00	-1.3412E-04	4.157E-06
4.0000E+00	-9.9841E-05	4.157E-06
6.0000E+00	-6.5560E-05	4.157E-06
8.0000E+00	-3.1280E-05	4.157E-06
1.0000E+01	3.0000E-06	4.157E-06
1.0000E+01	6.6613E-22	1.665E-22

Figure B.17: Output screen displaying static stress response in tabular format.

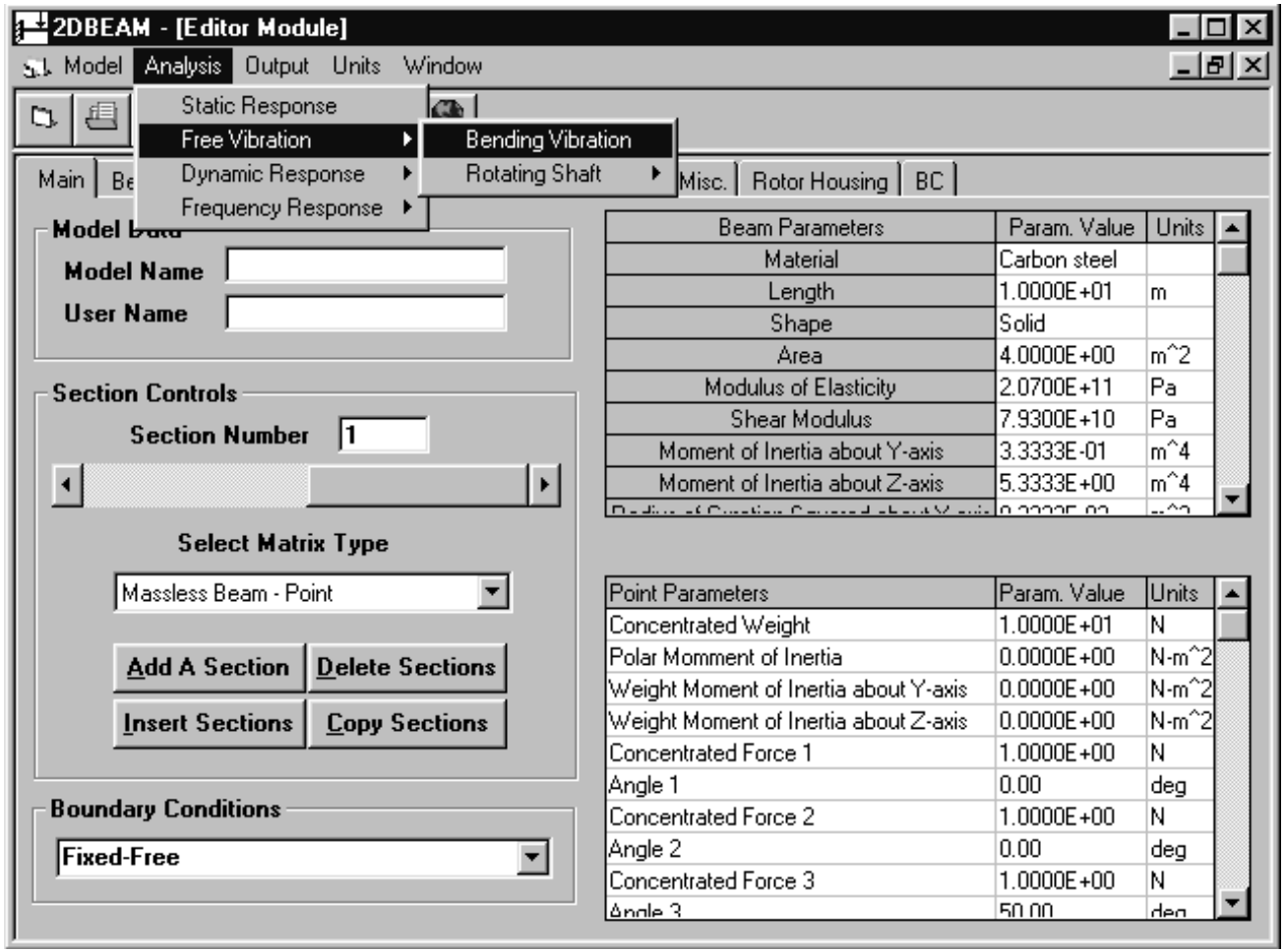

Figure B.18: Drop down menu of free vibration from which the different types of vibrations may be selected.

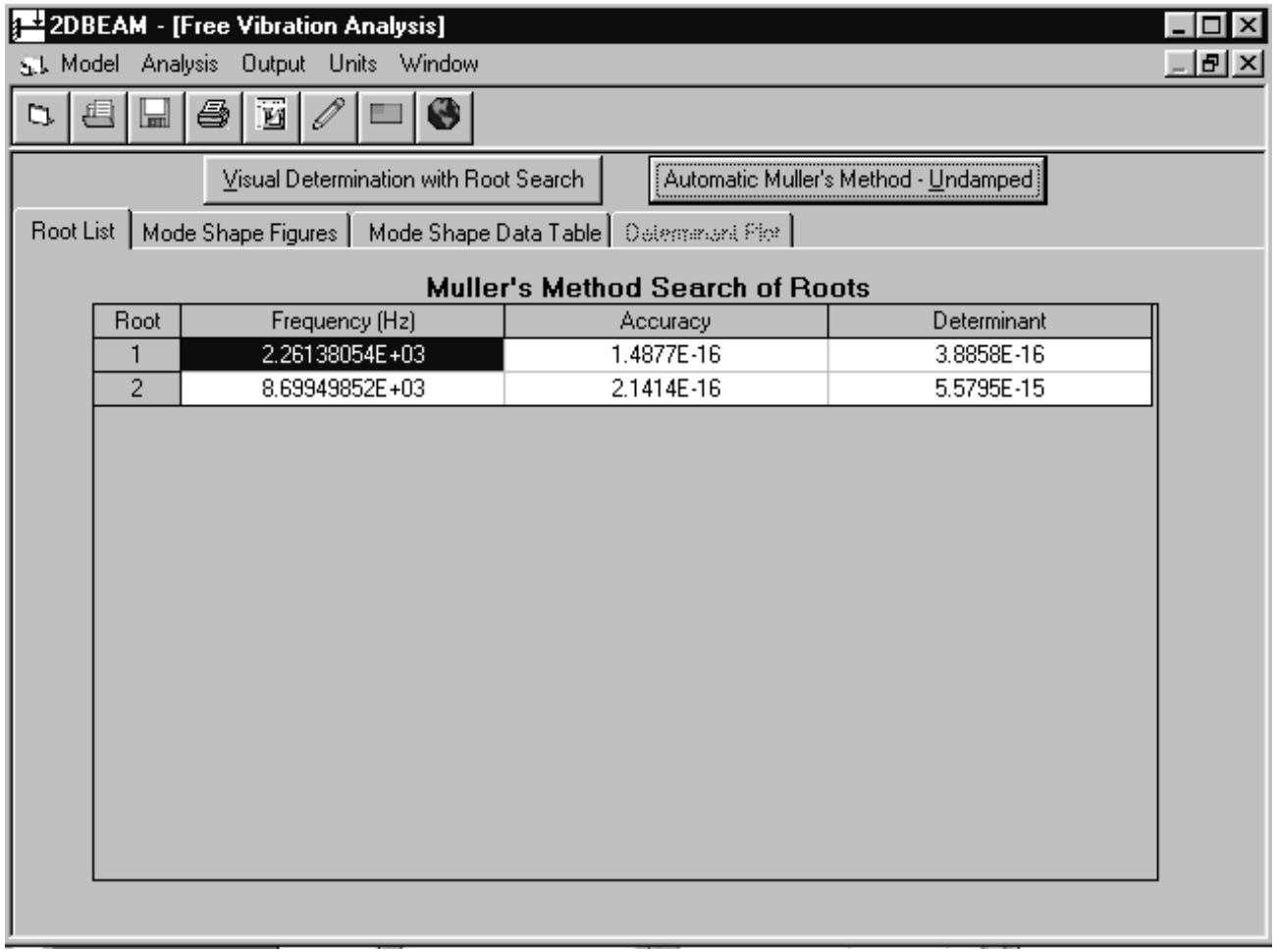

Figure B.19: Output screen displaying eigenvalues obtained from the automatic Muller method.

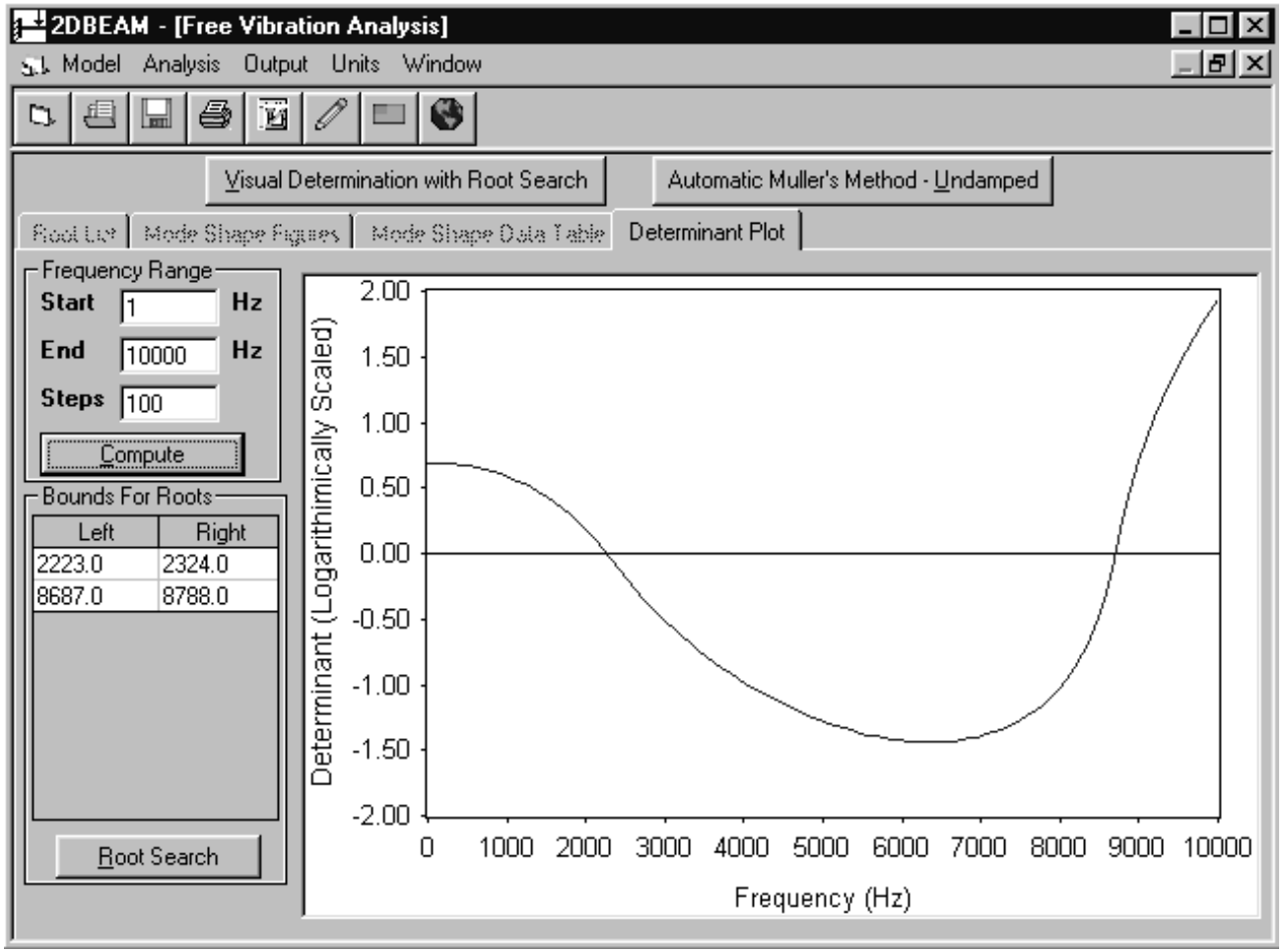

Figure B.20: Output screen allowing user to obtain eigenvalues using the Visual Root Search method.

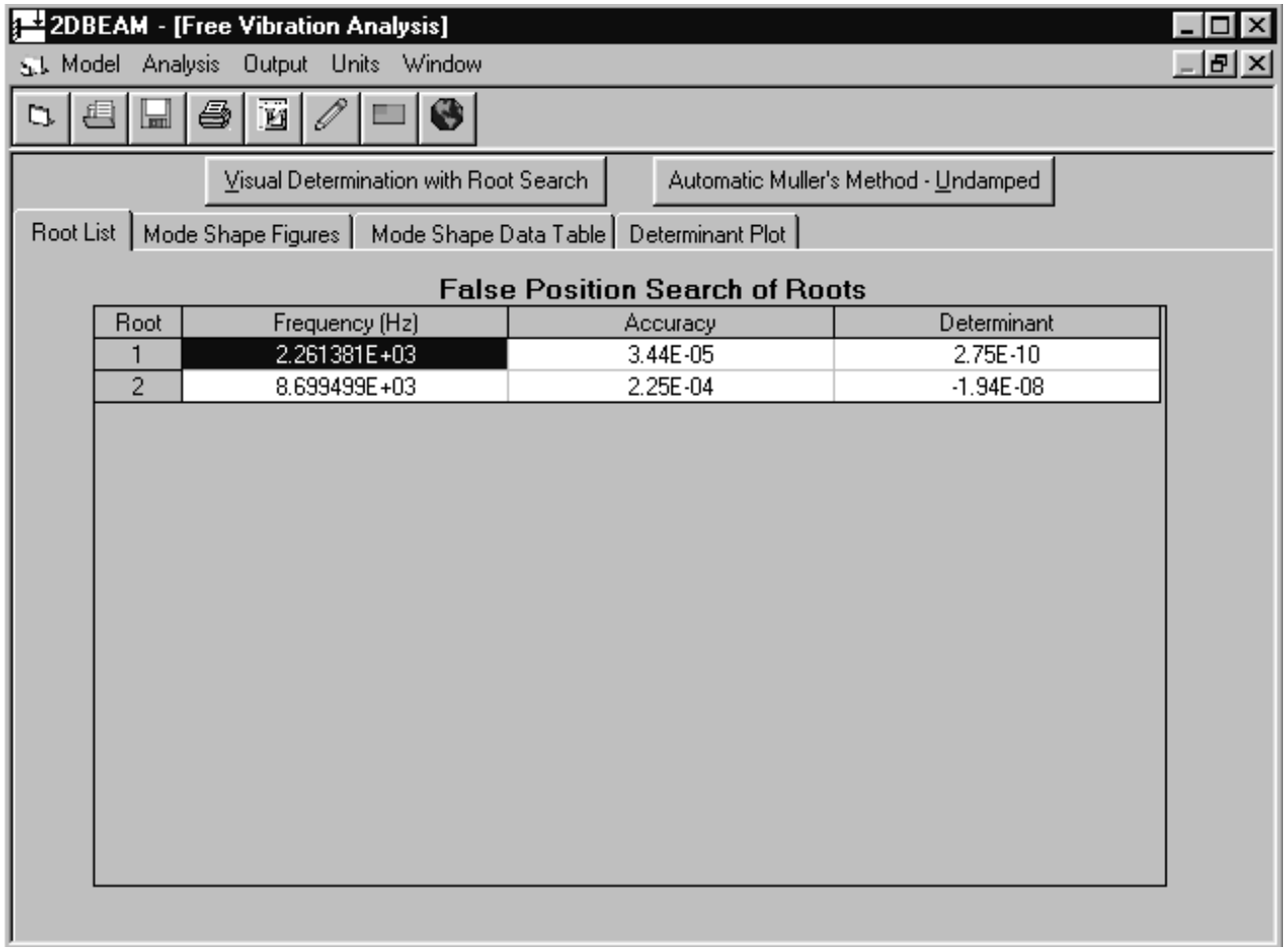

Figure B.21: Output screen displaying eigenvalues obtained from using the Visual Root Search method.

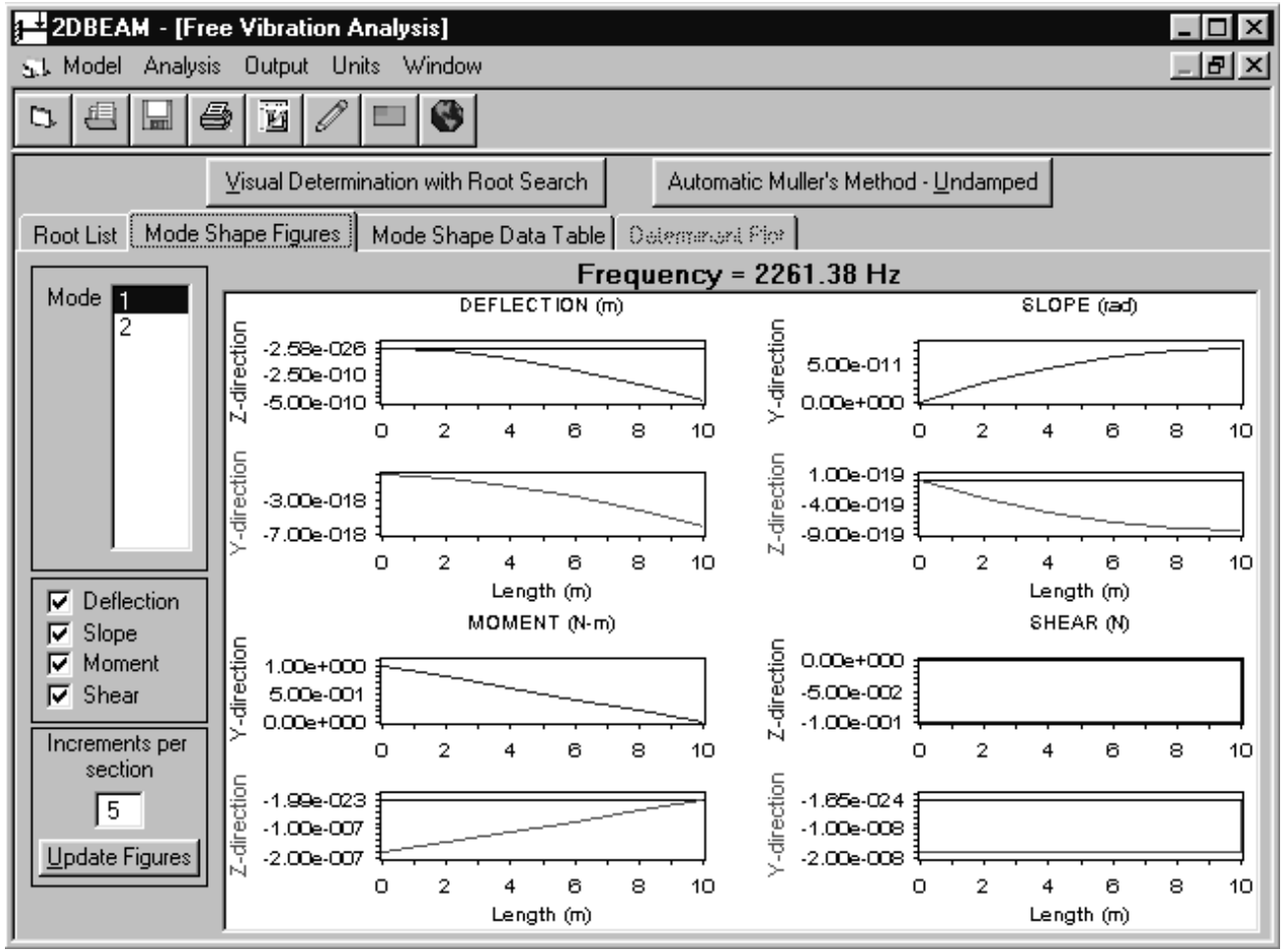

Figure B.22: Output screen graphically displaying mode shapes of the natural frequencies.

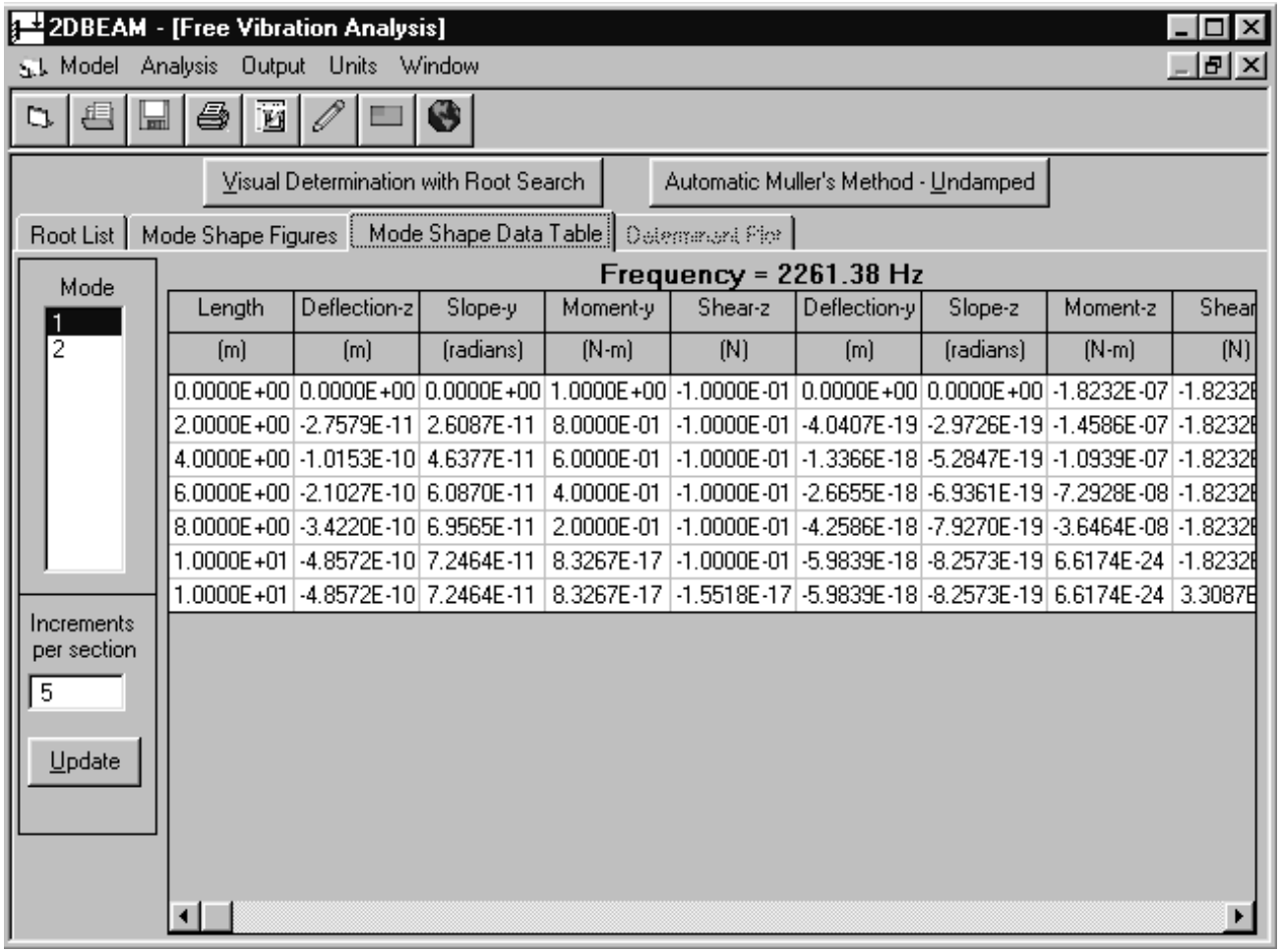

Figure B.23: Output screen displaying mode shapes of the natural frequencies in tabular format.

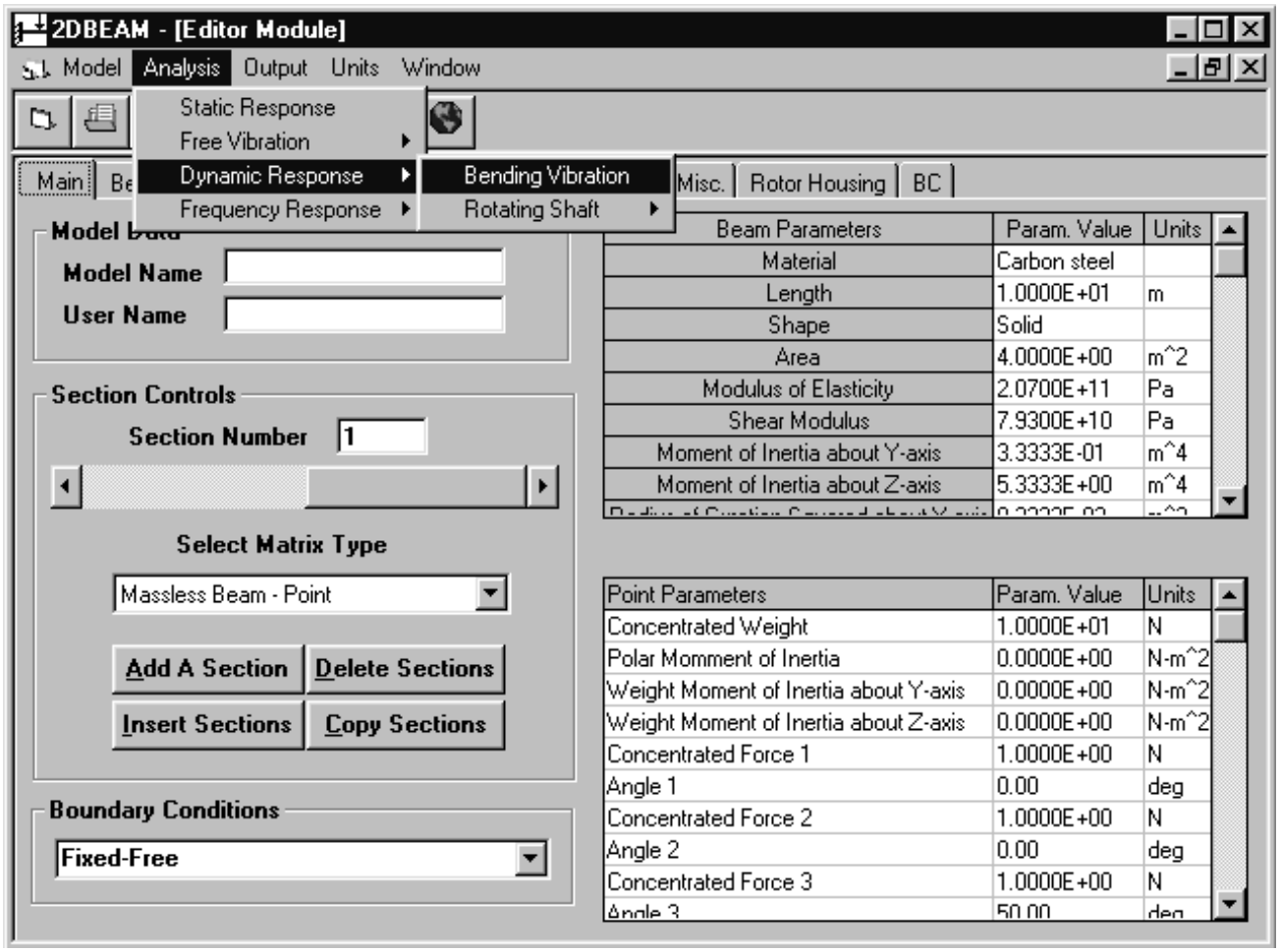

Figure B.24: Drop down menu of forced dynamic response from which the different types of vibrations may be selected.

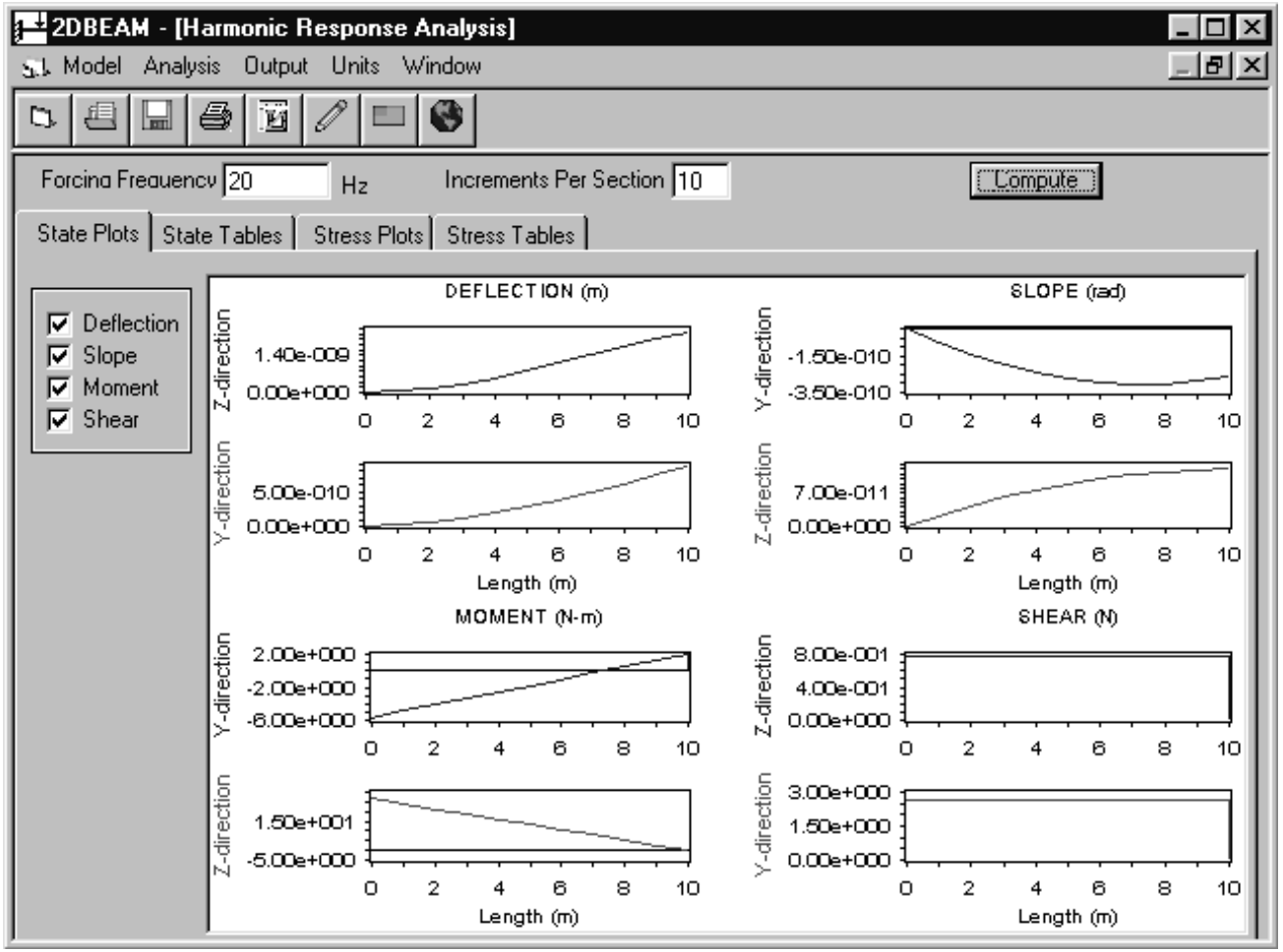

Figure B.25: Output screen graphically displaying the forced response at a specified forcing frequency.

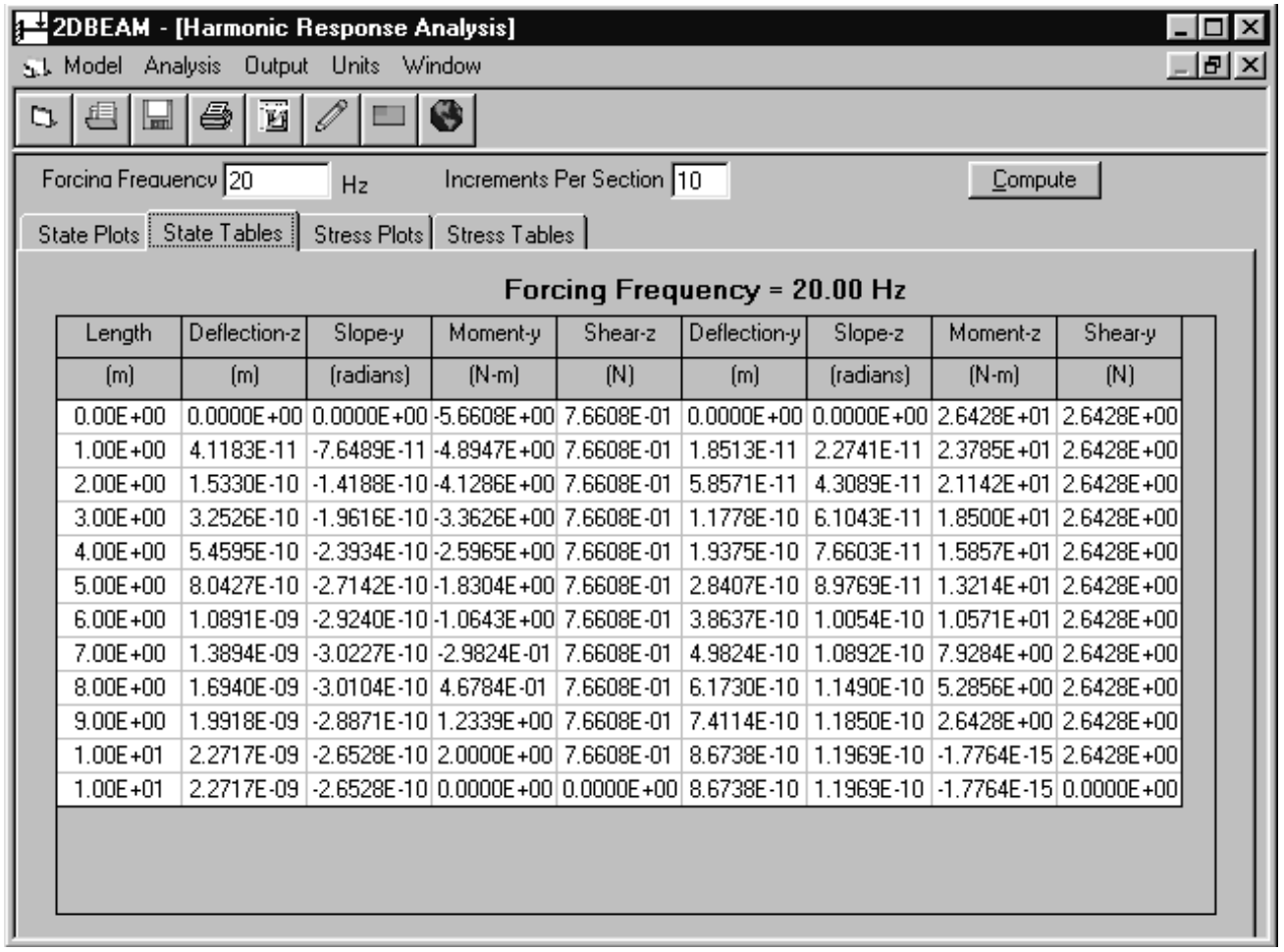

Length (m)	Deflection-z (m)	Slope-y (radians)	Moment-y (N-m)	Shear-z (N)	Deflection-y (m)	Slope-z (radians)	Moment-z (N-m)	Shear-y (N)
0.00E+00	0.0000E+00	0.0000E+00	-5.6608E+00	7.6608E-01	0.0000E+00	0.0000E+00	2.6428E+01	2.6428E+00
1.00E+00	4.1183E-11	-7.6489E-11	-4.8947E+00	7.6608E-01	1.8513E-11	2.2741E-11	2.3785E+01	2.6428E+00
2.00E+00	1.5330E-10	-1.4188E-10	-4.1286E+00	7.6608E-01	5.8571E-11	4.3089E-11	2.1142E+01	2.6428E+00
3.00E+00	3.2526E-10	-1.9616E-10	-3.3626E+00	7.6608E-01	1.1778E-10	6.1043E-11	1.8500E+01	2.6428E+00
4.00E+00	5.4595E-10	-2.3934E-10	-2.5965E+00	7.6608E-01	1.9375E-10	7.6603E-11	1.5857E+01	2.6428E+00
5.00E+00	8.0427E-10	-2.7142E-10	-1.8304E+00	7.6608E-01	2.8407E-10	8.9769E-11	1.3214E+01	2.6428E+00
6.00E+00	1.0891E-09	-2.9240E-10	-1.0643E+00	7.6608E-01	3.8637E-10	1.0054E-10	1.0571E+01	2.6428E+00
7.00E+00	1.3894E-09	-3.0227E-10	-2.9824E-01	7.6608E-01	4.9824E-10	1.0892E-10	7.9284E+00	2.6428E+00
8.00E+00	1.6940E-09	-3.0104E-10	4.6784E-01	7.6608E-01	6.1730E-10	1.1490E-10	5.2856E+00	2.6428E+00
9.00E+00	1.9918E-09	-2.8871E-10	1.2339E+00	7.6608E-01	7.4114E-10	1.1850E-10	2.6428E+00	2.6428E+00
1.00E+01	2.2717E-09	-2.6528E-10	2.0000E+00	7.6608E-01	8.6738E-10	1.1969E-10	-1.7764E-15	2.6428E+00
1.00E+01	2.2717E-09	-2.6528E-10	0.0000E+00	0.0000E+00	8.6738E-10	1.1969E-10	-1.7764E-15	0.0000E+00

Figure B.26: Output screen displaying the forced response at a specified forcing frequency in tabular format.

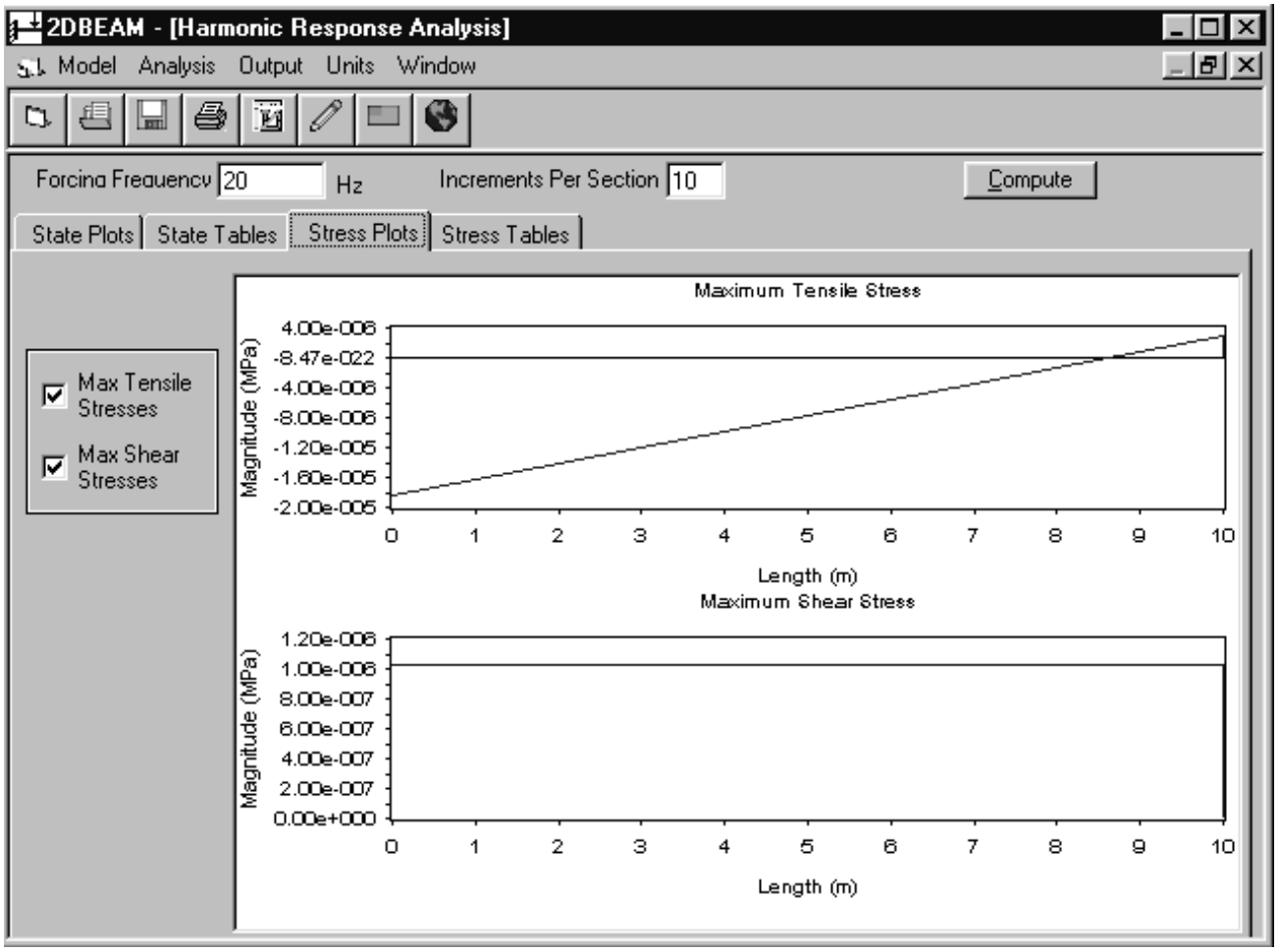

Figure B.27: Output screen graphically displaying the stress response at a specified forcing frequency.

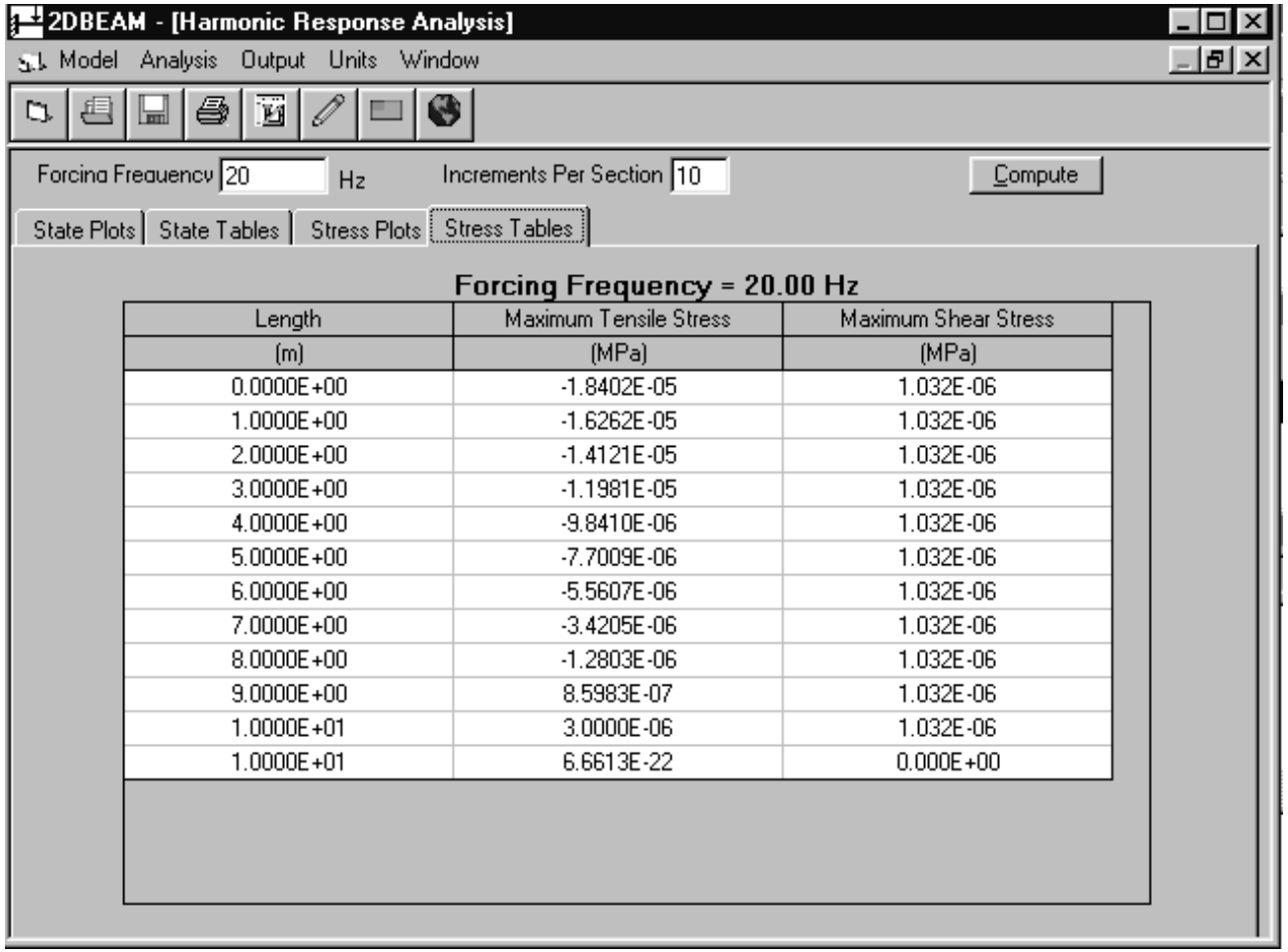

Length (m)	Maximum Tensile Stress (MPa)	Maximum Shear Stress (MPa)
0.0000E+00	-1.8402E-05	1.032E-06
1.0000E+00	-1.6262E-05	1.032E-06
2.0000E+00	-1.4121E-05	1.032E-06
3.0000E+00	-1.1981E-05	1.032E-06
4.0000E+00	-9.8410E-06	1.032E-06
5.0000E+00	-7.7009E-06	1.032E-06
6.0000E+00	-5.5607E-06	1.032E-06
7.0000E+00	-3.4205E-06	1.032E-06
8.0000E+00	-1.2803E-06	1.032E-06
9.0000E+00	8.5983E-07	1.032E-06
1.0000E+01	3.0000E-06	1.032E-06
1.0000E+01	6.6613E-22	0.000E+00

Figure B.28: Output screen displaying the stress response at a specified forcing frequency in tabular format.

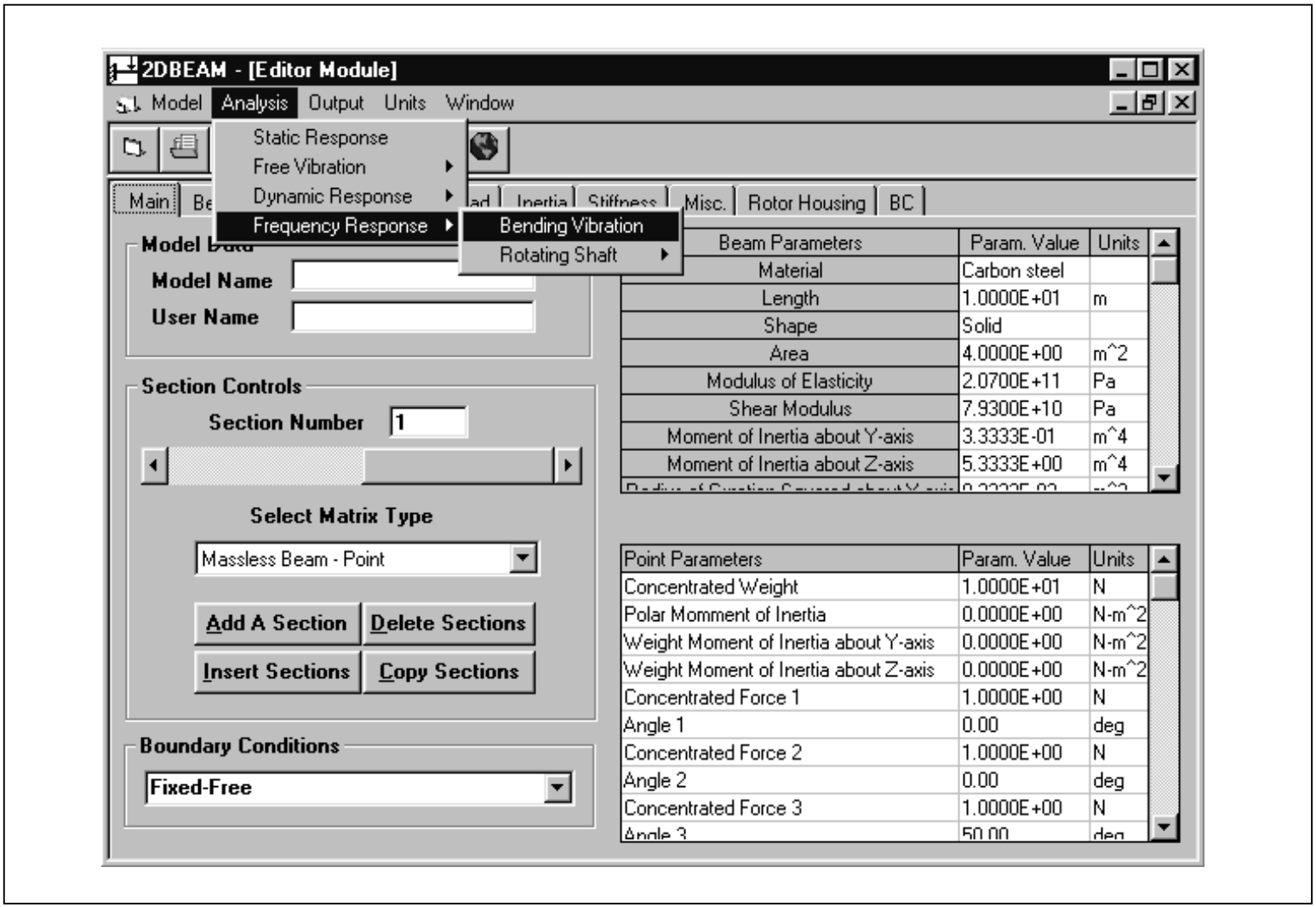

Figure B.29: Drop down menu of frequency response from which the different types of vibrations may be selected.

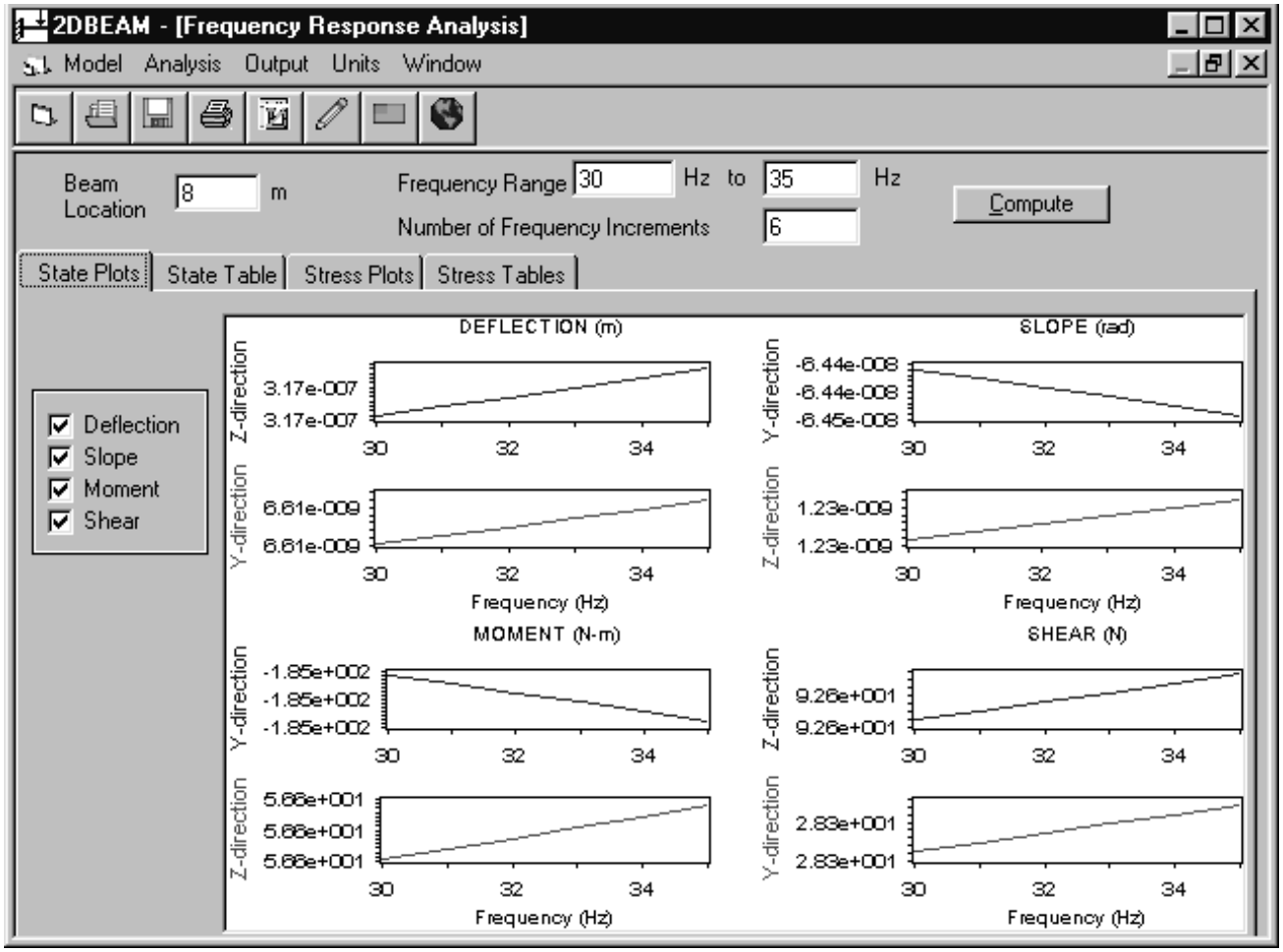

Figure B.30: Output screen graphically displaying the frequency response over a specified frequency range.

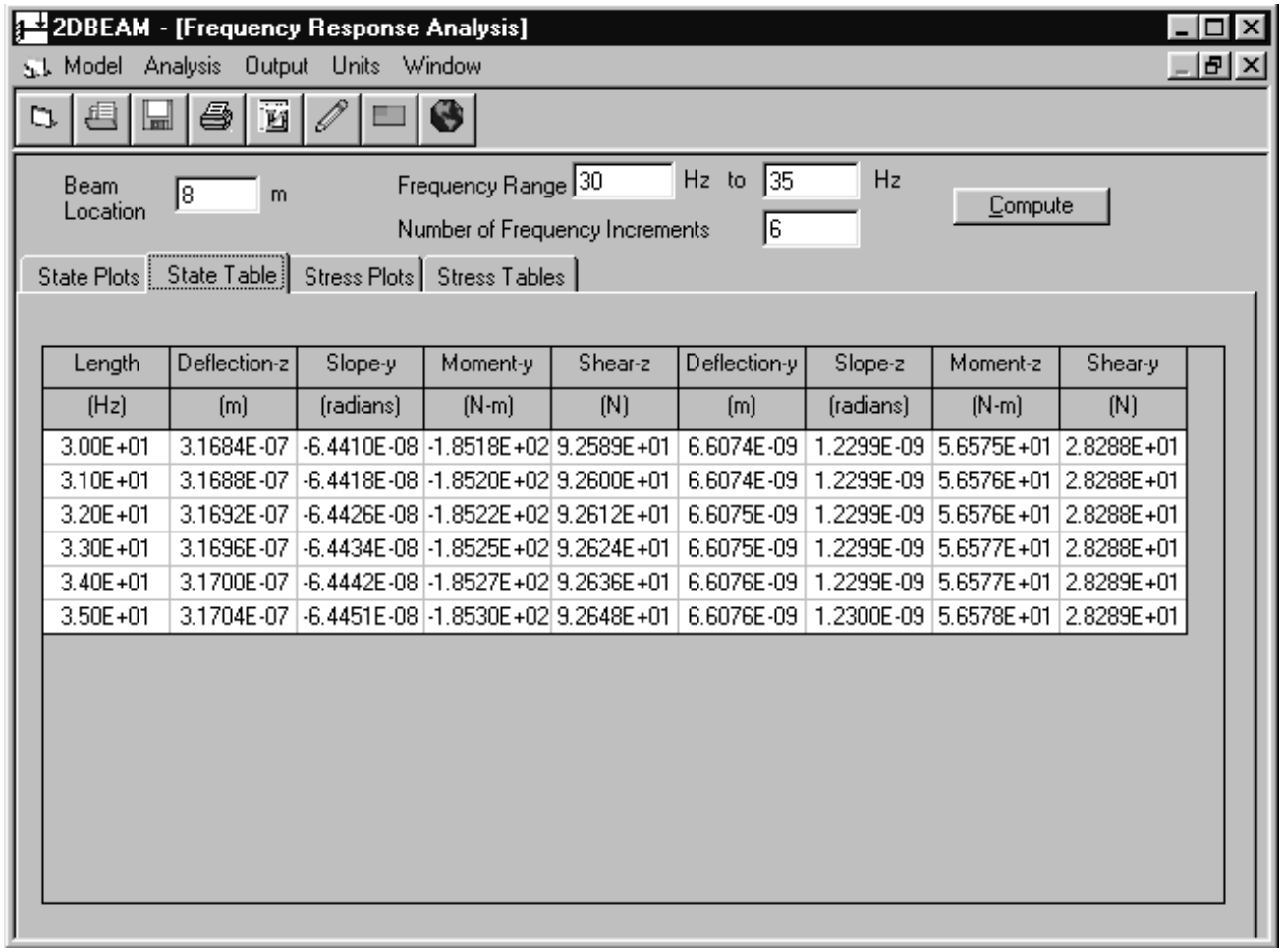

Length	Deflection-z	Slope-y	Moment-y	Shear-z	Deflection-y	Slope-z	Moment-z	Shear-y
(Hz)	(m)	(radians)	(N-m)	(N)	(m)	(radians)	(N-m)	(N)
3.00E+01	3.1684E-07	-6.4410E-08	-1.8518E+02	9.2589E+01	6.6074E-09	1.2299E-09	5.6575E+01	2.8288E+01
3.10E+01	3.1688E-07	-6.4418E-08	-1.8520E+02	9.2600E+01	6.6074E-09	1.2299E-09	5.6576E+01	2.8288E+01
3.20E+01	3.1692E-07	-6.4426E-08	-1.8522E+02	9.2612E+01	6.6075E-09	1.2299E-09	5.6576E+01	2.8288E+01
3.30E+01	3.1696E-07	-6.4434E-08	-1.8525E+02	9.2624E+01	6.6075E-09	1.2299E-09	5.6577E+01	2.8288E+01
3.40E+01	3.1700E-07	-6.4442E-08	-1.8527E+02	9.2636E+01	6.6076E-09	1.2299E-09	5.6577E+01	2.8289E+01
3.50E+01	3.1704E-07	-6.4451E-08	-1.8530E+02	9.2648E+01	6.6076E-09	1.2300E-09	5.6578E+01	2.8289E+01

Figure B.31: Output screen displaying the frequency response over a specified frequency range in tabular format.

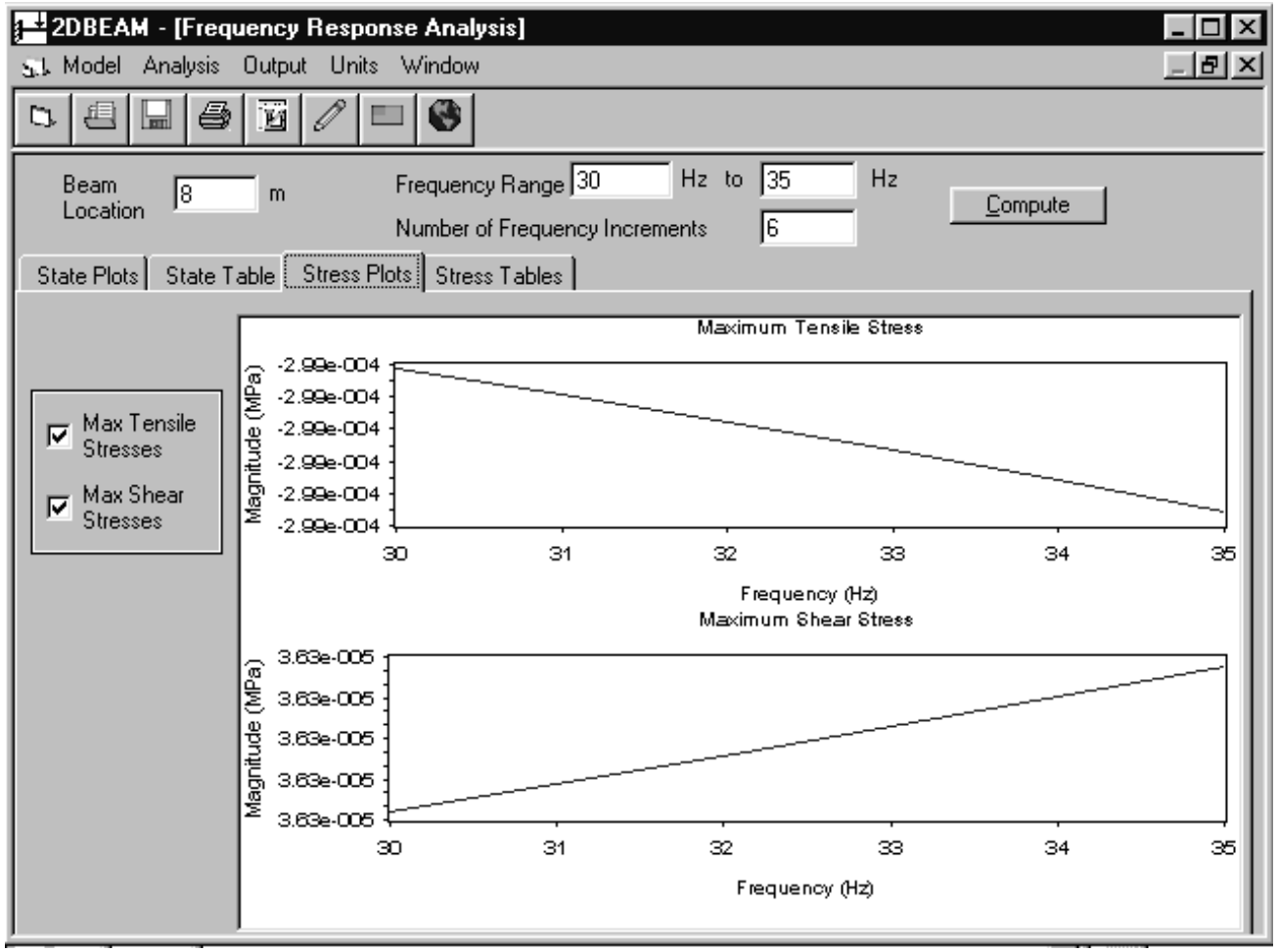

Figure B.32: Output screen graphically displaying the stress response over a specified frequency range.

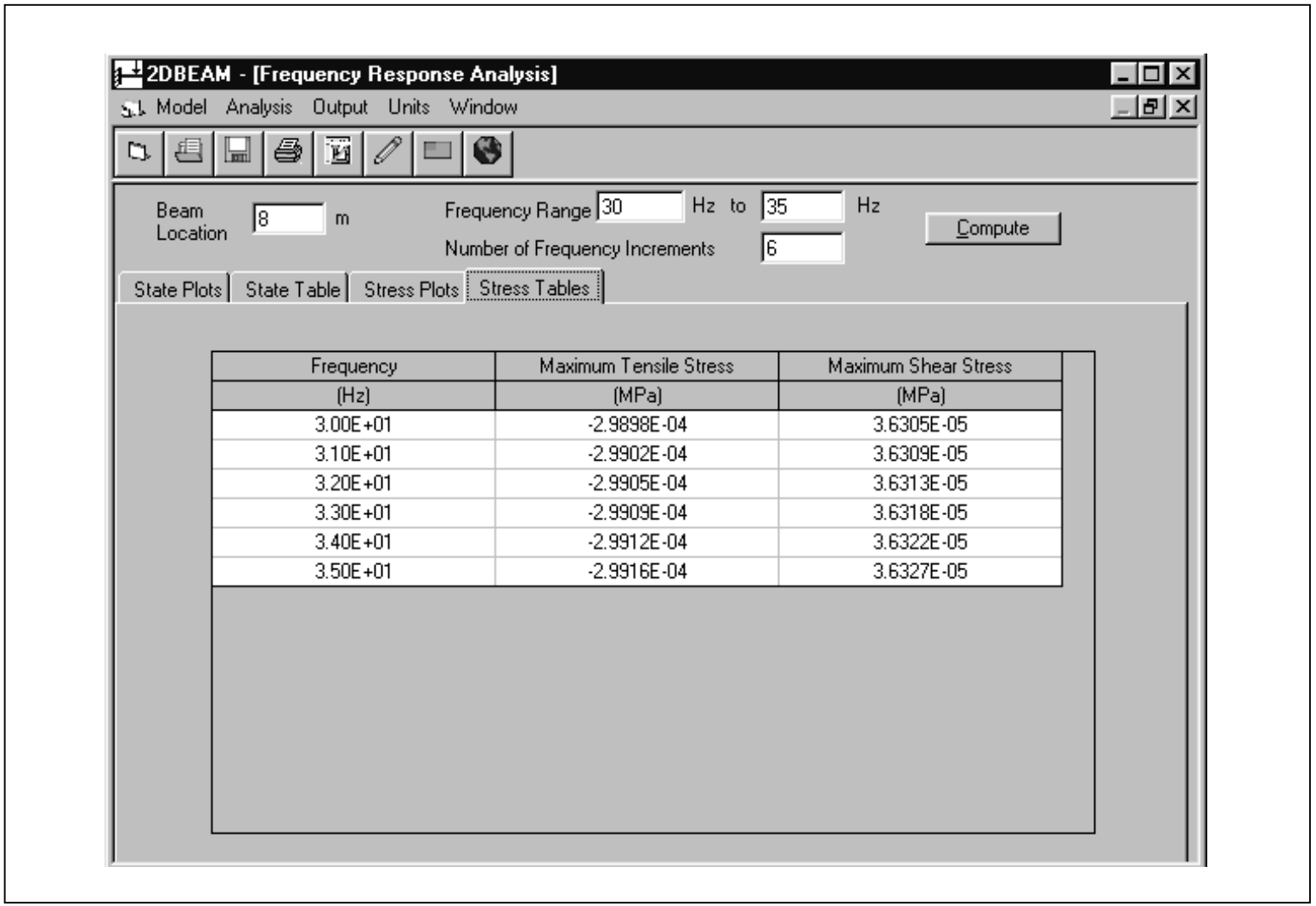

Figure B.33: Output screen displaying the stress response over a specified frequency range in tabular format.

References

1. Pestel, E. C. and Leckie, F. A., *Matrix Methods in Elastomechanics*, McGraw-Hill Book Company, Inc., New York, 1963.

2. Burden, R. L. and Faires, J. D., *Numerical Analysis*, Fourth Edition, Pws-Kent Publishing Company, Boston, 1989, pp. 73–81.

3. Reference 1, pp. 51-94.

4. Reference 1, p. 52.

5. Reference 1, p. 375.

6. Reference 1, p. 125.

7. Reference 1, p. 57.

8. Reference 1, p. 60.

9. Reference 1, p. 55.

10. Reference 1, p. 61.

11. Reference 1, p. 82.

12. Mitchell, L. D. and Young, R.J., *User's Guide-BEAM V*, AMDF Publication, Virginia Polytechnic Institute and State University, Blacksburg, October 1989, p. 6.

13. Reference 1, pp. 71-72.

14. Reference 1, p. 72.

15. Reference 1, p. 58.

16. Rao, J. S., *Rotor Dynamics*, John Wiley & Sons, Inc., New York, 1983, p. 108.

17. Reference 1, p. 5.

18. Reference 1, p. 6.

19. Shigley, J. E. and Mitchell, L. D., *Mechanical Engineering Design*, Fourth Edition, McGraw-Hill Book Company Inc., New York, 1983, pp. 804–811.

20. Hibbeler, R. C., *Mechanics of Materials*, Second Edition, Macmillan College Publishing Company, New York, 1994, p. 310.

21. Reference 20, p. 373.

22. Harris, C. M. and Crede, C. E., *Shock and Vibration Handbook*, Volume 1, McGraw-Hill Book Company, New York, 1961, p. 1-14.

23. Young, D. and Felgrar, R. P., *Tables of Characteristic Functions Representing Normal Modes of Vibration of a Beam*, The University of Texas Publication, No. 4913, Austin, 1949.

24. Reference 12, pp. 27-28.

25. Reference 22, pp. 2-8 to 2-9.

26. Reference 16, pp. 119-120.

27. Reference 16, p. 116.

28. Cook, R. D. and Young, W. C., *Advanced Mechanic of Materials*, Second Edition, Prentice-Hall, Inc., New Jersey, 1999, pp. 314-337.

29. Reference 16, p. 132.

30. Reference 16, p. 133.

31. Reference 1, p. 382.

32. Reference 1, p. 126.

33. Pilkey, W. D., *Manual for the Response of Structural Members,* Volume II, Engineering Mechanics Division, IIT Research Institute, Chicago, pp. III-111-III-112.

34. Reference 1, p. 380.

35. Reference 1, pp. 384-385.

36. Reference 1, pp. 127 and 381.

37. Reference 1, p. 382.

38. Reference 32, pp. III-129.

39. Reference 32, p. III-130.

Vita

Anaita R. Dolasa was born on June 24, 1973 in Baroda, India and was raised in Nairobi, Kenya. After graduating from high school she attended Michigan Technological University in Houghton, Michigan. In May 1996 she received a Bachelor of Science degree in Computer Science with a minor in Mechanical Engineering. In the Fall of 1996 she began her graduate study in Mechanical Engineering at Virginia Polytechnic Institute and State University. Upon completion of her Masters degree Anaita plans to begin work with the Bechtel Corporation located in Frederick, Maryland.